UNIVERSITY OF SOUTHAMPTON

THE KINETICS OF ADSORPTION, REACTION AND DESORPTION ON SINGLE CRYSTAL SILICON SURFACES

STEVEN WRIGHT

DOCTOR OF PHILOSOPHY

DEPARTMENT OF CHEMISTRY

JUNE 1996

UNIVERSITY OF SOUTHAMPTON

ABSTRACT

FACULTY OF SCIENCE

CHEMISTRY

Doctor of Philosophy

THE KINETICS OF ADSORPTION, REACTION AND DESORPTION ON SINGLE CRYSTAL SILICON SURFACES

By Steven Wright

Some aspects of adsorption, reaction and desorption reactions on single crystal silicon surfaces have been investigated in detail. Full use is made of the very extensive structural information that is currently available. The dissociative adsorption of D_2O on silicon surfaces involves a molecular precursor and is rapid at paired dangling bond sites but becomes very much slower when only isolated dangling bonds remain. Desorption of most of the deuterium occurs via the β_1 channel with an activation energy which increases with initial D_2O coverage due to an extended and cumulative interaction with adsorbed oxygen. Hydrogen atom adsorption at dangling bond sites on Si(100) and efficient Eley-Rideal abstraction seem to be inconsistent with a saturation coverage of one monolayer at 635 K. However, hydrogen atom uptake can be completely interpreted by including the surface dihydride species in the kinetic scheme. Both hydrogen atom adsorption on Si(100) and molecular hydrogen desorption from Si(100) are described by calculating the quasi-equilibrium distribution of singly occupied dimers, doubly occupied dimers and unoccupied dimers. A simple model considering only the pairing energy is sufficient at high coverages but the effective clustering interaction is also included in a detailed lattice gas model for equilibrium at low coverages. Similarly, the desorption of molecular hydrogen from Si(111)-7x7 can be modelled by calculating the equilibrium distribution of hydrogen atoms adsorbed at rest atom and adatom dangling bond sites.

CONTENTS

Acknowledgments

It is my pleasure to thank Neville Jonathan for the tireless and complete support which has brought this work to a successful conclusion. I am indebted to Michael Flowers, Alan Morris and Yong Liu for their many and valuable contributions. During my time in Southampton and Berlin I have also enjoyed and benefited from the company of Alex King, Adam Gee, Mark Newton, Dave Pegg, Brian Hayden, Susan Hill, Jon Davies, Olaf Dippel, Karl-Heinz Bornscheuer, Winfried Nessler, Marcello Binetti, Eckart Hasselbrink and many other friends and colleagues. Although my parents might not read past here, this thesis is for them.

Abbreviations

EELS	Electron energy loss spectroscopy
E_F	Fermi level
LEED	Low energy electron diffraction
LITD	Laser induced thermal desorption
ML	Monolayer
SHG	Second harmonic generation
SSIMS	Static secondary ion mass spectroscopy
STM	Scanning tunneling microscopy
STS	Scanning tunneling spectroscopy
TPD	Temperature programmed desorption
UHV	Ultra high vacuum
UPS	Ultraviolet photoelectron spectroscopy
XPS	X-ray photoelectron spectroscopy

CHAPTER 1

INTRODUCTION TO THE ELECTRONIC AND GEOMETRIC STRUCTURES OF THE Si(100)-2x1 AND Si(111)-7x7 SURFACES

The free energy of the cleaved Si(100) surface is reduced by dimerisation of the surface atoms. This reconstruction was identified by LEED [1, 2] and photoemission studies [3] together with theoretical modeling [4, 5] prior to direct observation by STM [6]. It now seems likely that the lowest energy dimer geometry is buckled as illustrated in figure (1) but STM images show that most dimers are symmetric [6, 7]. It is believed that the buckling orientation flips rapidly at room temperature and hence a time averaged configuration is seen by an STM tip which takes approximately 10 ms to image a dimer [8]. A very small energy barrier to dimer flipping through a symmetric transition state is also reflected by numerous theoretical calculations which variously find that either the symmetric or buckled dimer is the lowest energy geometry [8-12]. Photoemission from surface dimers has been identified with a distinct Si 2p surface core level shift but has been variously attributed to symmetric [13, 14] or buckled dimers [15-17]. A dimer geometry buckled by 19° with respect to the surface plane and with a dimer bond length of 2.25 Å has recently been deduced by analysis of angle-resolved photoelectron diffraction intensities [18]. Similarly, dimers are buckled by 17.7° and have a bond length of 2.29 Å in the lowest energy geometry of the c(4x2) reconstruction calculated using the local density approximation [19].

In addition to the σ–bond between the two silicon atoms of each dimer, there is some interaction between the remaining half filled p-orbitals (the dangling bonds). There is some controversy regarding the nature of this interaction with some preferring to describe it as a weak π-bond while others discuss dimer buckling in terms of a Peierls distortion. An important difference is that Peierls distortion requires that both bonding electrons are associated with a lone pair orbital on the up atom leaving an empty orbital on the down atom whereas the electron density is shared equally by π-bonding. Calculations using density functional theory [20] and the buckled geometries

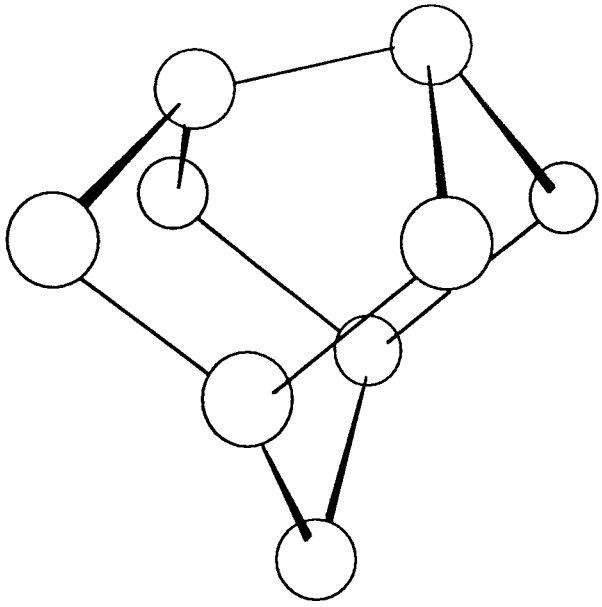

Figure (1). Buckled dimer reconstruction of the Si(100) surface.

have identified three phonons that may assist the flipping process. A dimer rocking vibration at 20 meV (involving essentially vertical displacements of the dimer atoms) also involves oscillation of the charge density between the up and down dimer atoms and is likely to be intimately linked to dimer flipping. In addition, very low frequency shear horizontal (in the direction of the dimer rows) and dimer twisting vibrations at 8.3 and 7.1 meV respectively may also have an important role.

Some rows of dimers are clearly asymmetric in room temperature STM images and appear to be pinned by defect sites, adsorbates and at step edges. The two second layer atoms bound to the up end of a buckled dimer are pulled together whereas those bound to the down end are pushed apart and hence the lattice strain is minimised when adjacent dimers buckle in opposite orientations. Adjacent rows of buckled dimers can be arranged in two configurations corresponding to in-phase and anti-phase buckling. The unit cells for these configurations are p(2x2) and c(4x2) respectively as shown in figure (2) and are both observed by STM [6]. Wolkow [21] has reported that at

120 K, 80% of the surface dimers are frozen in a buckled geometry with the c(4x2) arrangement five times more common than p(2x2), presumably also as a result of lattice strain. There is no prospect of identifying an order-disorder phase transition since it is presently impossible to prepare a Si(100) surface without steps or defects.

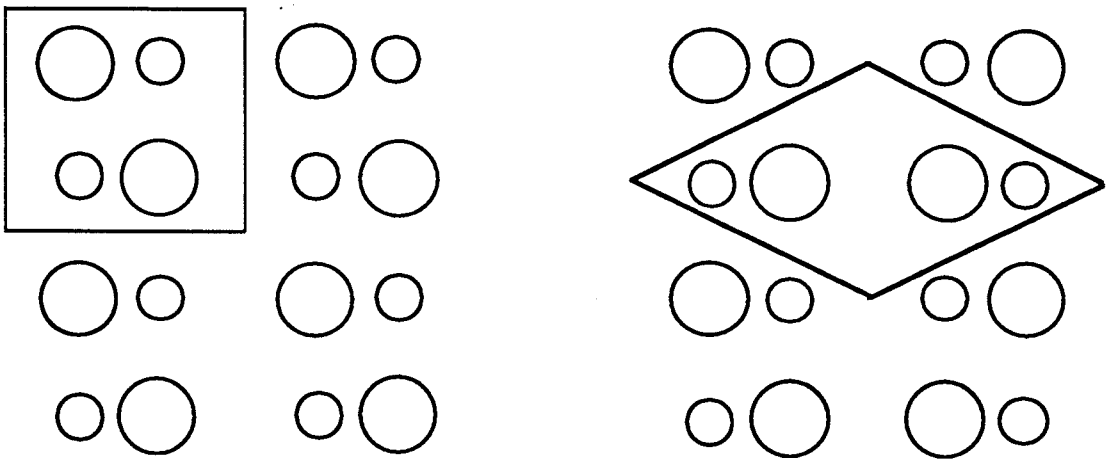

Figure (2). Buckled dimers in p(2x2) and c(4x2) reconstructions. Up atoms are large circles and down atoms are small circles. The unit cells are outlined.

Any misorientation away from the (100) plane and towards the [110] and [1$\bar{1}$0] axis is accommodated by single atomic height or double atomic height steps. Typically single crystal silicon samples can be obtained with a misorientation of ±0.5° from the (100) plane. When the misorientation is 0.5°, the average terrace width is 155 Å which corresponds to 40 dimers or 20 dimer rows. The bulk crystallography requires that the direction of dimerisation is rotated through 90° by a single atomic height step and hence spots for both (2x1) and (1x2) domains are found in the LEED pattern. The areas of the (1x2) and (2x1) domains are normally the same to within 1% but if mechanical strain is applied to the crystal [22] or if the surface is prepared by high temperature epitaxy [23] then one domain is preferred and observed over as much as 90% of the surface area.

It is thought that at some misorientation from the (100) plane, double atomic height steps become energetically more favourable than single atomic height steps. Surfaces with only single atomic height steps have been reported for misorientation by 1.5° [24] and 1.37° [25] whereas only double atomic height steps are found when the misorientation is 4.7° [26], 6° [27] and 8° [24, 25, 28] towards the [110] direction. At intermediate angles, a temperature dependent distribution of both double and single atomic height steps exists [25-27, 29, 30]. Steps are invariably labelled using S_A and S_B for single atomic height steps and D_A and D_B for double atomic height steps as described by Chadi [31]. The A and B subscripts denote that the dimer axis on the upper terrace is perpendicular and parallel to the step edge respectively. No D_A steps are observed experimentally but there must be equal numbers of S_A and S_B steps on surfaces with only single atomic height steps. Step edge sites are often important and sometimes dominant in adsorption, surface reaction and desorption processes on metal surfaces [32-34] as a consequence of the lower coordination of step atoms compared with terrace atoms. Isolated dangling bonds are found on nominally flat Si(100)-2x1 at both dimerised and undimerised S_B steps as shown in figure (3) but are generally ignored in many discussions.

Transmission electron diffraction [35, 36] and STM [37] have established the dimer-adatom-stacking fault (DAS) model of the Si(111)-7x7 reconstruction. Lattice coordinates for two hundred atoms in the top five layers of the reconstruction have been calculated by Tong *et al.* using the dynamical theory of LEED [38] and a unit cell based on these coordinates is illustrated in figure (4). The 7x7 unit cell has a total of nineteen dangling bonds of seven different geometries. In the top layer of the reconstruction there are twelve adatoms arranged in two triangular sub-units which have 2x2 periodicity and are alternately faulted and unfaulted with respect to the bulk lattice. Each adatom contributes one dangling bond and is bonded to three rest atoms in the second

layer leaving six unsaturated rest atom dangling bonds. The triangular sub units are bounded by rows of rest atom dimers which intercept at the corner holes. At each corner hole there is one dangling bond from an atom in the fourth layer. STM images of the Si(111)-7x7 reconstruction generally show only the adatoms since the rest atoms and corner holes are not easily accessed. However, the 1x1 periodicity of the underlying rest atom layer has been imaged after removal of the adatoms by chemical reaction [39].

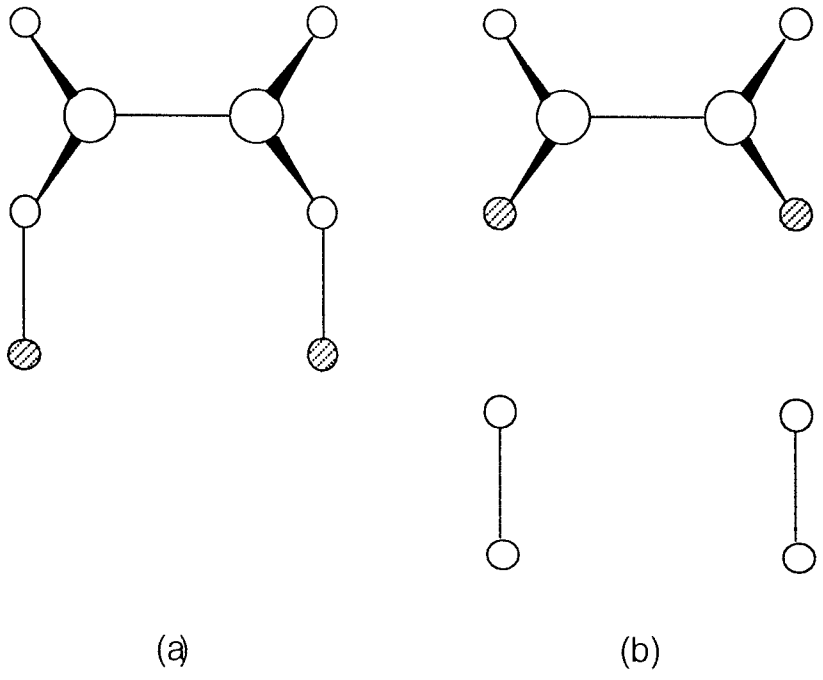

Figure (3). Bonding at (a) dimerised S_B steps and (b) non-dimerised S_B steps. Large circles represent the upper layer and small circles represent the lower layer. In both (a) and (b) the hatched circles are isolated (unpaired) dangling bond sites.

Step edges are found with normals along the high symmetry $[11\bar{2}]$ and $[\bar{1}\bar{1}2]$ axis [40, 41]. The 7x7 reconstruction is maintained up to and including the step edge on both upper and lower terraces and any kinks are accommodated by loss or gain of whole unit cells. Although the edges of the rhombohedral unit cells are flush with the step edges, some slip in the registry between upper and lower terraces has been observed.

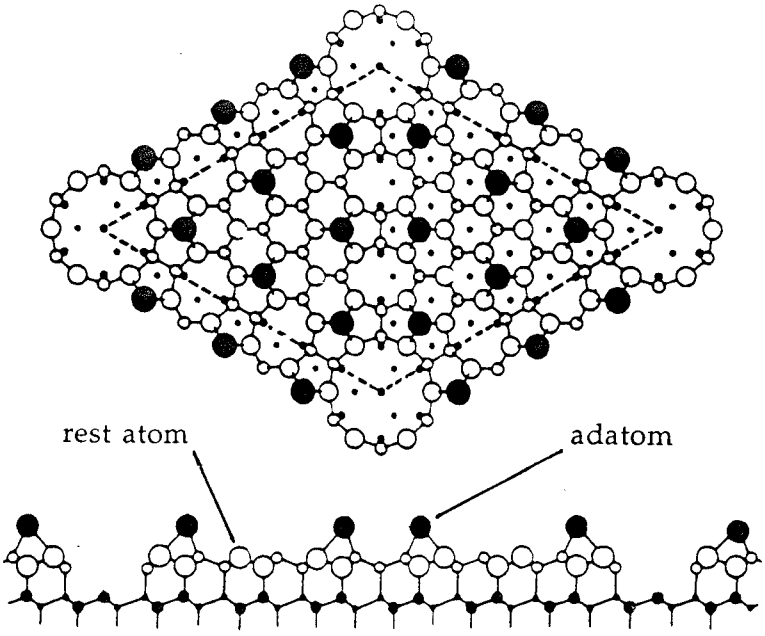

Figure (4). A Si(111)-7x7 unit cell based on the DAS model for the reconstruction. The long and short diagonals measure 46.6 Å and 26.9 Å respectively.

It has become clear that some reactions on the Si(111)-7x7 surface are very site specific and it is thought that this is a consequence of interaction and charge transfer between center adatom, corner adatom, rest atom and corner hole dangling bond sites [42, 43]. A fully occupied rest atom dangling bond state is found at 0.8 eV below E_F by STS [42]. Adatom sites are characterised by occupied and unoccupied states at 0.4 eV below and 0.5 eV above E_F respectively but the center adatom dangling bond state is found to be nearly empty. These data and theoretical considerations [44, 45] suggest that the rest atom dangling bond state is filled by charge transfer from the adatoms. More electron density is withdrawn from the center adatoms compared with the corner adatoms because each center adatom has two rest atom neighbours whereas each corner adatom has only one. The reactivity of each site has been predicted using *ab initio* density functional theory to calculate donor and acceptor charge transfer [43].

Much of the chemistry of the Si(111)-7x7 reconstruction involves reaction of the adatom back-bonds which are strained compared with rest atom back-bonds as shown in figure (5). Theoretical calculations [44-47] predict that these weakened back-bonds result in a surface state at about 2 eV below E_F and that there is some bonding interaction between the adatom and the silicon atom directly below it in the third layer. Whereas the electron density associated with the adatom dangling bond is withdrawn and somewhat delocalised by both charge transfer and sub-surface bonding, the rest atom dangling bond is very much more localised. Indeed, there is sufficient Coulomb repulsion between the fully occupied rest atom dangling bond and the rest atom back-bonds to push the rest atom higher than its bulk position.

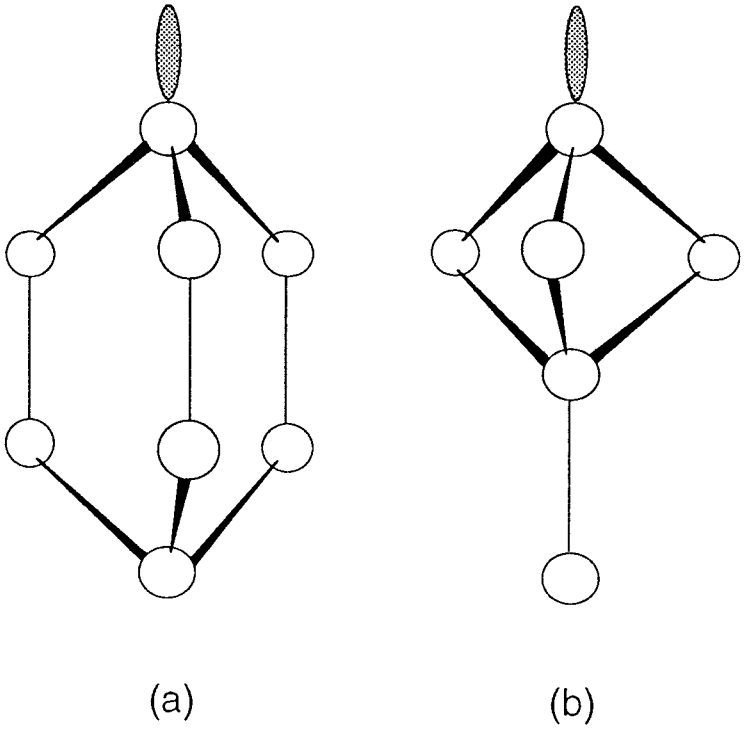

Figure (5). Local bonding at (a) rest atom and (b) adatom dangling bond sites.

The position of the Fermi level in bulk silicon can be moved between the top of the valence band and the bottom of the conduction band by n-type and p-type doping. However, the presence of surface states can have a

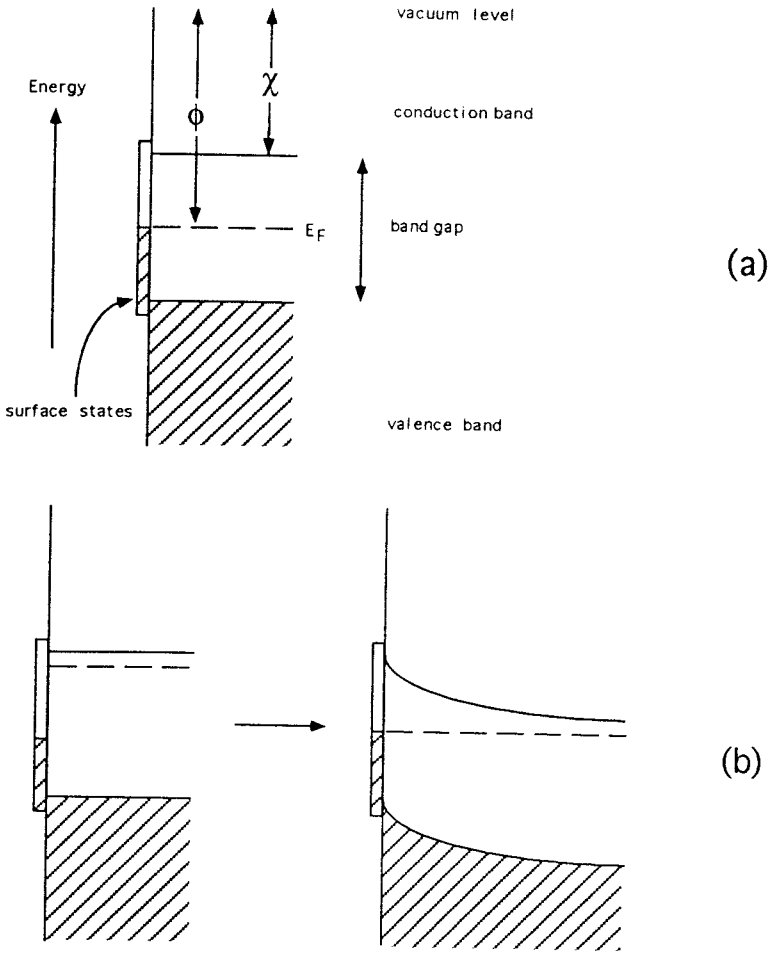

Figure (6). Band structure at (a) intrinsic and (b) n-type semiconductor surfaces. The work function, ϕ, is not changed by doping but the electron affinity, χ, is changed due to band bending.

profound effect on the band structure near the surface as will any change of the surface states as a result of chemisorption. If empty surface states are available below the bulk Fermi level (n-type doping) or if occupied surface states are available above the bulk Fermi level (p-type doping), then electrons will flow between the surface states and the near surface region until thermodynamic equilibrium is reached. The occupation of surface states is hardly changed since the density of surface states is approximately 10^{15} cm^{-2} whereas the bulk doping density of states in a single plane of atoms is typically between only 10^{8} and 10^{12} cm^{-2}. Consequently, the Fermi level at the surface and the measured work function [48] are nearly independent of the bulk doping (Fermi level pinning).

An electrostatic potential (a space - charge layer) is established by the transfer of electrons between surface states and dopant atoms in the near surface region. The response of the electron energy levels to this potential is known as band bending and causes the electron affinity at the surface to change. Fermi level pinning and band bending are illustrated in figure (6) for n-type doping.

[1] R.E. Schlier and H.E. Farnsworth, J. Chem. Phys. 30 (1959) 917.

[2] S.Y. Tong and A.L. Maldondo, Surf. Sci. 78 (1978) 459.

[3] J.E. Rowe, Phys. Rev. Lett. 46A (1974) 400.

[4] J.A. Appelbaum, G.A. Baraff and D.R. Hammann, Phys. Rev. Lett. 35 (1975) 729.

J.A. Appelbaum, G.A. Baraff and D.R. Hammann, Phys. Rev. B11 (1975) 3822.

J.A. Appelbaum, G.A. Baraff and D.R. Hammann, Phys. Rev. B12 (1975) 5749.

J.A. Appelbaum, G.A. Baraff and D.R. Hammann. Phys. Rev. B14 (1976) 588.

J.A. Appelbaum, G.A. Baraff and D.R. Hammann, Phys. Rev. B15 (1977) 2408.

[5] G.P. Kerker, S.G. Louie and M.L. Cohen, Phys. Rev. B 17 (1978) 706.

[6] R.J. Hamers, R.M. Tromp and J.E. Demuth, Phys. Rev. B34 (1986) 5343.

[7] J.J. Boland, J. Vac. Sci. Technol. A10, (1992) 2458.

[8] J. Dabrowski and M. Scheffler, Appl. Surf. Sci. 56-58 (1992) 15.

[9] Z. Zhu, N. Shima and M. Tsukada, Phys. Rev B40 (1989) 11868.

[10] B.I. Craig and P.V. Smith, Surf. Sci. 218 (1989) 569.

[11] G.P. Kochanski and J.E. Grifith, Surf. Sci. 249 (1991) L293.

[12] P.C. Weakleim and E.A. Carter, J. Chem. Phys. 96 (1992) 3240.

[13] X. Yang, R. Cao, J. Terry and P. Pianetta, J. Vac. Sci. Technol. B10 (1992) 2013.

R. Cao, X. Yang, J. Terry and P. Pianetta, Phys. Rev. B45 (1992) 13749.

[14] D.H. Rich, T. Miller and T.-C. Chiang, Phys. Rev. B37 (1988) 3124.
D.-S. Lin, T. Miller and T.C. Chiang, Phys. Rev. Lett. 67 (1991) 2187.
D.-S. Lin, J.A. Carlisle, T. Miller and T.-C. Chiang, Phys. Rev. Lett. 69 (1992) 553.

[15] G.K. Wertheim, D.M. Riffe, J.E. Rowe and P.H. Citrin, Phys. Rev. Lett. 67 (1991) 120.
J.E. Rowe and J.K. Wertheim, Phys. Rev. Lett. 69 (1992) 550.

[16] E. Landemark, C.J. Karlsson, Y.-C. Chao and R.I.G. Uhrberg, Phys. Rev Lett. 69 (1992) 1588.

[17] E. Pehlke and M. Scheffler, Phys. Rev. Lett. 71 (1993) 2338.

[18] E.L. Bullock, R. Gunnella, L. Patthey, T. Abukawa, S. Kono, C.R. Natoli and L.S.O. Johansson, Phys. Rev. Lett. 74 (1995) 2756.

[19] J.E. Northrup, Phys. Rev. B47 (1993) 10032.

[20] J. Fritsch and P. Pavone, Surf. Sci. 344 (1995) 159.

[21] R.A. Wolkow, Phys. Rev. Lett. 68 (1992) 2636.

[22] M.B. Webb, Surf. Sci. 299/300 (1994) 454.

[23] T. Abukawa, T. Okane and S. Kono, Surf. Sci. 256 (1991) 370.

[24] E. Schröder-Bergen and W. Ranke, Surf. Sci. 259 (1991) 323.

[25] I. Vilfan, Surf. Sci. 289 (1993) L604.

[26] L. Barbier and J. Lapajoulade, Surf. Sci. 253 (1991) 303.

[27] C.E. Aumann, C.E. de Miguel, R. Kariotis and M.G. Lagally, Surf. Sci. 275 (1992) 1.

[28] X. Tong and P.A. Bennett, Phys. Rev. Lett. 67 (1991) 101.

[29] B. Salanon, L. Barbier and L. Lapajoulade, J. Appl. Surf. Sci. 65/66 (1993) 575.

[30] J.J. de Miguel, C.E. Aumann, R. Kariotis and M.G. Lagally, Phys. Rev. Lett. 67 (1991) 2830.

[31] D. J. Chadi, Phys. Rev. Lett. 59 (1987) 1691.

[32] D.F. Johnson and W.H. Weinberg, J. Chem. Phys. 101, 6289, (1994).

[33] H. Karner, M. Luger, H.P. Steinrack, A. Winkler and K.D. Rendulic, Surf. Sci. 163, L641, (1985).

[34] J.A. Serri, J.C. Tully, M.J. Cardillo, J. Chem. Phys, 19, 1530, (1983).

[35] K. Takayanagi, Y. Tanishiro, M. Takahashi and S. Takahashi, J. Vac. Sci. Technol. A3 1052 (1985).

[36] K.Takayanagi, Y. Tanishiro, M. Takahashi and S. Takahashi, Surf. Sci. 164 367 (1985).

[37] J.J. Boland, Surf. Sci. 244 1 (1991).

[38] S.Y. Tong, H. Huang, C.M. Wei, W.E. Packard, F.K. Men, G. Glander and M.B. Webb, J. Vac. Sci. Technol. A6 (1988) 615.

[39] J.J. Boland and J.S. Villarrubia, Phys. Rev. B41 (1990) 9865.

[40] X.-S. Wang, J.L. Goldberg, N.C. Bartelt, T.L. Einstein and E.D. Williams, Phys. Rev. Lett. 65 (1990) 2430.

[41] R.S. Becker, J.A. Golovchenko, E.G. McRae and B.S. Swartzentruber, Phys. Rev. Lett. 55 (1985) 2028.

[42] R. Wolkow and Ph. Avouris, Phys. Rev. Lett. 60 (1988) 1049.

[43] K.D. Brommer, M. Galván, A. Dal Pino. Jr. and J.D. Joannopoulos, Surf. Sci. 314 (1994) 57.

[44] J.E. Northrup, Phys. Rev. Lett. 57 (1986) 154.

[45] R.D. Meade and D. Vanderbilt, Phys. Rev. B40 (1989) 3905.

[46] G.-X. Qian and D.J. Chadi, J. Vac. Sci. Technol. A5 (1987) 906.

[47] Ph. Avouris and R. Wolkow, Phys. Rev. B39 (1989) 5091.

[48] F.J. Allen and G.W. Gobeli, Phys. Rev. 127 (1962) 152.

CHAPTER 2

EXPERIMENTAL

2.1. CRYSTAL MOUNT AND SURFACE PREPARATION

The single crystal samples (15x10x1.5 mm) were cut from (100)±0.5° orientated, p-type wafers with a resistivity of 0.01-0.02 Ω cm and (111)±0.5° orientated, n-type wafers with a resistivity of 5 Ω cm. A 0.3 mm wide and 2 mm deep slot was cut in the long edge of each sample so that the thermocouple (K-type), contained in a tantalum sleeve, could be inserted as a tight fit. The silicon samples were wrapped with tantalum foil and clamped to a sapphire plate with molybdenum screws and tantalum clips such that a 10x10 mm area of the front surface was exposed. The sample mount shown in figure (1) was constructed entirely from refractory materials and connected to the power supply with oxygen free, high conductivity copper wire. After degassing the sample and mount at 800 K during bake-out, the native oxide was removed from the silicon surface by repetitively heating to a maximum temperature of 1150 K. At no time was the pressure allowed to exceed $5x10^{-10}$ mbar during a heating ramp. This procedure results in low carbon contamination and the LEED patterns characteristic of the (100)-2x1 and (111)-7x7 reconstructions [1]. The Si(111)-7x7 reconstruction seems to be very robust [2] and is easily prepared but the Si(100)-2x1 reconstruction is easily damaged by heating to above 1350 K [3]. After the oxide layer had been removed, the surface was always protected overnight with a monolayer coverage of deuterium. It has been noted elsewhere [4] that the EELS spectrum of hydrogen on Si(100) does not change after several days in UHV.

In common with most other surfaces prepared in UHV, silicon surfaces are often found to be contaminated by carbon which is probably introduced by degreasing in organic solvents or by adsorption of pump oil cracking products. It is common to remove this by argon ion sputtering but this may introduce metal contamination from the ion gun itself and cause damage that is not healed by thermal annealing. Nickel is a tenacious contaminant of silicon

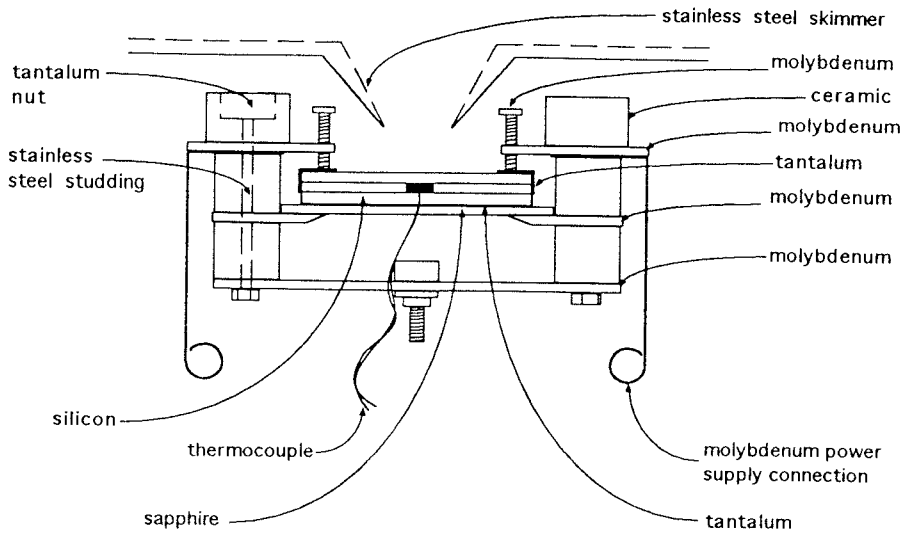

Figure (1). The silicon crystal was mounted as shown and positioned in front of a skimmer during TPD experiments.

surfaces and its effect on both surface structure and chemistry have been studied in some detail [5, 6]. Each "split off dimer" defect seen in many STM images of Si(100)-2x1 is caused by a single nickel atom [5] and involves a total of eight surface silicon atoms. These defects aggregate into vacancy channels with 2 x 10 periodicity at low coverages and eventually 2x7 periodicity as the nickel coverage increases to 1% [7, 8]. Similar nickel coverages on Si(111)-7x7 result in the well known ($\sqrt{19}$ x $\sqrt{19}$)R23.5° LEED pattern [9, 10]. It is of particular interest here that a nickel coverage of less than 5% prevents desorption of silane from hydrogen covered Si(111) and causes the β_1 and β_2 TPD peaks to shift to lower temperatures by 50 K [6]. Nickel contamination of the surface is reduced by a factor of about 10^7 when it rapidly dissolves into the bulk at temperatures above 600 K [5], although it segregates at the surface again on cooling. Hence, it is puzzling that surface processes occurring at above 600 K, notably the molecular hydrogen β_1 TPD peak, are in any way affected by nickel contamination. It is generally appreciated that contact with stainless steel during handling and cutting can introduce transition metal contamination [11]. Recently,

evaporation of nickel from K-type thermocouples (containing 90% nickel) at 1440 K has been identified as another source of contamination [5] and it may be that C-type thermocouples (containing only tungsten and rhenium) will become more popular [12]. However, in the present study, the maximum surface temperature was only 1150 K and the tantalum envelope containing the thermocouple extended to at least 3 mm from the top of the crystal.

2.2. TEMPERATURE PROGRAMMED DESORPTION

The 70 dm^3 main chamber was pumped by a 2000 $dm^{-3}s^{-1}$ diffusion pump with liquid nitrogen trap and had a base pressure of less than $2x10^{-10}$ mbar. The desorbing flux was sampled through a conic skimmer with a 3 mm aperture positioned approximately 4 mm from the crystal surface and measured by a mass spectrometer (VG SXP400) housed in a separate, differentially pumped detection chamber.

A variable transformer driven by a synchronous motor supplied a 0-250 V linear voltage ramp to the primary winding of a step-down transformer. The voltage obtained across the secondary winding was used to generate the temperature program by resistive heating of the crystal. It should be noted that a smooth and reproducible but not necessarily linear temperature ramp was required for these experiments.

A general purpose, 12 bit data acquisition card (PC - Labcard PCL-812PG) was installed in a 486 DX PC at a vacant I/O address and used to control the experiment and record the data. Typically, data aquisition was facilitated by third party (Adventech) application software, however, greater flexibility could be achieved by programming the card using QBASIC 4.5. Although it is possible to write to and read the I/O port directly, it is more convenient to use the machine code driver routines supplied by the manufacturer. These are

loaded into a memory segment from the QBASIC command line and are subsequently implemented using the QBASIC CALL statement.

Several signal intensities could be recorded almost simultaneously during a single TPD experiment by multiplexing the mass spectrometer. The required ion signal could be selected by supplying a DC voltage proportional to the mass number to the radio frequency generator. An amplifier (integrating) time constant appropriate to the rate of change of the signal was chosen when only a single signal was recorded. However, when several signals were recorded, the time constant was set equal to the rate of mutiplexing if this was faster than the rate of change of any of the signals. The thermocouple voltage was amplified by a calibrated isolation amplifier and recorded after time intervals during which up to three different ion signals were measured.

The desorption of molecular hydrogen from tantalum sample mounts has resulted in anomolous data from TPD studies of hydrogen desorption from diamond [13, 14]. Although the experimental geometry was such that only a very small fraction of the flux desorbing from the tantalum clips and foil was sampled, the possible contribution to the TPD data was calculated. Using published kinetic parameters for the recombinative desorption of molecular deuterium from tantalum [15], it was concluded that desorption from the tantalum components may increase slowly after the β_1 TPD peak if the deuterium exposure was particularly high. Occasionally such a feature was observed after very high exposures, especially of hydrogen, but was always small compared with the genuine TPD peaks.

2.3 EXPOSURE TO WATER AND ATOMIC HYDROGEN

Atomic deuterium (D·) and atomic hydrogen (H·) were generated by dissociating D_2 (99.7 atom %) and H_2 (99.9 atom %) respectively with a thoroughly degassed hot tungsten filament (1750±50 K) positioned approximately 100 mm from and at 135° with respect to the normal of the silicon surface. This arrangement is somewhat unusual in that there are no line-of-sight trajectories from the filament to the silicon surface but reduces the likelihood of radiative heating and contamination by tungsten compared with line-of-sight geometries [16]. The rate of atomisation is linear in hydrogen pressure when the pressure is less than 10^{-6} torr [17]. Although H· and D· are pumped by reaction with the Cr_2O_3 surface of the stainless steel UHV chamber, the gas load required to achieve saturation of the silicon surface is reasonable and a base pressure of $6x10^{-10}$ mbar could generally be achieved after 3-5 minutes. The relative D· and H· exposures were measured by integration of the ion gauge controller output but the absolute flux at the surface was not determined. Deuterium was used in preference to hydrogen in order to minimise the background contribution to the signal. The H_2^+ mass spectrometer signal is typically found to be large and noisy in residual gas analysis as a result of hydrocarbon cracking (in diffusion pump systems) [18].

The D_2O was degassed by several freeze-pump-thaw cycles prior to each set of experiments and introduced into the vacuum chamber through a leak valve. The ion gauge was switched off during D_2O exposures in order to avoid dissociation at its hot filament. The relative D_2O exposures were measured by integration of the mass spectrometer signal at m/e=20 with the sample moved out of line-of-sight of the detection chamber sampling orifice to ensure that exposure to dissociation products from the mass spectrometer filaments was insignificant.

2.4 REFERENCES

[1] L.A. Okada, M.L. Wise and S.M. George, Appl. Surf. Sci. 82/83 (1994) 410.

[2] J.J. Boland, Adv. Phys. 42 (1993) 129.

[3] R.J. Hamers, R.M. Tromp and J.E. Demuth, Phys. Rev. B34 (1986) 5343.

[4] N. Takagi, N. Minami, T. Furukawa and M. Nishijima, Surf. Sci. 297 (1993) L443.

[5] V.A. Ukraintsev and J.T. Yates, Jr., Surf. Sci. 346 (1996) 31.

[6] R.M. Wallace, C.C. Cheng, P.A. Taylor, W.J. Choyke and J.T. Yates, Jr., App. Surf. Sci. 45 (1990) 201.

[7] K. Kato, T. Ide, S. Miura, A. Tamura and T. Ichinokawa, Surf. Sci. 194 (1988) L87.

[8] A.E. Dolbak, B.Z. Olshanetsky, S.I. Stenin, S.A. Teys and T.A. Gavrilova, Surf. Sci. 218 (1989) 37.

[9] A.J. van Bommel and F. Meyer, Surf. Sci. 8 (1967) 467.

[10] J.G. Clabes, Surf. Sci. 145 (1984) 87.

[11] D.R. Sparks, R.G. Chapman and N.S. Alvi, Appl. Phys. Lett. 49 (1986) 525.

[12] V.S. Smentkowski and J.T. Yates, Jr., J. Vac. Sci. Technol. A14 (1996) 260.

[13] Y.L. Yang, L.M. Struck, L.F. Sutcu and M.P. D'Evelyn, Thin Solid Films, 225 (1993) 203.

[14] G.D. Kubiak, M.T. Schulberg and R.H. Stulen, Surf. Sci. 277 (1992) 234.

[15] W.R. Wampler, J. Appl. Phys. 69 (1991) 3063.

[16] K.-H. Bornscheuer, S.R. Lucas, W.J. Choyke, W.D. Partlow and J.T. Yates, Jr., J. Vac. Sci. Technol. A11 (1993) 2822.

[17] D. Brennan and P.C. Fletcher, Proc. Roy. Soc. A, 250 (1959) 389.

[18] J.F. O'Hanlon, A User's Guide to Vacuum technology, Wiley-Interscience, Chapt. 5.

CHAPTER 3

THE ADSORPTION AND REACTIONS OF WATER ON Si(100)-2x1 AND Si(111)-7x7 SURFACES

3.1. INTRODUCTION.

Despite the technological importance of wet oxidation in device fabrication, many fundamental aspects of the adsorption and reactions of water on silicon surfaces have not previously been addressed. The transition between active oxidation (SiO desorption) and passive oxidation (growth of SiO_2) is determined by the surface temperature and the pressure of H_2O and by the rate constants for adsorption of H_2O (the sticking probability) and desorption of H_2 and SiO [1]. This chapter explores in detail the kinetics and mechanisms of D_2O adsorption on single crystal silicon surfaces and the subsequent desorption of D_2 and SiO using TPD.

The majority of the vast literature pertaining to water adsorption on silicon surfaces is concerned with the identity and characterisation of the adsorbed species. Although UPS spectra have been variously described in terms of molecular and dissociative adsorption, infrared spectroscopy has unequivocally identified surface Si-H and Si-OH groups following adsorption at 300 K [2, 3]. The dissociative mechanism is also supported by STM images which show that two dangling bonds are occupied simultaneously as the result of each chemisorption event [4] and that these occupied sites can be resolved into atomic features of different intensities [5]. However, at low coverages only dark, unresolved features can be imaged which, it is argued, are consistent with molecular chemisorption [5]. At surface temperatures in excess of about 500 K, the Si-OH decomposes rapidly to give Si-O-Si and further Si-H. This is evidenced by a doubling of the integrated infrared absorption due to the Si-H stretching vibration with concurrent loss of integrated absorption due to the O-H stretching vibration and the detection of fragments resulting from the concomitant appearance of Si-O-Si in SSIMS [6] and LITD [7] experiments.

3.2. COVERAGE CALIBRATION

The D_2O coverages on Si(100) and Si(111) have been determined from the integrated D_2 TPD peak areas. An absolute and independent calibration can be obtained by considering the adsorption of atomic deuterium. Initially, atomic deuterium adsorbs at dangling bond sites on Si(100) and Si(111) but can subsequently react with and break Si-Si bonds. The desorption of molecular deuterium from both Si(100) and Si(111) is characterised by two TPD peaks which are labelled β_1 and β_2 and represent desorption from monodeuteride and from dideuteride species respectively.

At 380±20 K, the saturation hydrogen atom coverage on Si(100) is characterised by an ordered 3x1 phase consisting of alternating rows of dihydride (HSiH) and monohydride (HSi-SiH) units [9, 10] whereas at temperatures in excess of 600 K a saturated monohydride phase can be prepared [9]. The uptake plots for atomic deuterium adsorption on Si(100) at 373 K and 650 K are presented in figure (1). By equating the saturation coverage at 650 K to 1 ML, the saturation coverage at 373 K is found to be 1.50±0.06 ML. A coverage of 1.33 ML is expected for a perfect lattice of alternating rows of dideuteride and monodeuteride units, however, adjacent rows of dideuteride units at domain boundaries [9] accounts for the present calibration. The TPD data also indicate that at 373 K, the β_2 peak first appears at a coverage of approximately 0.85 ML and is consistent with Boland's observation [9] that a saturated monohydride phase cannot be prepared at temperatures below 600 K.

There is no structural evidence available to suggest a convenient coverage calibration for hydrogen (or deuterium) adsorbed on Si(111). However, a saturation hydrogen atom coverage of 1.25±0.13 ML has been measured using nuclear reaction analysis [11]. The Si(111)-7x7 DAS reconstruction can accommodate a hydrogen coverage of 19/49 (approximately

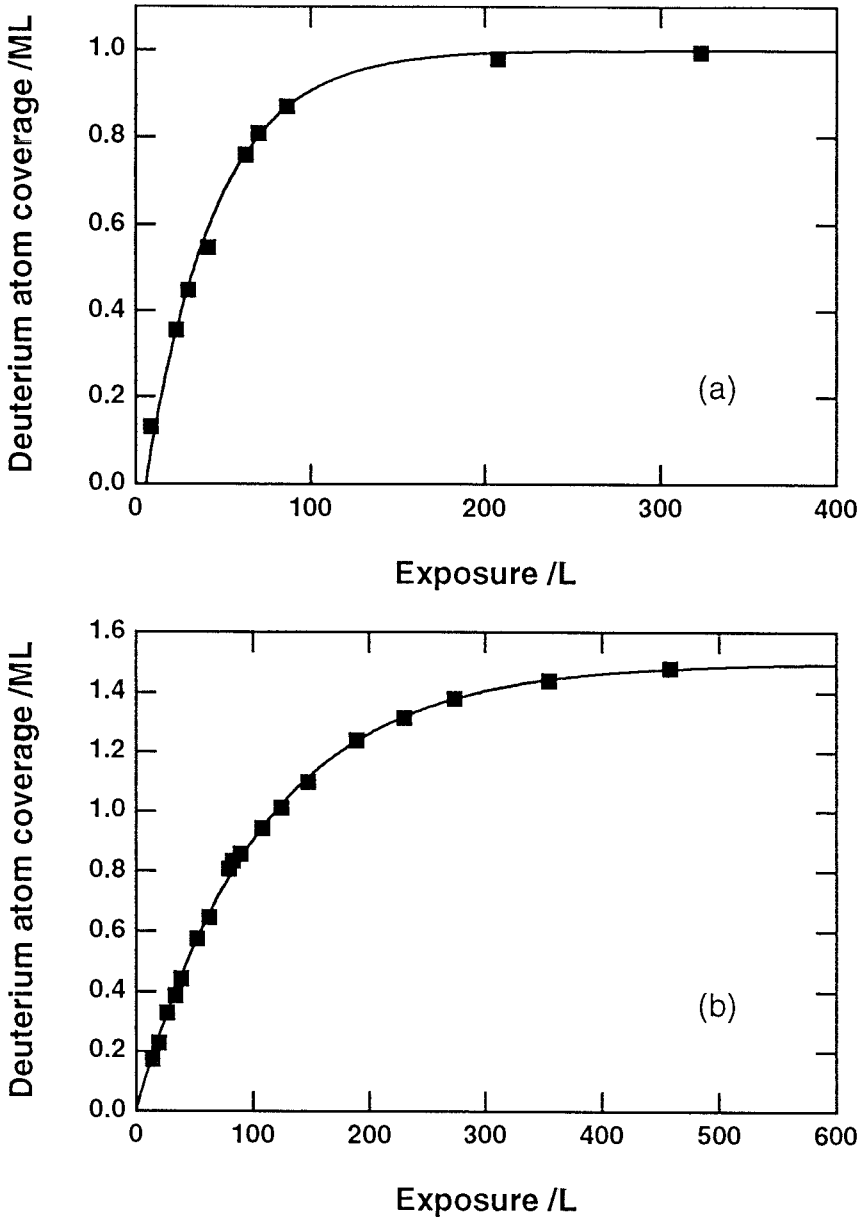

Figure (1). Deuterium atom uptake plots for Si(100) at (a) 650 K and (b) 373 K; experimental data (■) and spline through data (—).

0.39) ML at dangling bond sites. Scission of all adatom-rest atom bonds to give adatom trihydride and further rest atom monohydride species is equivalent to a maximum hydrogen coverage of 1.37 ML. However, at room temperature and above, the aggregation of adatoms into islands [12] competes with adatom trihydride formation and results in a lower saturation coverage. In figure (2), the uptake plot for deuterium atom adsorption on Si(111) at 373 K has been

scaled to give a saturation coverage of 1.25 ML. Using this calibration, the β_2 peak first appears at a coverage of approximately 0.42 ML. This is in good agreement with the expected onset of adatom dideuteride and trideuteride formation at a coverage of 0.39 ML after saturation of all the dangling bonds of the Si(111)-7x7 reconstruction.

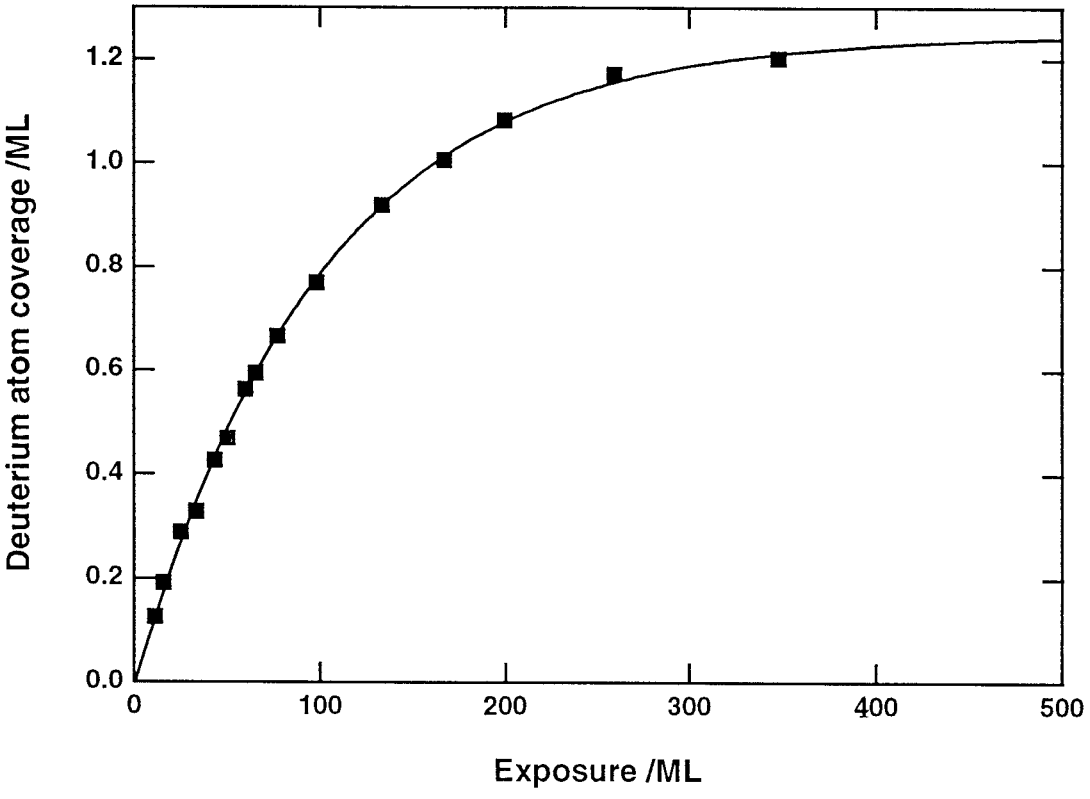

Figure (2). Deuterium atom uptake plot for Si(111) at 373 K; experimental data (■) and spline through data (—).

Figure (3) demonstrates that there is a linear correlation between the yields of D_2 and SiO from both Si(100) and Si(111). The SiO TPD peak areas and oxygen atom coverages have been calibrated by setting the gradients of these plots equal to 0.5 as required by the stoichiometry of D_2O. The extrapolated SiO TPD area when the D_2 TPD area is zero is approximately 0.01-0.02 ML and is the consequence of residual H_2O adsorption despite a base pressure of less than $2x10^{-10}$ mbar.

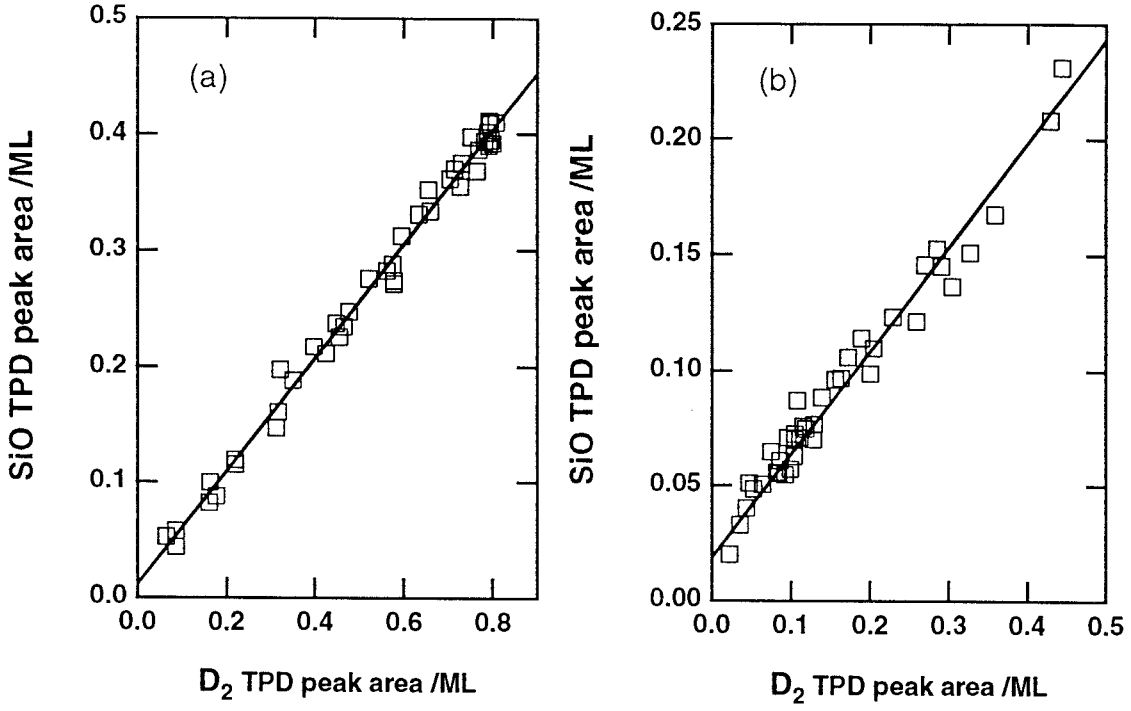

Figure (3). Correlation between D_2 and SiO TPD peak areas for (a) Si(100) and (b) Si(111); experimental data (□) and linear regression through data (—).

3.3. RESULTS AND DISCUSSION

A. Adsorption

The D_2O coverage on Si(100) is plotted as a function of exposure (at an average D_2O pressure of $1x10^{-8}$ mbar) in figures (4a) and (4b) for surface temperatures of 300 K and 423 K respectively. Absolute D_2O exposures were determined by adjusting the experimentally measured exposures to give an initial sticking probability on Si(100) of unity at 300 K in accord with quantitative UPS and other measurements [13-18]. Using the calibration described above, the saturation D_2O coverage is determined as 0.41±0.02 ML and corresponds to 0.18 ML of vacant sites if it is assumed that each D_2O molecule dissociates and reacts with two dangling bonds. The saturation coverage was measured for surface temperatures between 300 K and 523 K and was found to

be constant. Previously, a saturation coverage of 0.5 ML after exposure to 2 L of H_2O has been inferred from XPS data [18].

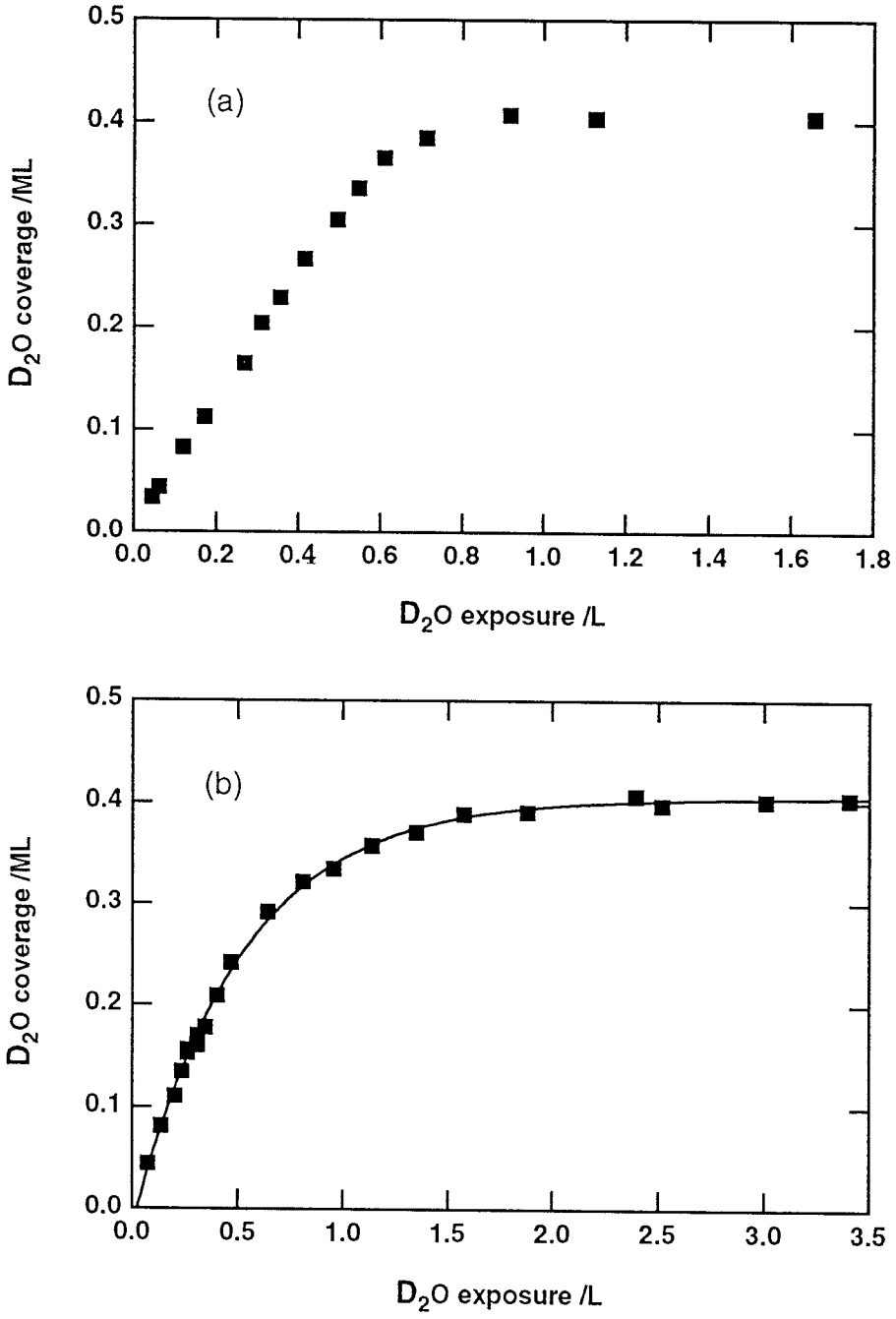

Figure (4). D_2O coverage on Si(100) as a function of exposure at (a) 300 K and (b) 423 K; experimental data (■) and fit to first order Langmuir kinetics (—).

At 300 K, the sticking probability is constant up to 95% of the saturation coverage and then decreases rapidly. This behaviour is characteristic of adsorption involving a long-lived, mobile extrinsic precursor which is able to migrate over occupied sites and eventually adsorb at vacant sites. A long-lived precursor is not unreasonable since a relatively strong interaction is expected between D_2O and Si-OD and Si-D through hydrogen bonding. STM images [4, 5] show that following H_2O adsorption at 300 K, occupied sites are clustered rather than distributed randomly which requires that an H_2O molecule incident at an unoccupied site can migrate to and dissociate at the perimeter of an island via a mobile intrinsic precursor state. At higher surface temperatures the life-time of the extrinsic precursor and hence the probability of chemisorption at vacant sites are reduced. In the limit that the rate of desorption from the extrinsic precursor state is much greater than the rate of migration to other sites, the coverage dependence of the sticking probability is determined by the site requirement for chemisorption (Langmuir adsorption kinetics). Since dissociative adsorption requires two adjacent sites, the coverage dependence of the sticking probability, s, might be expected to be described by

$$s = s_0(1 - \theta/\theta_s)^2 \tag{1}$$

where θ is the coverage, θ_s is the saturation coverage and s_o is the initial sticking probability. However, a single site is required by first order Langmuir adsorption kinetics and thus the sticking probability is given by

$$s = \frac{d\theta}{d\varepsilon} = s_o(1 - \theta/\theta_s) \tag{2}$$

where ε is the exposure. Integration of equation (2) gives

$$\theta/\theta_s = 1 - \exp(-s_0\varepsilon) \tag{3}$$

and hence a plot of $-\ln(1-\theta/\theta_s)$ against exposure is linear. At 423 K, the sticking probability decreases with coverage and surprisingly, the experimental data can be fitted to first order adsorption kinetics (using equation (3)) as shown in figure (4b). However, it is clear from figure (5) that adsorption at a surface temperature of 300 K cannot be described by first order Langmuir kinetics.

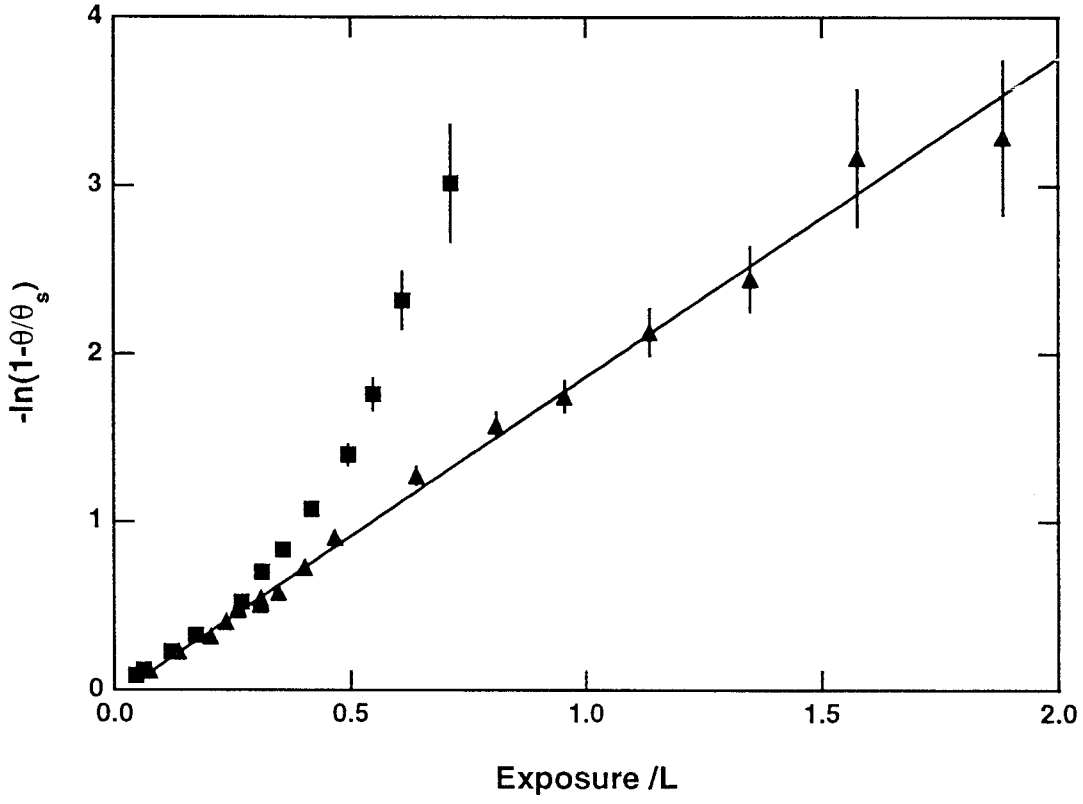

Figure (5). Plot of $-\ln(1-\theta/\theta_s)$ against exposure for surface temperatures of 300 K (■) and 423 K (▲).

First order Langmuir adsorption kinetics can only be reconciled with either a single or two correlated adsorption sites. STM images have shown that both dangling bonds of a single dimer or occasionally diagonally adjacent dangling bonds are occupied simultaneously as the result of each chemisorption event [4]. Furthermore, the absence of chemical splitting of the Si-H stretching mode [19] indicates that HSi-SiH, which would arise from random adsorption across two dimers, is not present in detectable

concentrations. Hence, each dimer can be considered as a single adsorption site or two correlated dangling bonds and it follows that adsorption is described by first order kinetics.

The initial sticking probability for D_2O adsorption on Si(100) was measured as a function of surface temperature by integration of D_2 TPD peak areas and is plotted in figure (6). The observed decrease in sticking probability with increasing surface temperature is characteristic of precursor mediated adsorption kinetics. The precursor model predicts that the surface temperature dependence of the initial sticking probability is given by

$$s_o(T) = \frac{\alpha}{1 + \upsilon_d/\upsilon_c \exp[-(E_d - E_c)/RT]} \qquad (4)$$

where α is the probability of trapping into the precursor state, υ_d and υ_c are the pre-exponential factors for desorption and chemisorption from the precursor state respectively and E_d and E_c are the corresponding activation energies [20]. The model assumes that α does not vary with surface temperature and that there is no contribution from a direct chemisorption channel. Weighted linear regression of $\ln(1/s_o - 1)$ against $1/T$ gives $E_d - E_c = 6.72 \pm 0.15$ kcal mol^{-1} and $\upsilon_d/\upsilon_c = 1120 \pm 140$ for D_2O adsorption on Si(100)-2x1. An initial sticking probability of unity at low temperatures requires that $\alpha = 1$. The fit to the experimental data obtained using these parameters is plotted in figure (6). The values of s_o, $E_d - E_c$ and υ_d/υ_c for some molecular adsorbates on Si(100) and Ge(100) are collated in table (1). The initial sticking probabilities are generally high and precursor mediated adsorption has been suggested in all cases. It can be seen that the value for $E_d - E_c$ obtained here is comparable to that for HCl adsorption on Ge(100) but is somewhat higher than the rest. This may be the result of a relatively strong dipole - induced dipole interaction between D_2O and Si(100) and between HCl and Ge(100) compared to the weak van der Waals interaction

of the molecular halogens and hydrocarbons with Si(100). However, the equilibrium bond lengths and bond energies for chemisorption and the orbital overlap between adsorbate and dimer may also determine the cross-over between precursor and chemisorption potential wells [26, 35]. It has been proposed that the chemisorption of hydrides on Si(100) and Ge(100) involves a four center transition state [33, 35]. Thus the nine degrees of freedom of D_2O in a precursor state which resembles a two dimensional gas, become eight vibrations and the reaction coordinate in the highly constrained transition state. It is not surprising, therefore, that the entropy of activation for chemisorption is large and negative and hence that the pre-exponential factor for desorption from the precursor state greatly exceeds that for chemisorption.

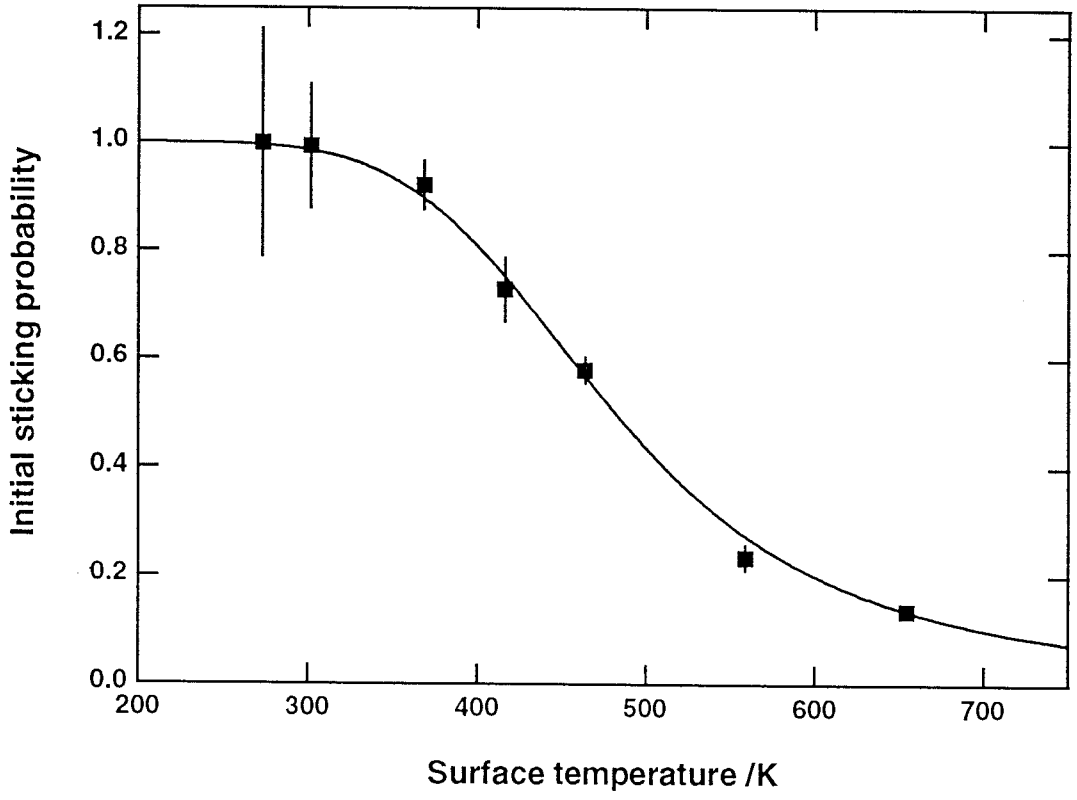

Figure (6). Temperature dependence of the initial sticking probability of D_2O on Si(100); experimental data with 90 % confidence limits (■) and fit to precursor model (—).

Table (1). Comparison of saturation coverages and adsorption kinetics for some molecular adsorbates on Si(100) and Ge(100).

Substrate	Adsorbate	s_0 (surface temperature)	Saturation coverage /ML	E_d-E_c /kcal mol^{-1}	υ_d/υ_c	Reference
Si(100)	H_2O	1 (350 K)	0.5 0.41±0.02 0.2-0.3	6.7±0.2	1120±140	[13] This work [21]
Si(100)	H_2S	1(<550 K)	0.5			[13]
Si(100)	NH_3	1 (120 K)	0.58±0.18 0.25			[22] [23]
Si(100)	CH_3I	1 (273 K)	0.43±0.04			[24]
Si(100)	Cl_2	1 (100 K) 0.54 (300 K)	0.44 0.5±0.05	0.7±0.1	5	[25] [26] [27]
Si(100)	F_2	0.46 (<600 K)				[28]
Si(100)	Br_2	0.55 (300 K)		0.7±0.2		[26]
Si(100)	I_2	0.80 (300 K)		2.5±0.7	70±10	[26]
Si(100)	C_2H_2	1 (105 K)	0.42 0.37	1.9±0.6	19±10	[29] [30]
Si(100)	C_2H_4	1 (105 K)	0.4±0.03 0.37	2.9	27	[31] [30]
Si(100)	HCl		0.25			[32]
Ge(100)	H_2O	0.28 (173 K)				[33]
Ge(100)	H_2S	0.23 (<373 K) 0.2 (300 K)				[33] [34]
Ge(100)	HCl	0.6 (270 K)		6.3	70000	[35]
Ge(100)	HBr	0.7 (<400 K)				[35]

Adsorption on Si(100) is apparently complete at a coverage of 0.41 ML. The remaining 0.18 ML of unoccupied sites can be identified with isolated (unpaired) dangling bonds which are characterised by bright spots in both occupied and unoccupied state STM images [4, 36]. In figure (3) of reference [4] these bright spots can be clearly distinguished on the lower terrace and are easily counted. If each bright spot represents a single unoccupied dangling bond then the coverage of H_2O is estimated as 0.42 ML in excellent agreement with the present result. These isolated dangling bonds are presumably the consequence of adsorption across diagonally adjacent dangling bonds. The saturation coverages of some molecular adsorbates, all of which require two adjacent dangling bond sites for adsorption, are given in table (1). Saturation at less than 0.5 ML has been attributed to defect sites [24, 29, 31] despite an intrinsic defect density on Si(100) of 1% or less [4, 5, 36, 37]. However, it seems more reasonable to propose that in many, if not all cases, isolated dangling bonds remain as a result of adsorption across two adjacent dimers.

The D_2O coverage on Si(111) at 373 K is plotted as a function of exposure (at average D_2O pressures between $1x10^{-7}$ and $1x10^{-6}$ mbar) in figure (7). Adsorption is initially rapid but becomes very much slower for coverages in excess of 0.1 ML. Experiments with the main chamber ion gauge switched on demonstrated that dissociation of D_2O at the hot filament and the subsequent adsorption of D· or OD· is significant when the sticking probability for molecular water is low (see figure (7)). The saturation coverage of D_2O on Si(111)-7x7 is measured as 0.22±0.02 ML and corresponds to saturation of all the dangling bonds of the 7x7 DAS reconstruction if it is assumed that each D_2O molecule dissociates and occupies two such sites. This is consistent with the observation [38] that the 7x7 LEED pattern remains after large exposures although the spot intensities are decreased and suggests that the Si-Si bonds are not broken. The saturation coverages of NH_3 [39, 40], PH_3 [41] and H_2S [42], all of

which require two sites for dissociative adsorption are also approximately 0.2 ML.

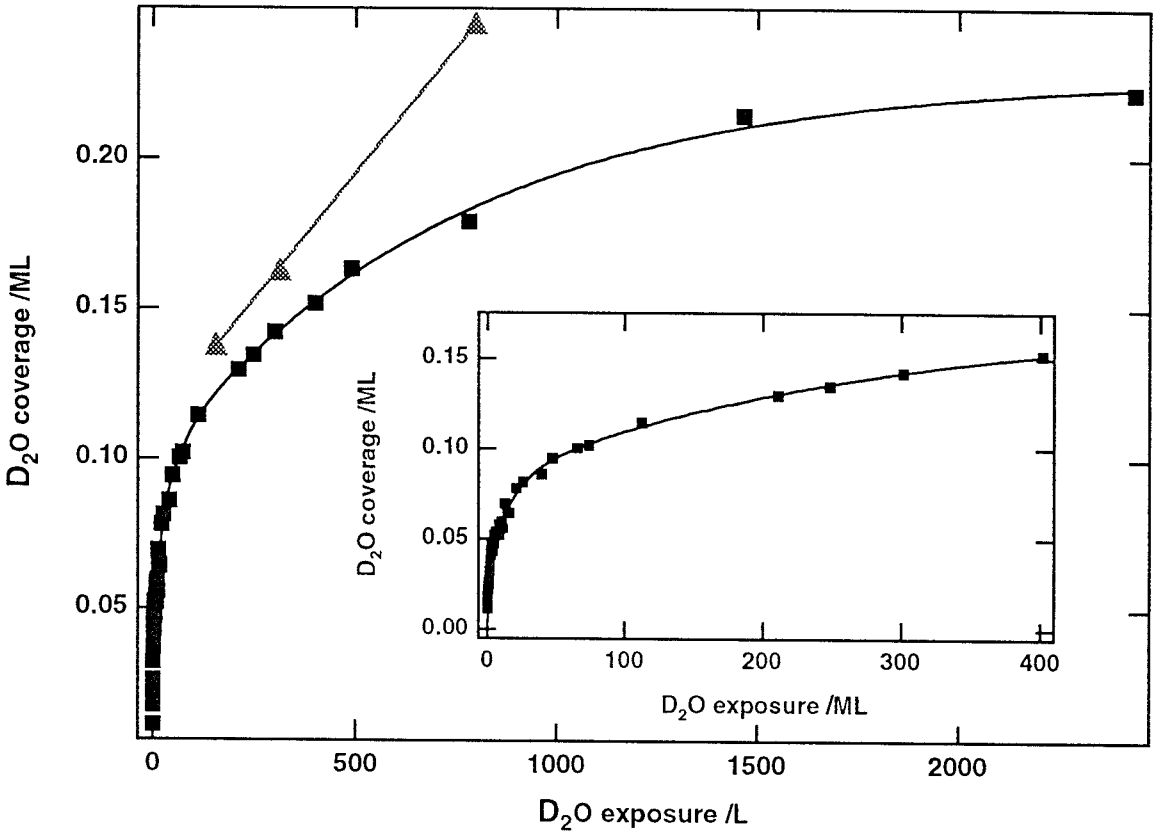

Figure (7). D_2O coverage on Si(111) at 373 K as a function of exposure; ion gauge off (■), ion gauge on (▲), spline through data (—).

Dissociative adsorption is most likely to involve adatom - rest atom dangling bond pairs which are separated by approximately 4.6 Å [43]. The closest adatom - adatom and rest atom - rest atom dangling bond pairs are separated by approximately 6.7 Å and 19.2 Å respectively. An STM "reaction map" [44] has shown that twice as many center adatoms as corner adatoms react (the total number of reacted adatoms is approximately 0.1 ML) since each center adatom has two rest atom neighbours whereas each corner adatom has only one rest atom neighbour. Similarly, it has been proposed that C_2H_2 adsorbs

across adjacent adatom - rest atom dangling bond pairs but without dissociation such that twice as many center adatoms as corner adatoms and only three adatoms in each triangular sub unit (corresponding to the number of rest atoms) are observed to react [45]. Saturation of all the adatom - rest atom pairs (twelve of the nineteen dangling bonds) corresponds to a D_2O coverage of 0.12 ML. The inset in figure (7) indicates that the initially rapid uptake is complete by about 0.1 ML which approximately correlates with saturation of all the adatom - rest atom pairs. Reaction at the remaining 0.14 ML of isolated dangling bonds is characterised by a very much lower sticking probability which is reasonable since these sites will be separated by at least 6.7 Å. A saturation coverage of approximately 0.4 ML of H_2O has been obtained by George *et al.* [7] but this value seems unlikely given the evidence presented above.

Despite the very large exposures required to achieve saturation, the initial sticking probability on Si(111)-7x7 is high and measured as 0.23±0.08. Since this is associated with adsorption across an adatom - rest atom pair, it is not surprising to find that occasionally adsorption on Si(100) involves diagonally adjacent dangling bonds which are also separated by about 4.6 Å, although the loss of two π-bonds rather than one makes this thermodynamically less favourable. The initial rapid uptake on Si(111)-7x7, Si(100)-2x1 and other reconstructions has been reported previously and an initial sticking probability of unity has been established for Si(100)-2x1 at room temperature [13-18]. Subsequently adsorption is very much slower on all planes including Si(100)-2x1. Indeed, it is found that although the initial rapid adsorption on Si(100) is complete after an exposure of less than 1 L, saturation is not complete by 1000 L [14]. The adsorption of D_2O on Si(100)-2x1 and Si(111)-7x7 has been described and interpreted above in terms of adsorption at adjacent dangling bond sites. Clearly, saturation at 0.5 ML for Si(100)-2x1 and at 0.2 ML for Si(111)-7x7 can only be achieved by adsorption at the remaining isolated

dangling bonds and it is entirely reasonable to find that this is associated with a low sticking probability. Other adsorbates behave similarly; the adsorption of both Cl_2 [25, 27] and NH_3 [22] on Si(100)-2x1 is initially rapid but is followed by slow adsorption until saturation.

B. Desorption

Representative TPD data for the two desorption products, D_2 and SiO, are presented in figure (8) for both Si(100) and Si(111). Qualitatively similar data for D_2 desorption from Si(100) and H_2 and SiO desorption from Si(111) have been reported elsewhere [10, 11]. The D_2 TPD peaks are similar to the β_1 peaks which are characteristic of deuterium desorption from Si(100) and Si(111) [46, 47] except that a small and coverage independent fraction of the deuterium is retained to higher temperatures. For Si(100) this fraction is about 10% of the total peak area and appears as a shoulder whereas for Si(111) it is less clearly resolved but represents approximately 15% of the total peak area and contributes to a considerable broadening of the peak. The SiO TPD data are similar to those resulting from oxygen adsorption on Si(100) and Si(111) [48, 49]. The shoulder observed at high temperatures on Si(111) is believed to be a consequence of the complex desorption kinetics [51]. These data have a poorer signal-to-noise ratio and are superimposed on a relatively large background due to the coincidence of the SiO^+ and ambient CO_2^+ signals at m/e=44 and the lower sensitivity of the mass spectrometer to SiO compared with D_2.

The peak temperature of the D_2 TPD peak from both Si(100) and Si(111) is dependent on the initial water coverage; this has not been reported previously. In figures (9a) and (10) the D_2TPD peak temperature is plotted as a function of initial water coverage on Si(100) and Si(111) respectively and compared with the expected peak temperature [50] for an equivalent coverage of atomic deuterium only. The equivalent coverage of atomic deuterium corresponds to

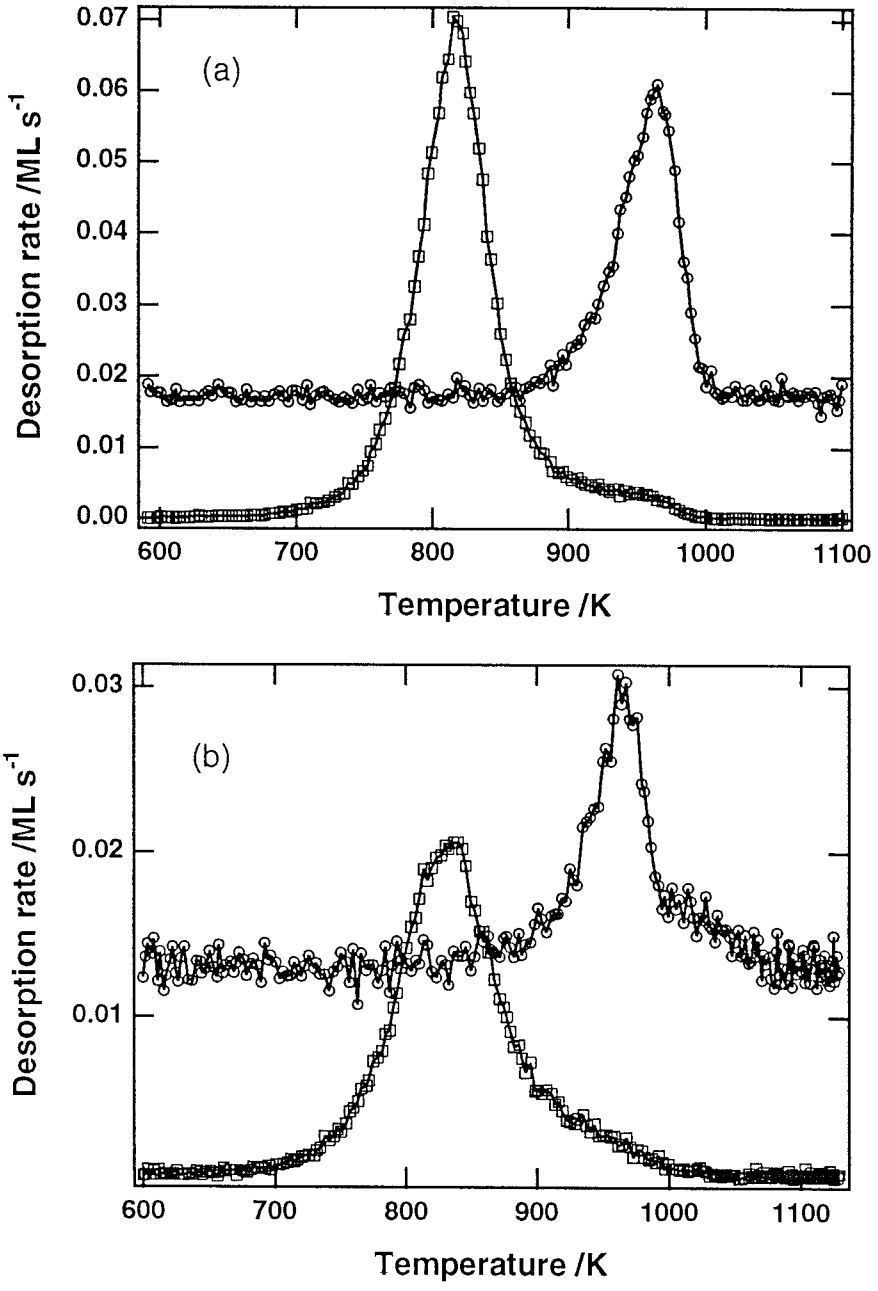

Figure (8). D_2(□) and SiO (○) TPD data for initial D_2O coverages of (a) 0.3 ML on Si(100) and (b) 0.15 ML on Si(111).

90 % of twice the initial water coverage in figure (9a) and to 85% of twice the initial water coverage in figure (10). It is necessary to take into account the small amount of ambient H_2O adsorption (0.01-0.02 ML) since this results in desorption of H_2, HD and D_2 but only the D_2^+ signal (and any overlap with the HD^+ signal) is detected. This is only of any consequence at very low D_2O

coverages and in particular at the lowest measured coverages on Si(111). Kinetic models have been developed to describe the desorption of deuterium via the β_1 channel from both Si(100) and Si(111) [46, 47] and can be applied to the present data if it is assumed that the same desorption mechanisms are involved.

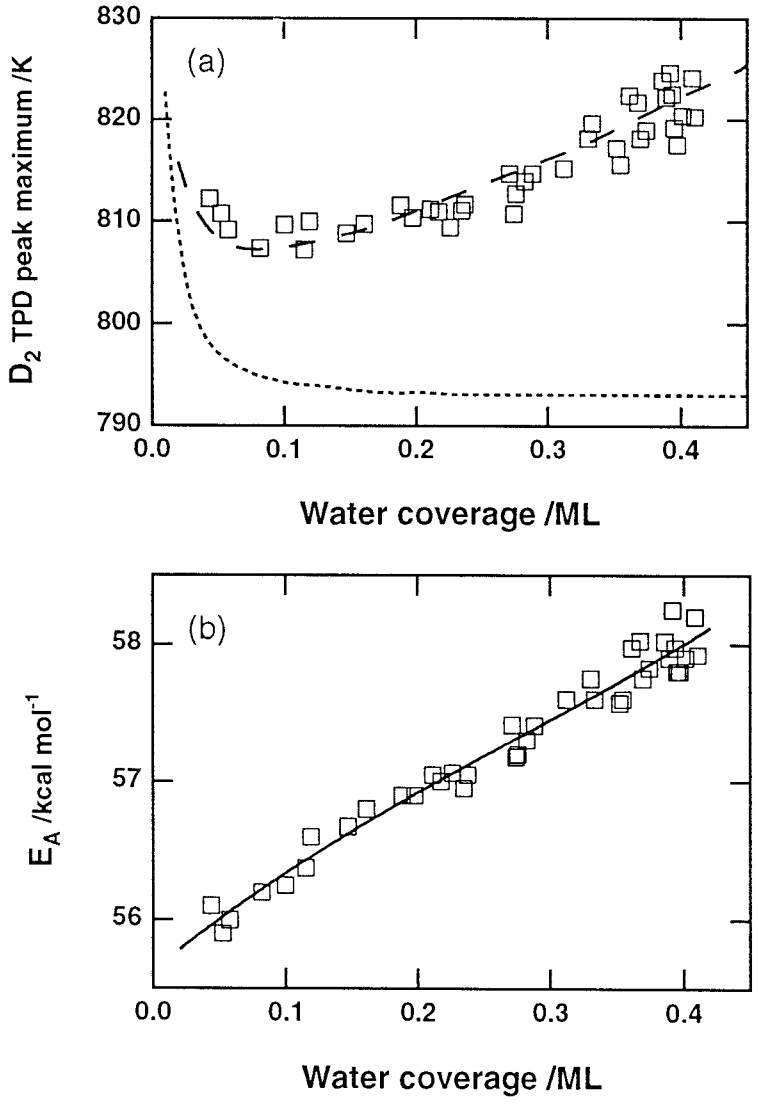

Figure (9). (a) D_2 TPD peak temperature and (b) activation energy for desorption as a function of initial water coverage on Si(100); experimental data (□), regression through data (—), peak temperatures for atomic deuterium coverage only (---) and peak maxima calculated using regressed activation energies (— —).

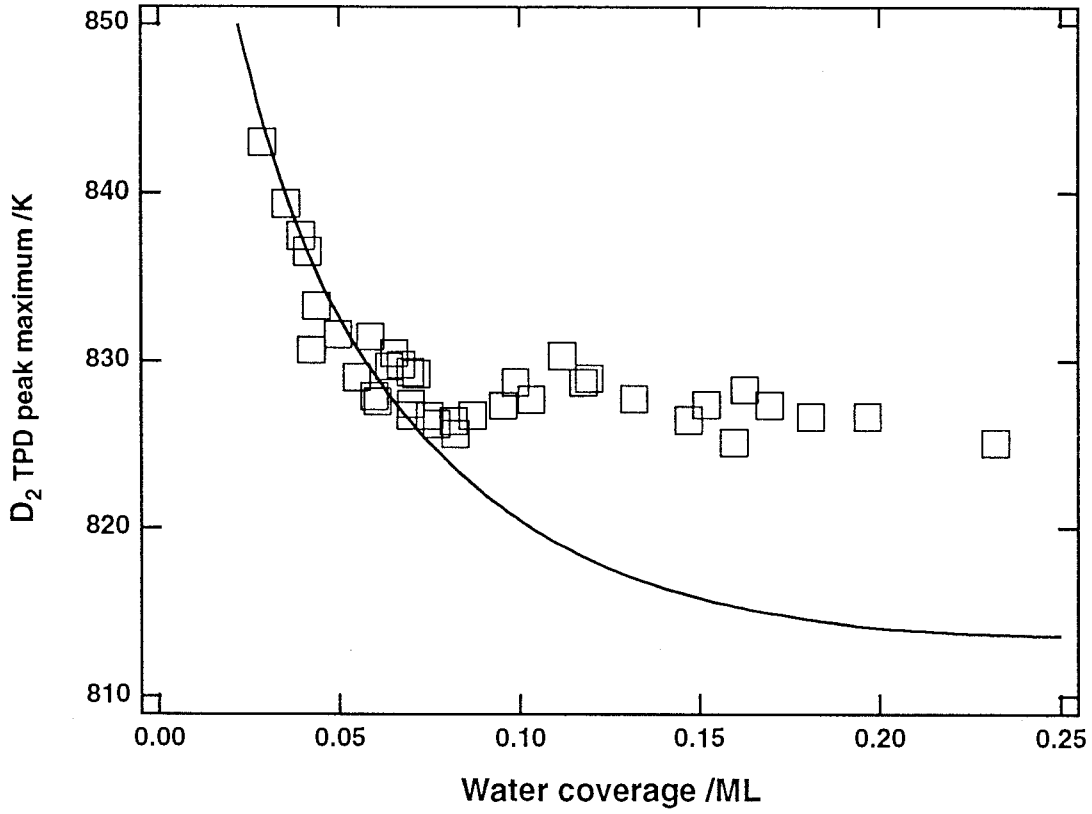

Figure (10). D_2 TPD peak temperature as a function of initial water coverage on Si(111); experimental data (□), expected peak temperature for an equivalent coverage of atomic deuterium only (—).

It has been proposed that unoccupied dimers (Si=Si), singly occupied dimers (D-Si-Si·) and doubly occupied dimers (D-Si-Si-D) are in dynamic equilibrium [51] on Si(100).

$$\text{D-Si-Si-D} + \text{Si=Si} \rightleftharpoons 2\ \text{D-Si-Si}\cdot \tag{5}$$

The equilibrium coverage of doubly occupied dimers can be obtained from a simple lattice gas model [46] in which the enthalpy for the forward reaction is approximately equal to the π-bond energy. If it is assumed that desorption of molecular deuterium occurs exclusively from doubly occupied dimers, then the rate of change of fractional coverage can be written as

$$-\frac{d\Theta}{dt} = \nu \times \theta_{11} \times \exp(-E_A / kT) \tag{6}$$

where Θ is the total coverage, θ_{11} is the coverage of doubly occupied dimers, υ is the pre-exponential factor and E_A is the activation energy for desorption. The Si(100) D_2 TPD data were fitted using this model and an activation energy for desorption that was allowed to vary with initial water coverage. A π-bond energy of 4 kcal mol^{-1} and a pre-exponential factor of $1x10^{15}$ s^{-1} were required to fit the peaks and to give the appropriate peak temperatures at low coverages. The activation energy for desorption is approximately 56 kcal mol^{-1} at low initial water coverages and for coverages of deuterium atoms only [50]. However, the activation energy for desorption increases almost linearly with increasing initial water coverage to a maximum of about 58 kcal mol^{-1} as shown in figure (9b). A typical fit is shown in figure (11) and clearly demonstrates that the model described above is appropriate for the 90% of adsorbed deuterium represented by the main peak.

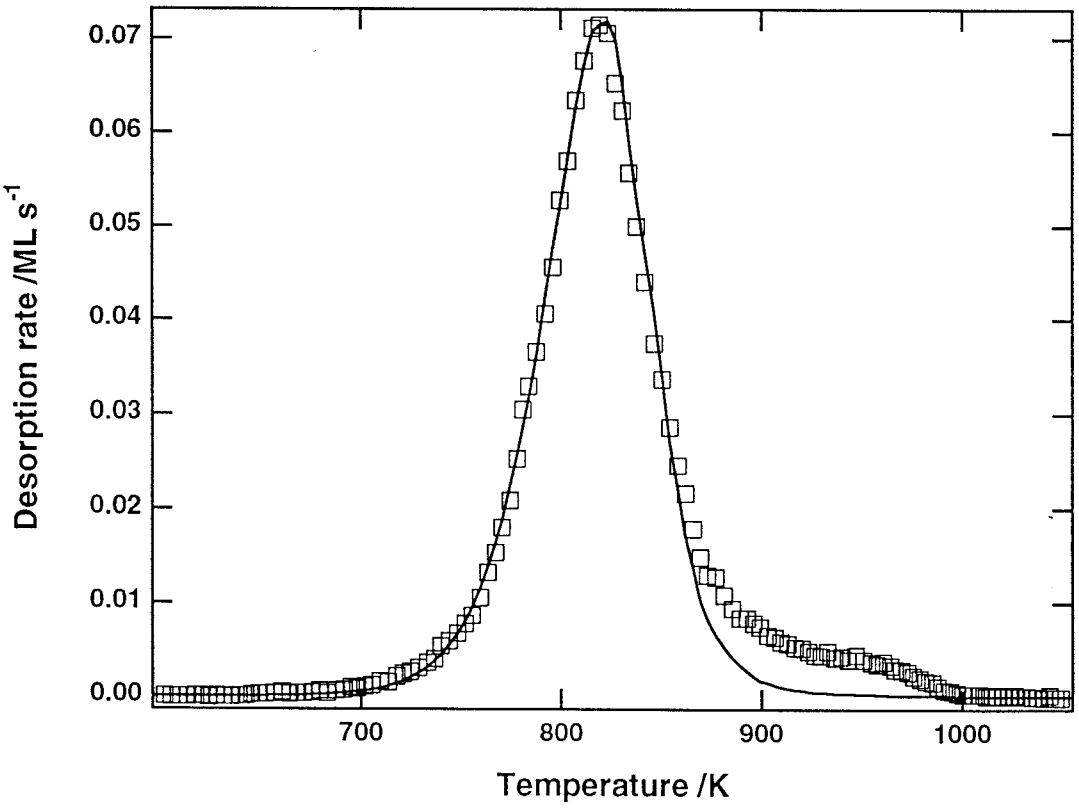

Figure (11). D_2 TPD data for an initial D_2O coverage of 0.29 ML on Si(100) (□) and fit using model described in text for an equivalent deuterium atom coverage of 0.52 ML (—).

For Si(111), it has been proposed that two second order desorption channels, designated AA and AB, constitute the β_1 TPD peak and represent recombinative desorption from adjacent A sites and adjacent A and B sites respectively [47]. It is required that adsorption of deuterium atoms at A sites is energetically more favourable than adsorption at B sites by an amount denoted as ΔE. The equilibrium coverages of deuterium adsorbed at A sites, θ_A, and at B sites, θ_B, can be calculated for a given value of ΔE and as a function of temperature since diffusion is much faster than desorption [52]. Hence, the rate of desorption is then given by

$$-N\frac{d\Theta}{dt} = \nu_{AA}\theta_A^2 \exp(-E_{AA}/RT) + \nu_{AB}\theta_A\theta_B \exp(-E_{AB}/RT) \qquad (7)$$

where N is the number of silicon atoms in one monolayer, Θ is the total deuterium atom coverage, υ_{AA} and υ_{AB} are pre-exponential factors and E_{AA} and E_{AB} are activation energies for desorption. STM images [12] have shown that low hydrogen atom coverages can be accommodated at the dangling bond sites without disruption of the 7x7 reconstruction. Hence, for coverages less than the dangling bond density, the A and B sites have been correlated with rest atom and adatom sites respectively which implies that of the 19/49 ML of sites available, 7/49 ML are A sites and 12/49 ML are B sites. At low coverages the AA desorption channel dominates but at higher coverages the AB channel has an increasingly important influence on both the peak shape and peak temperature [47].

In previous studies, the appropriate values of υ_{AA}, υ_{AB}, E_{AA}, E_{AB} and ΔE have been established as 2×10^{15} s^{-1}, 1×10^{15} s^{-1}, 56.4 kcal mol^{-1}, 57.0 kcal mol^{-1} and 2.5 kcal mol^{-1} respectively by simulation of the TPD data [47, 50]. However, only the leading edge of the TPD peak is available in the present study (since there is considerable broadening) and hence it proved impossible to extract E_{AA} and E_{AB} as a function of initial water coverage. The experimental peak temperatures

plotted in figure (10) are in good agreement with the model described above for initial water coverages less than 0.07 ML. Thus it can be concluded that the AA route is largely unaffected by the presence of oxygen at low initial water coverages. At higher coverages, the expected and experimental peak temperatures deviate, presumably as a consequence of the effect of oxygen atoms on the AB desorption channel in particular and the AA desorption channel to a lesser extent. It is noted here that adatom back bonds react with chlorine [53], atomic hydrogen [12] and molecular oxygen [44, 54] but rest atom back bonds do not. Thus it is reasonable to suppose that the insertion of oxygen atoms into the surface is associated mainly with the adatoms whereas rest atoms, and hence the AA desorption channel, are affected less.

The reaction of molecular oxygen with Si(111) and Si(100) is characterised by four chemically shifted features in Si $2p_{3/2}$ X-ray photoelectron spectra which have been assigned to surface and sub-surface silicon atoms bonded to one (SiO), two (SiO_2), three (SiO_3) and four (SiO_4) oxygen atoms respectively [55-57]. Annealing at and above 773 K causes a considerable increase in the concentration of SiO_3 and SiO_4 units for both surfaces and regardless of coverage with a concomitant decrease in the concentration of SiO units. Thermal decomposition of Si-OH to Si-H and Si-O-Si occurs at surface temperatures above 300 K but is rapid at temperatures in excess of 500 K [6]. Consequently, Si $2p_{3/2}$ features corresponding to SiO and SiO_2 develop after annealing at 640 K whereas SiO_3 and SiO_4 units appear after annealing to 870 K. The insertion of oxygen into silicon - silicon bonds is most likely to involve the strained dimer bonds and the disappearance of the 2x1 LEED pattern above 500 K [58] supports this assumption. In addition to the Si $2p_{3/2}$ features resulting from Si-O bonding, surface core level shifts, which are a characteristic of the clean surface, are also observed after annealing to 870 K. This suggests that

oxygen penetrates the lattice and is incorporated into the sub - surface bonding prior to desorption.

Infrared spectroscopy [19, 59-63] and EELS [16, 38, 64-67] identify the dissociative adsorption of H_2O on Si(100) and Si(111) at 300 K with a single Si-H stretching mode at 2073 - 2097 cm^{-1}. The Si-H stretching mode is found at 2087 cm^{-1} by transmission infrared spectroscopy of H_2O adsorbed on porous silicon but is replaced by four new features at 2102, 2119, 2176 and 2268 cm^{-1} after annealing to 640 K [60]. These absorptions have been assigned to Si-H stretching vibrations with no oxygen nearest neighbours (H-Si) and one (H-SiO), two (H-SiO_2), and three (H-SiO_3) oxygen nearest neighbours respectively by comparison with molecular analogues. Similarly, internal reflection infrared spectroscopy can resolve a number of Si-H absorptions after annealing H_2O adsorbed on Si(100) at only 420 K [19, 61]. Some typical Si-H stretching frequencies for molecular compounds are plotted in figure (12). Hence the Si-H stretching frequency is increased a little by interaction with distant oxygen atoms and one oxygen nearest neighbour but is shifted much further by two and three oxygen nearest neighbours. Four Si-H stretching modes are observed at 2090, 2155, 2220 and 2285 cm^{-1} by EELS after atomic hydrogen adsorption on Si(100) pre-exposed to molecular oxygen and correspond to H-Si, H-SiO, H-SiO_2 and H-SiO_3 respectively [75, 76]. As the surface temperature is increased most of the hydrogen desorbs between 700 and 850 K from H-Si and H-SiO but some is retained as H-SiO_2 and H-SiO_3 and desorbs at about 1050 K. Moreover, an increase in the integrated intensity due to H-SiO_2 and H-SiO_3 suggests that hydrogen diffuses from H-Si and H-SiO to SiO_2 and SiO_3 sites between 600 and 800 K.

The evidence described above suggests that aggregation of oxygen as SiO_2, SiO_3 and SiO_4 occurs prior to and during the desorption of molecular

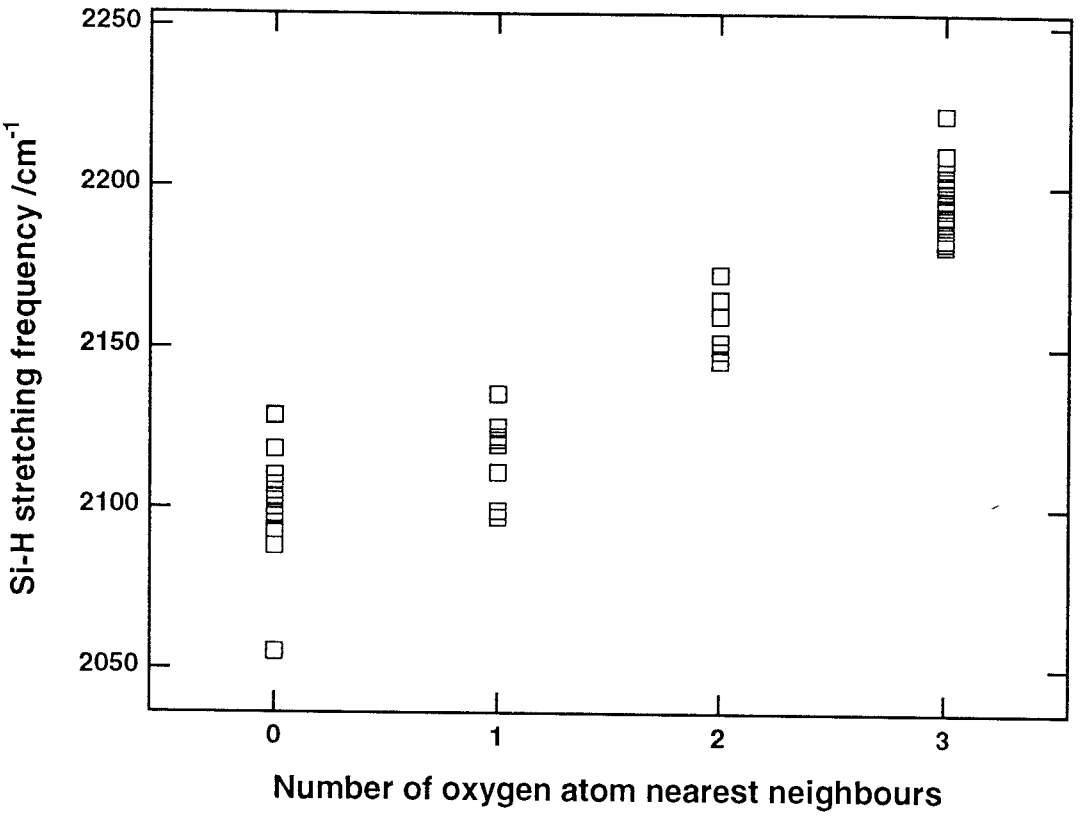

Figure (12). The effect of oxygen nearest neighbours on the Si-H stretching frequency in molecular compounds [68-74]. Only R_3Si-H, $(RO)R_2Si$-H, $(RO)_2RSi$-H and $(RO)_3Si$-H where R are saturated alkyl or silylalkyl groups are considered.

deuterium. The number of SiO_2 and SiO_3 surface sites will be smaller than the deuterium atom coverage and hence most deuterium will desorb from surface silicon atoms with no oxygen nearest neighbours. It is not surprising, therefore, that most of the adsorbed deuterium desorbs via the β_1 channel. However, the data presented in figures (9b) and (10) indicate that the activation energy for desorption from such sites increases with oxygen atom coverage. This is probably a consequence of an extended and cumulative electronic interaction [77] between Si-D bonds and oxygen atoms which may be third and fifth nearest neighbours. It has been suggested that the shoulder on the D_2 peak from Si(100) is the result of hydrogen bonding between Si-D and oxygen defect sites [7]. In view of the evidence regarding Si-H stretching frequencies discussed above, it is proposed here that deuterium adsorbed at SiO_2 and SiO_3 sites is

considerably more strongly bound than deuterium adsorbed at surface silicon atoms with only one oxygen nearest neighbour or with distant oxygen neighbours and is therefore retained to higher temperatures on both Si(100) and Si(111).

In their detailed studies of oxygen adsorbed on Si(100), Engel *et al.* report that desorption of SiO is heterogeneous for coverages as low as 0.3 ML and may occur at the perimeters of shrinking oxide islands or expanding voids [48, 49]. They conclude that desorption can be described by first order kinetics at coverages less than 0.3 ML but that the kinetics are more complex at higher coverages. The SiO TPD peak temperature is plotted as a function of initial D_2O coverage in figure (13). These data are in agreement with the results of Engel *et al.* [49] which show that the peak temperature increased rapidly with increasing initial oxygen coverage below about O.1 ML but more slowly at higher coverages [49]. The absolute peak temperatures are similar but cannot be compared in detail because of the different heating rates used. Some representative SiO TPD data are plotted in figure (14) for a range of initial D_2O coverages. These data can be simulated and are fitted well by first order desorption kinetics with a pre-exponential factor of 2.5×10^{17} s^{-1} and an activation energy that increases with initial D_2O coverage from 75 kcal mol^{-1} at 0.05 ML to 80 kcal mol^{-1} at 0.4 ML as shown in figure (14). If heterogeneous desorption occurs in this case also, it may be more appropriate to vary the pre-exponential factor rather than (or as well as) the activation energy. Reasonable but somewhat less satisfactory fits were obtained with a fixed activation energy of 75 kcal mol^{-1} and a pre-exponential factor that decreases with initial D_2O coverage from 2.5×10^{17} s^{-1} at 0.05 ML to 2.5×10^{16} s^{-1} at 0.4 ML. Regardless of which combination of pre-exponential factor and activation energy is chosen to represent the data, the overall rate constants are very similar to those reported by Engel *et al.* [49] for SiO desorption in the absence of adsorbed deuterium.

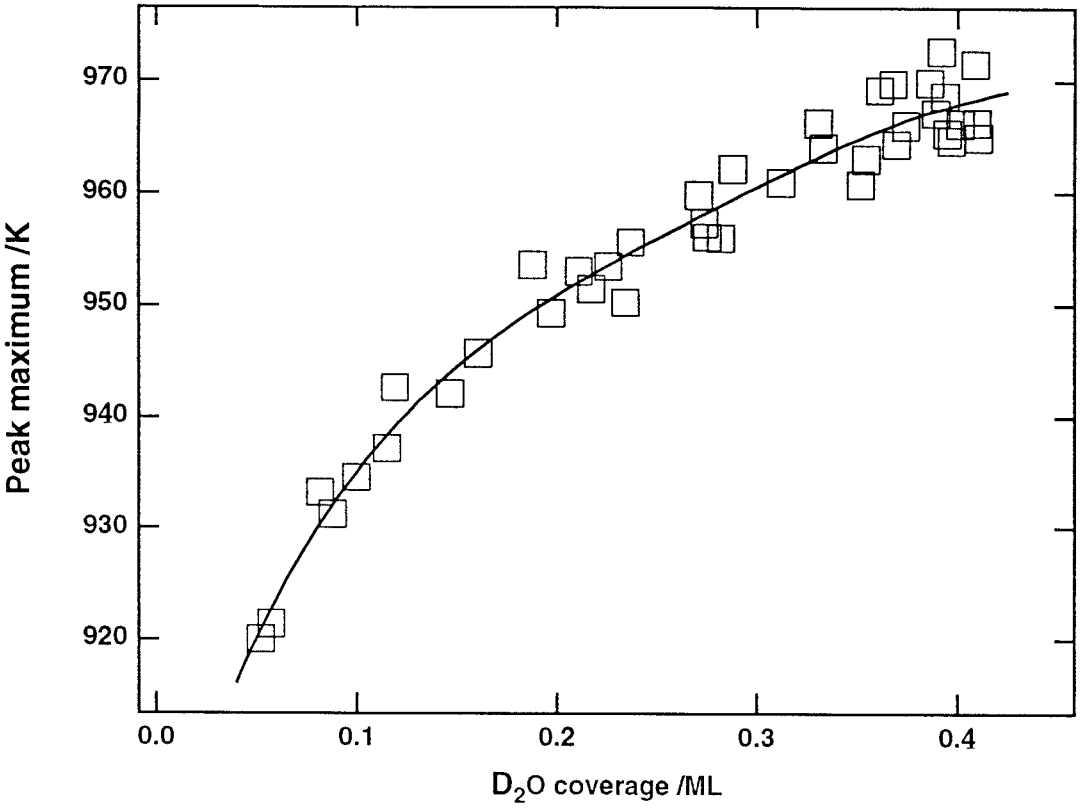

Figure (13). SiO TPD peak temperatures as a function of D_2O coverage on Si(100); experimental data (□) and regression through data (—).

Since first order kinetics seem appropriate, it follows that the most likely transition state would result from the breaking of a single surface - SiO bond so liberating SiO. The measured pre-exponential factor is two orders of magnitude higher than that found and justified for D_2 desorption [47] but can be rationalized solely on transition state theory arguments. In order to do this, it is necessary to consider the six vibrational degrees of freedom of SiO in the surface that become the reaction coordinate and five vibrational/internal rotational modes in the transition state leading to the gaseous SiO product. To a first approximation, the Si=O stretching vibration can be considered as being unchanged in going from the reactant to the transition state and hence contributes zero to the entropy of activation ($\Delta S^{\ddagger}$). If the transition state is then considered to consist of three bending modes (υ = 100 cm^{-1}) and one free

internal rotation of the O atom about a single Si - surface bond (S^0 = 9.2 cal K^{-1} mol^{-1} at 1000 K) and if the five remaining stretching/deformation modes of the reactant SiO group are assigned a geometric mean frequency of 700 cm^{-1}, a calculated frequency factor, $(ekT/h).\exp(\Delta S^{\ddagger}/R)$, equal to $2x10^{17}$ s^{-1} for a temperature of 1000 K results. Hence, in spite of its seemingly high value, the pre-exponential factor is not unreasonable.

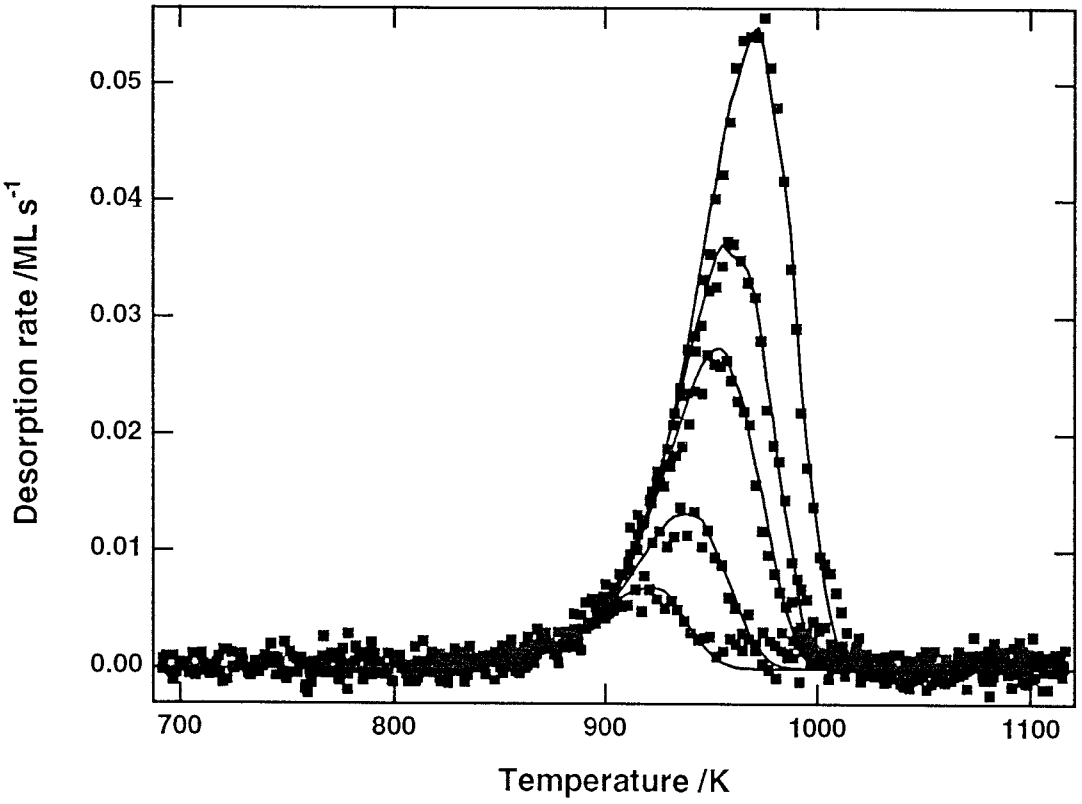

Figure (14). SiO TPD from Si(100) for initial D_2O coverages of 0.05, 0.09, 0.2, 0.28 and 0.4 ML; experimental data (■) and fit to first order desorption kinetics (—). The background signal due to CO_2^+ has been subtracted.

C. Reaction with atomic deuterium

The coverages of deuterium and oxygen on Si(100) have been measured after reaction of an initial D_2O coverage of 0.41 ML (apparent saturation) with atomic deuterium at 300 K. In figure (15), the oxygen atom coverage, as determined by the SiO TPD peak area, is plotted as a function of deuterium

atom exposure. Surprisingly, it was found that some (approximately 17% or 0.07 ML) but not all of the surface oxygen could be removed. However, if the surface was annealed at 600 K for 10 minutes after exposure to D_2O at 300 K, none of the oxygen could be removed. A total hydrogen coverage of about 1.5 ML was achieved at a surface temperature of 300 K, regardless of whether or not the surface had been annealed. The initial sticking probability for atomic deuterium is approximately five times greater than the initial reaction probability for loss of oxygen. Exposure to 140 L of undissociated molecular deuterium did not result in any reaction on the surface.

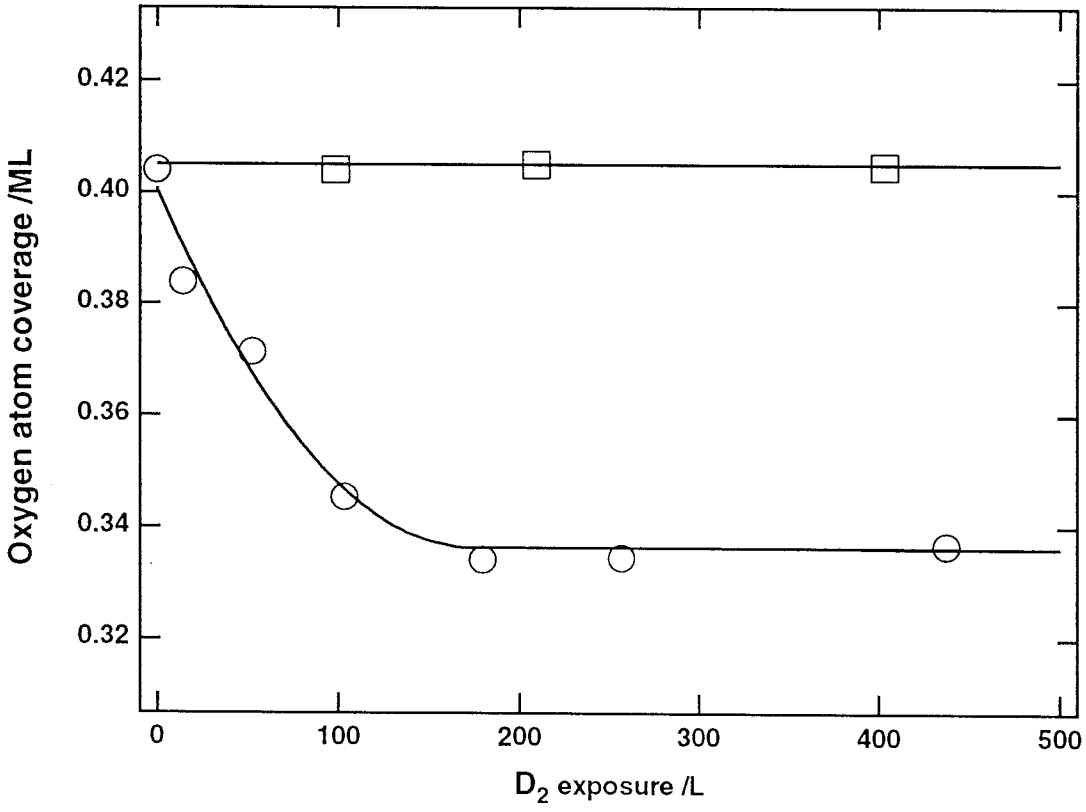

Figure (15). Reaction of surface oxygen with atomic deuterium; no annealing (○) annealed at 600K for 10 minutes prior to reaction with atomic deuterium at 300 K (□).

Atomic hydrogen or deuterium is known to react with a number of adsorbates on silicon surfaces [78-86]. Chabal has noted (without giving details) that the vibrational spectrum of Si(100) exposed to 2L of H_2O is modified

following reaction with atomic hydrogen [62]. Recently, Ikeda *et al.* [86] have measured EELS intensities during the reaction at room temperature of H_2O adsorbed on Si(100) with atomic hydrogen. Their data show that exposure to atomic hydrogen induces the decomposition of Si-OH as evidenced by an increase in intensity of the signal due to Si-O-Si and led them to propose reaction (8).

$$\text{Si-Si-OH} + \text{H}\cdot \rightarrow \text{Si-O-Si}\cdot + \text{H}_2 \qquad (8)$$

However, the rate of production of Si-O-Si was less than the rate of loss of Si-OH in the early stages of reaction and hence another competing process was suggested which is represented by reaction (9).

$$\text{Si-OH} + \text{H}\cdot \rightarrow \text{Si}\cdot + \text{H}_2\text{O} \qquad (9)$$

The data given in figure (15) strongly support this suggestion by showing that reaction of Si-OD with atomic deuterium results in loss of oxygen (since no loss of oxygen is observed after thermal decomposition of all the Si-OD to Si-O-Si). It is unclear why reaction (9) does not proceed further although Ikeda *et al.* suggest that the presence of dihydride species may inhibit the reaction. In support of this, the present data indicate an approximate correlation between the completion of reaction (9) and the appearance of the β_2 desorption peak. However, it is clear that the chemistry of these processes is not well understood and deserves a thorough study, ideally using molecular beam techniques.

3.4. CONCLUSIONS

The adsorption of D_2O on Si(100) involves both intrinsic and extrinsic precursor states. At a surface temperature of 300 K the precursor can diffuse to many sites and hence the sticking probability is independent of coverage to 95% of the apparent saturation coverage. In the limit that the rate of desorption from the precursor states is much greater than the rate of diffusion, the coverage dependence of the sticking probability is described by first order Langmuir kinetics because adsorption across both dangling bonds of a single

dimer is preferred. Occasionally, adsorption involves two diagonally adjacent dangling bonds and as a result 0.18 ML of isolated dangling bonds are left at the apparent saturation coverage. Similarly, adsorption across all the available adatom - rest atom dangling bond pairs of the Si(111) - 7x7 reconstruction is associated with a high sticking probability but reaction of the remaining isolated adatom dangling bonds occurs with very much reduced probability.

Desorption of 90% of the adsorbed deuterium on Si(100) and 85% of the adsorbed deuterium on Si(111) involves the same mechanisms that have previously been invoked to describe the β_1 TPD peak in the absence of adsorbed oxygen. The remaining coverage independent fraction of adsorbed deuterium is more closely associated with the desorption of SiO. It is proposed that one oxygen nearest neighbour and more distant oxygen nearest neighbours do not strongly influence desorption although an extended and cumulative interaction does increase the activation energy. However, deuterium adsorbed at SiO_2 and SiO_3 sites is more strongly bound and desorbs at higher temperatures. The desorption of SiO from Si(100) can be simulated using first order kinetics with an activation energy that increases with initial D_2O coverage. Although the pre-exponential factor is high, it is nevertheless consistent with transition state theory. The presence of adsorbed deuterium seems to have little or no effect on the rate constant for desorption of SiO.

3.5. REFERENCES

[1] G. Ghidini and F. W. Smith, J. Electrochem. Soc. 131 (1984) 2924.

[2] P.A. Thiel and T.E. Madey, Surf. Sci. Rep. 7 (1987) 211.

[3] R.K. Schulze and J.F. Evans, Appl. Surf. Sci. 81 (1994) 449.

[4] L. Andersohn and U. Köhler, Surf. Sci. 284 (1993) 77.

[5] M. Chander, Y.Z. Li, J.C. Patrin and J.H. Weaver, Phys. Rev. B48 (1993) 2493.

[6] X.-L. Zhou, C.R. Flores and J.M. White, Appl. Surf. Sci. 62 (1992) 223.

[7] B.G. Koehler, C.H. Mak and S.M. George, Surf. Sci. 221 (1989) 565.

[8] M.C. Flowers, N.B.H. Jonathan, Y. Liu and A. Morris, J. Chem. Phys. 99 (1993) 7038.

[9] J.J. Boland, Surf. Sci. 261 (1992) 17.

[10] Y.J. Chabal and K. Raghavachari, Phys. Rev. Lett. 54 (1985) 1055.

[11] R.J. Culbertson, L.C. Feldman and P.J. Silverman, J. Vac. Sci. Technol. 20 (1982) 868.

[12] J.J. Boland Surf. Sci. 244 (1991) 1.

[13] E. Schröder-Bergen and W. Ranke, Surf. Sci. 236 (1990) 103.

[14] W. Ranke and D. Schmeisser, Surf. Sci. 149 (1985) 485.

[15] D. Schmeisser, Surf. Sci. 137 (1984) 197.

[16] H. Ibach, H. Wagner and D. Buchmann, Solid State Comms. 42 (1982) 457.

[17] Y.J. Chabal and S. B. Christman, Phys. Rev. B29 (1984) 6974.

[18] W. Ranke and Y.R. Xing, Surf. Sci. 157 (1985) 339.

[19] Y. J. Chabal, Phys. Rev. B29 (1984) 3677.

[20] W.H. Weinberg, Kinetics of Interface Reactions, Eds. M. Grunze and H.J. Kreuzer (Springer, New York, 1987).

[21] J.P. Lacharme, C. Sébenne, S.M. Chérif, M. Chikhi, N. Safta and M.A. Zaibi, Appl. Surf. Sci. 65/66 (1993) 598.

[22] M.J. Dresser, P.A. Taylor, R.M. Wallace, W.J. Choyke and J.T. Yates, Jr., Surf. Sci. 218 (1989) 75.

[23] S.M. Chérif, J.P. Lacharme and C.A. Sébenne, Surf. Sci. 262 (1992) 33.

[24] H. Gutleben, S.R. Lucas, C.C. Cheng, W.J. Choyke and J.T. Yates, Jr., Surf. Sci. 257 (1991) 146.

[25] Q. Gao, C.C. Cheng, P.J. Chen, W.J. Choyke and J.T. Yates, Jr., J. Chem. Phys. 98 (1993) 8308.

[26] H.C. Flaum, D.J.D. Sullivan and A.C. Kummel, J. Phys. Chem. 98 (1994) 1719.

[27] A. Szabó, P.D. Farrall and T. Engel, Surf. Sci. 312 (1994) 284.

[28] J.R. Engstrom, M. M. Nelson and T. Engel, Surf. Sci. 215 (1989) 437.

[29] P.A. Taylor, R.M. Wallace, C.C. Cheng, W.H. Weinberg, M.J. Dresser, W.J. Choyke and J.T. Yates, Jr., J. Am. Chem. Soc. 114 (1992) 6754.

[30] C.C. Cheng, R.M. Wallace, P.A. Taylor, W.J. Choyke and J.T. Yates, Jr., J. Appl. Phys. 67 (1990) 3693.

[31] L. Clemen, R.M. Wallace, P.A. Taylor, M.J. Dresser, W.J. Choyke, W.H. Weinberg and J.T. Yates, Jr., Surf. Sci. 268 (1992) 205.

[32] Q. Gao, C.C. Cheng, P.J. Chen, W.J. Choyke and J.T. Yates, Jr., Thin Solid Films, 225 (1993) 140.

[33] S.M. Cohen Y.L. Yang, E. Rouchouze, T. Jin and M.P. D' Evelyn, J. Vac. Sci. Technol. A10 (1992) 2166.

[34] H.J. Kuhr, W. Ranke and J. Finster, Surf. Sci. 178 (1986) 171.

[35] M.P. D' Evelyn, Y.L. Yang and S.M. Cohen. J. Chem. Phys. 101 (1994) 2463.

[36] J.J. Boland, J. Vac. Sci. Technol. A10 (1992) 2458.

[37] J.J. Boland, Surf. Sci. 261 (1992) 17.

[38] N. Nishijima, K. Edamoto, Y. Kubota, S. Tanaka and M. Onchi, J. Chem. Phys. 84 (1986) 6458.

[39] S.M. Cherif, J.-P. Lacharme and C.A. Sçbenne, Surf. Sci. 243 (1991) 113.

[40] B.G. Koehler, P.A. Coon and S.M. George, J. Vac. Sci. Technol. B7 (1989) 1303.

[41] P.A. Taylor, R.M. Wallace, W.J. Choyke, J.T. Yates, Jr., Surf. Sci. 238 (1990) 1.

[42] K. Fujiwara and H. Ogata, Surf. Sci. 72 (1978) 157.

[43] S.Y. Tong, H. Huang, C.M. Wei, W.E. Packard, F.K. Men, G. Glander and M.B. Webb, J. Vac. Sci. Technol. A6 (1988) 615.

[44] Ph. Avouris and I-W. Lyo, Surf. Sci. 242 (1991) 1.

[45] J. Yoshinobu, D. Fukushi, M. Uda, E. Nomura, M. Aono, Phys. Rev. B 46 (1992) 9520.

[46] M.C. Flowers, N.B.H. Jonathan, Y. Liu and A. Morris, J. Chem. Phys. 99 (1993) 7038.

[47] M.C. Flowers, N.B.H. Jonathan, Y. Liu and A. Morris, J. Chem. Phys. 102 (1994) 1034.

[48] J.R. Engstrom, D.J. Bonser, M.M. Nelson and T. Engel, Surf. Sci. 256 (1991) 317.

[49] Y.-K. Sun, D.J. Bonser and T. Engel, J. Vac. Sci. Technol. A10 (1992) 2314.

[50] M.C. Flowers, N.B.H. Jonathan, A. Morris and S. Wright, to be published.

[51] M.P. D' Evelyn, Y.L. Yang and L.F. Sutcu, J. Chem. Phys. 96 (1992) 852.

[52] G.A. Reider, U. Höfer and T.F. Heinz, Phys. Rev. Lett. 66 (1991) 1994.

[53] J.S. Villarrubia and J.J. Boland, Phys. Rev. Lett. 63 (1989) 306.

[54] J.P. Pelz and R.H. Koch, J. Vac. Sci. Technol. B9 (1991) 775.

[55] G. Hollinger, J.F. Morar, F.J. Himpsel, G. Hughes and J.L. Jordan, Surf. Sci. 168 (1986) 609.

[56] G. Hollinger and F.J. Himpsel, J. Vac. Sci. Technol. A1 (1983) 640.

[57] G. Hollinger and F.J. Himpsel, Phys. Rev. B28 (1983) 3651.

[58] E.M. Oellig, R. Butz, H. Wagner and H. Ibach, Solid State Commun. 51 (1984) 7.

[59] P. Gupta, A.C. Dillon, A.S. Bracker and S.M. George, Chem. Phys. Lett. 176 (1991) 28.

[60] P. Gupta, A.C. Dillon, A.S. Bracker and S.M. George, Surf. Sci. 245 (1991) 360.

[61] Y.J. Chabal and K. Rahavachari, Phys. Rev. Lett. 54 (1985) 1055.

[62] Y.J. Chabal, J. Vac. Sci. Technol. A3 (1985) 1448.

[63] Y.J. Chabal and S.B. Christman, Phys. Rev. B29 (1984) 6974.

[64] D. Schmeisser and J.E. Demuth, Phys. Rev. B33 (1986) 4233.

[65] J.A. Schaefer, F. Stucki, D.J. Frankel, W. Göpel and G.J. Lapeyre, J. Vac. Sci. Technol. B2 (1984) 359.

[66] F. Stucki, J. Anderson, G.L. Lapeyre and H.H. Farrell, Surf. Sci. 143 (1984) 84.

[67] H. Kobayashi, T. Kubota, M. Onchi and M. Nishijima, Phys. Lett. A95 (1983) 345.

[68] Hydrides of the Elements of Main Groups I-IV, E. Wiberg, 1971.

[69] McKean, J. Phys. Chem. 86 (1982) 307.

[70] McKean, Chem. Phys. Lett. 109 (1984) 347.

[71] McKean, Spectrochimica Acta, 41A (1985) 25.

[72] McKean, Spectrochimica Acta, 49A (1993) 1095.

[73] E. Popowski, Z. Anorg. Allg. Chem. 543 (1986) 219.

[74] Muller and Popowski, Z. Phys. Chimie, Liepzig, 271 (1990) 703.

[75] J.A. Schaefer, D. Frankel, F. Stucki, W. Göpel and G.J. Lapeyre, Surf. Sci. 139 (1984) L209.

[76] J.A. Schaefer, Surf. Sci. 178 (1986) 90.

[77] G. Lucovsky, Solid State Comms. 29 (1979) 571.

[78] W. Widdra, C. Huang, G.A.D. Briggs and W.H. Weinberg, J. Elect. Spec. Rel. Phenom. 64 (1993) 129.

[79] S. Tanaka, M. Onchi and M. Nishijima, J. Chem. Phys. 91 (1989) 2712.

[80] L. Chua, R.B. Jackman and J.S. Foord, Surf. Sci. 315 (1994) 69.

[81] M.J. Bozack, P.A. Taylor, W.J. Choyke and J.T. Yates, Jr., Surf. Sci. 179 (1987) 132.

[82] J.T. Yates, Jr., C.G. Cheng, Q. Gao, M.L. Colaianni, W.J. Choyke, Thin Solid Films 225 (1993) 150.

[83] D.D. Koleske, S.M. Gates and B. Jackson, J. Chem. Phys. 101 (1994) 3301.

[84] C.C. Cheng, S.R. Lucas, H. Gutleben, W.J. Choyke and J.T. Yates, Jr., J. Am. Chem. Soc. 114 (1992) 1249.

[85] W. Widdra, S.I. Yi, R. Maboudian, G.A.D. Briggs and W.H. Weinberg, Phys. Rev. Lett. 74 (1995) 2074.

[86] H. Ikeda, K. Hotta, T. Yamada, S. Zaima and Y. Yasuda, Jpn. J. Appl. Phys. 34 (1995) 2191.

CHAPTER 4

A QUASI-EQUILIBRIUM MODEL FOR THE UPTAKE KINETICS OF HYDROGEN ATOMS ON Si(100)

4.1. INTRODUCTION

The adsorption and abstraction mechanisms of hydrogen atoms (H·) and deuterium atoms (D·) incident on silicon surfaces remain speculative and controversial despite recent kinetic studies [1-4].

Discussions and analyses of adsorption kinetics and dynamics have extensively invoked the notion of both intrinsic (above empty sites) and extrinsic (above occupied sites) physisorbed precursors [5, 6]. In the simple Lennard-Jones description of an indirect adsorption process and kinetic analyses based on it, the incident atom or molecule becomes trapped in a physisorption well prior to chemisorption or return to the gas phase. Many sites can be investigated by the precursor when the rate constant for diffusion is much bigger than that for desorption and hence it is often found that the sticking coefficient for chemisorption is high and remains constant until near saturation. Kaesmo and Harris [7] have recognised that energy accommodation in the chemisorption potential well may be slow such that the adsorbate becomes trapped in vibrational levels above the barrier to diffusion. Although this has received relatively little attention, "hot precursors" may be important in both adsorption [8] and reaction [9, 10] mechanisms.

Conventionally, surface reactions are considered in terms of the Langmuir-Hinshelwood mechanism which involves reaction between chemisorbed species on adjacent sites, or the Eley-Rideal mechanism which requires a direct collision between a gas phase reactant and a chemisorbed species. Experimental evidence for the latter mechanism from kinetic studies is scarce and not entirely convincing. However, recent molecular beam studies [11-13] of H· abstraction of D adsorbed on Cu(111) and Cl adsorbed on Au(111) are regarded as definitive investigations of Eley-Rideal dynamics.

In this chapter the uptake kinetics of H· and D· on Si(100) are interpreted by considering adsorption, abstraction and desorption reactions. The initial gradients of the H· and D· uptake plots represent adsorption at dangling bond sites only. In the absence of an independent calibration of the H· and D· fluxes, the same rate constant, k_s is assumed in both equations (1) and (2).

$$H\cdot + \cdot Si \xrightarrow{k_s} H-Si \quad (1)$$

$$D\cdot + \cdot Si \xrightarrow{k_s} D-Si \quad (2)$$

The abstraction reactions are followed by measuring the H_2, HD and D_2 TPD yields after reaction of H· with adsorbed D or reaction of D· with adsorbed H. Previously [1, 2], an Eley-Rideal abstraction mechanism has been considered such that

$$H\cdot + H-Si \xrightarrow{k_{HH}} \cdot Si + H_2 \quad (3)$$

$$D\cdot + D-Si \xrightarrow{k_{DD}} \cdot Si + D_2 \quad (4)$$

$$H\cdot + D-Si \xrightarrow{k_{HD}} \cdot Si + HD \quad (5)$$

$$D\cdot + H-Si \xrightarrow{k_{DH}} \cdot Si + HD \quad (6)$$

where k_{HH}, k_{DD}, k_{HD} and k_{DH} are the corresponding rate constants. Both Widdra *et al.* [1] and Koleske *et al.* [2] have reported that there is no observable isotope effect for abstraction with the rate constant given as $0.36k_s$ and $(0.5\pm0.1)k_s$ respectively. If H· adsorption is described by first order Langmuir kinetics then the steady state saturation coverage is $1/(1+{}^{k_{HH}}/_{k_s})$ since

$$\frac{d\theta}{dt} = Fk_s(1-\theta) - Fk_{HH}\theta \quad (7)$$

where F is the H· flux and θ is the coverage. However, STM images [14] have shown that adsorption of H· on Si(100) at 600 K results in a saturation coverage of 1 ML which seems to be inconsistent with a high probability for abstraction. Koleske *et al.* [2] have suggested that either surface dihydride or sub-surface hydrogen exist during exposure to H· which then react to give surface monohydride when the H· source is turned off. More recently, Widdra *et al.* [1] have shown that incident D· can diffuse across the surface at 150 K despite the

high activation barrier and have proposed that a hot precursor is able to investigate a number of adsorption sites whilst in excited vibrational levels of the Si-D potential. They then argue that the rate of adsorption is consequently much greater than $Fk_s(1-\theta)$ at saturation and hence a coverage of almost 1 ML can be reconciled with abstraction. In the present study, new data concerning both adsorption and abstraction processes are presented and appropriate mechanisms are discussed.

4.2. RESULTS.

Uptake plots for D· and H· on Si(100) at 635 K are presented in figures (1a) and (1b) respectively. The measured exposures to H· have been scaled such that the initial sticking probability is the same as for D·. An independent calibration of the relative H· and D· fluxes is desirable but difficult to obtain with any accuracy. The rates of impingement of H_2 and D_2 on the filament cannot be calculated using the Hertz-Knudsen equation in the present experiment since this is not appropriate for an effusive beam source. Some fraction of the effusive beam will impinge on the filament and hence the relative rates of effusion should be considered. For a given chamber pressure of D_2 or H_2 and after correction for relative ion gauge sensitivities, the rate of effusion of H_2 into the chamber will be approximately $\sqrt{2}$ times greater than the rate of D_2 effusion due to the rates of pumping. However, this is a crude approximation since diffusion pump pumping speeds vary less rapidly than $(mass)^{1/2}$ at low molecular masses [15]. In view of the disparate ionisation gauge sensitivities reported in the literature [16], it has been suggested that the ionisation cross-section is the best indication of relative sensitivities [17]. The ionisation cross-section for D_2 has been found [18] to be only 1% greater than that for H_2 in agreement with the nearly identical ionisation gauge sensitivities measured by Walters and Craig [19]. An equilibrium thermodynamic model [20] predicts that H_2 atomisation is 10% more efficient than D_2 atomisation [2] but this must

be considered as a very approximate value in the absence of experimental data. These considerations combine to give an H· flux which is very approximately 1.6 times greater than the D· flux at a given uncorrected chamber pressure of H_2 or D_2 whereas a factor of 2.1 is determined from the initial sticking probabilities.

Previously, a considerable deviation from first order Langmuir adsorption kinetics has been reported by Widdra *et al.* [1] for D· adsorption on Si(100) at 600 K and their best fit to their data is reproduced in figure (1a). However, the present data for both D· and H· adsorption at 635 K, which are plotted in figure (1a) and (1b) respectively, show only minor deviations from first order Langmuir kinetics. It will be argued later that surface dihydride species must be considered in the kinetic scheme and hence this experiment, which aims to characterise the processes which lead to a saturated monohydride phase, may be greatly affected by the surface temperature. A surface temperature of 635 K was chosen since this gave no indication of a β_2 TPD peak at saturation yet the rate of desorption from the saturated monohydride phase is calculated to be very small (of the order of 10^{-5}ML s^{-1}) using the Arrhenius parameters given in reference [21]. If the surface lifetime of dihydride species become comparable with the time-scale of the experiment or if loss of monohydride via the β_1 channel becomes significant, then the amount of uptake measured by TPD becomes ill-defined. It should be noted that although a β_2 TPD may not be apparent, a significant dihydride coverage could desorb between terminating the exposure and recording the TPD, especially when long pump-down times are involved.

The rates of H· abstraction of adsorbed D and D· abstraction of adsorbed H were determined at 1 ML coverage and at a surface temperature of 635 K by measuring the H_2, HD and D_2 TPD yields after reaction. The data are plotted in figure (2) and indicate a distinct isotope effect with abstraction of H by D·

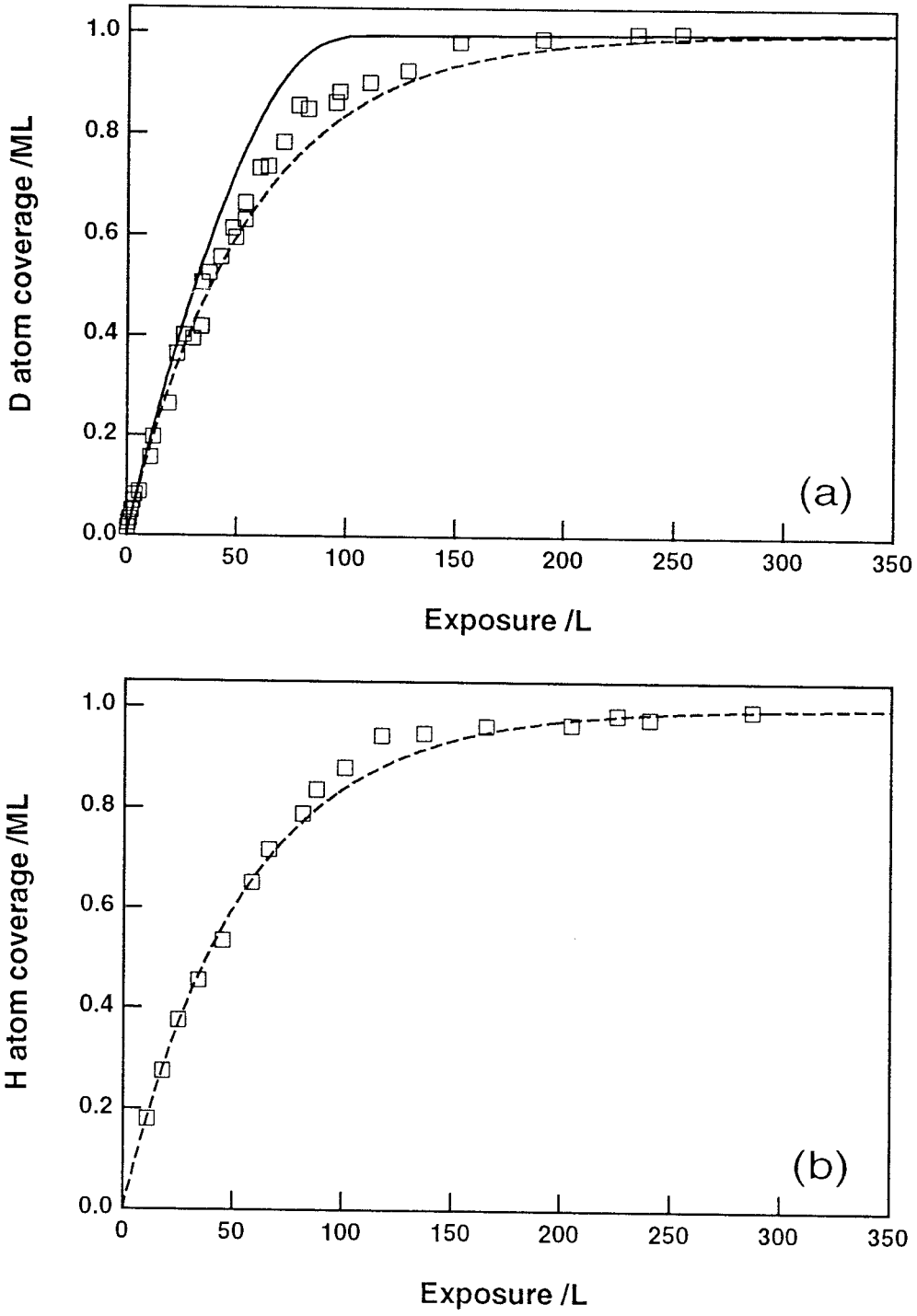

Figure (1). Uptake plots for (a) deuterium and (b) hydrogen at 635 K; experimental data (□), first order Langmuir kietics (---) and the best fit obtained by Widdra *et al.* [1] using their data (—).

calculated as (1.8±0.1) times faster than abstraction of D by H· from the initial rates. However, the rate of D abstraction becomes noticeably slower than expected for first order kinetics as the reaction proceeds and suggests that abstraction is not simply an Eley-Rideal reaction. Furthermore, the abstraction of D by H· when the initial coverage is less than 1 ML also shows the same trend with increasing exposure. In figure (3), the data for initial D coverages of 0.22 ML and 0.46 ML are consistent with first order kinetics and a rate constant determined by the initial slopes of the plots, however, the rate seems to be systematically slower than expected at higher exposures.

The D· uptake plot shown in figure (4) was obtained for a surface temperature of 373 K by integrating the β_1 and β_2 TPD peak areas. An excellent fit to first order Langmuir kinetics is obtained with a saturation coverage of 1.5 ML. In addition, the SiD_4 TPD yield was also measured since this represents another, albeit very minor channel for loss of D during desorption. It can be estimated from published data [22] that the yield of SiD_4 at saturation and at 373 K is approximately 0.007 ML. The onset of SiD_4 formation coincides with the first indication of a β_2 TPD peak at approximately 0.85 ML.

Although the initial gradients of the D· uptake plots at 373 and 635 K are the same, abstraction is slower at 373 K. It is found from the data in figure (5) that a rate constant equal to $(0.18\pm0.02)k_s$ represents the abstraction of adsorbed H by D· at 373 K regardless of the dihydride coverage. An activation energy of (1.9±0.1) kcal mol^{-1} is calculated for the abstraction of adsorbed H by D· using the rate constants measured at 373 and 635 K. This compares reasonably with the value of (1.06±0.11) kcal mol^{-1} measured by Koleske *et al.* [2] and also with the activation energy for the gas phase abstraction of H from SiH_4 by D· which is reported as (2.5±0.5) kcal mol^{-1} [23]. When D· reacts with a saturated monohydride phase at 373 K, the overall increase in coverage represents both

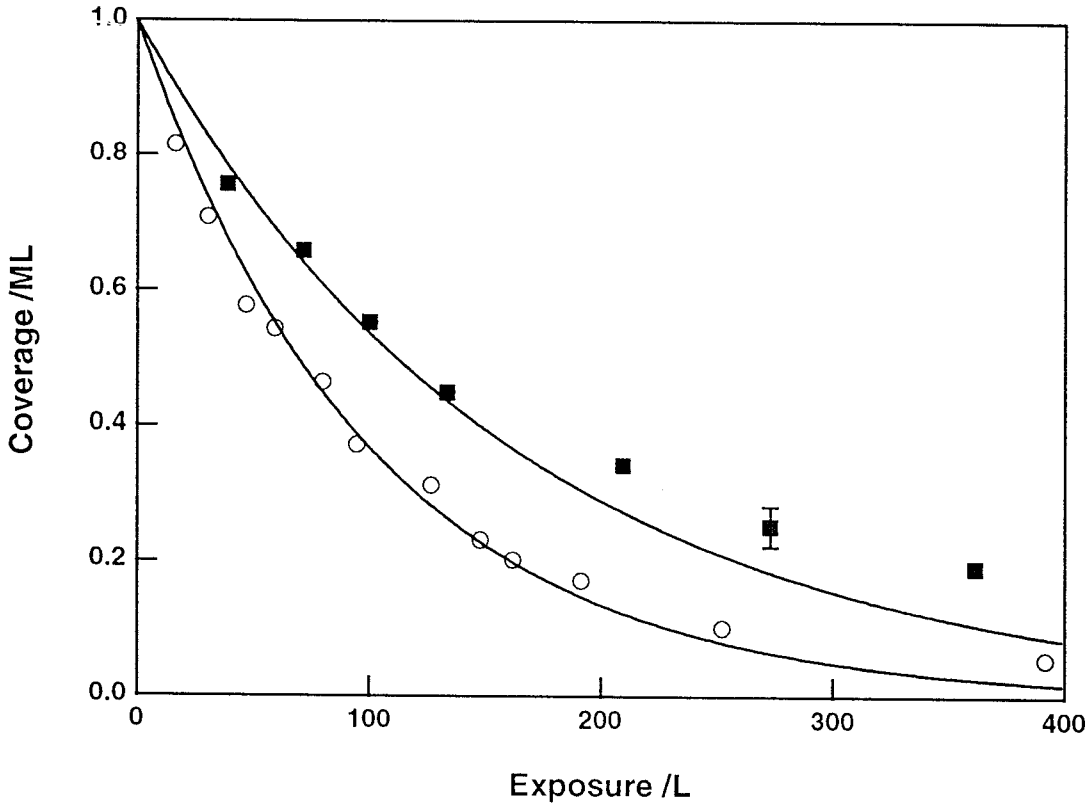

Figure (2). H coverage as a function of exposure to D· (○) fitted to first order kinetics with rate constant 0.55k_s and D coverage as a function of exposure to H· (■) fitted to first order kinetics with a rate constant of 0.31 k_s.

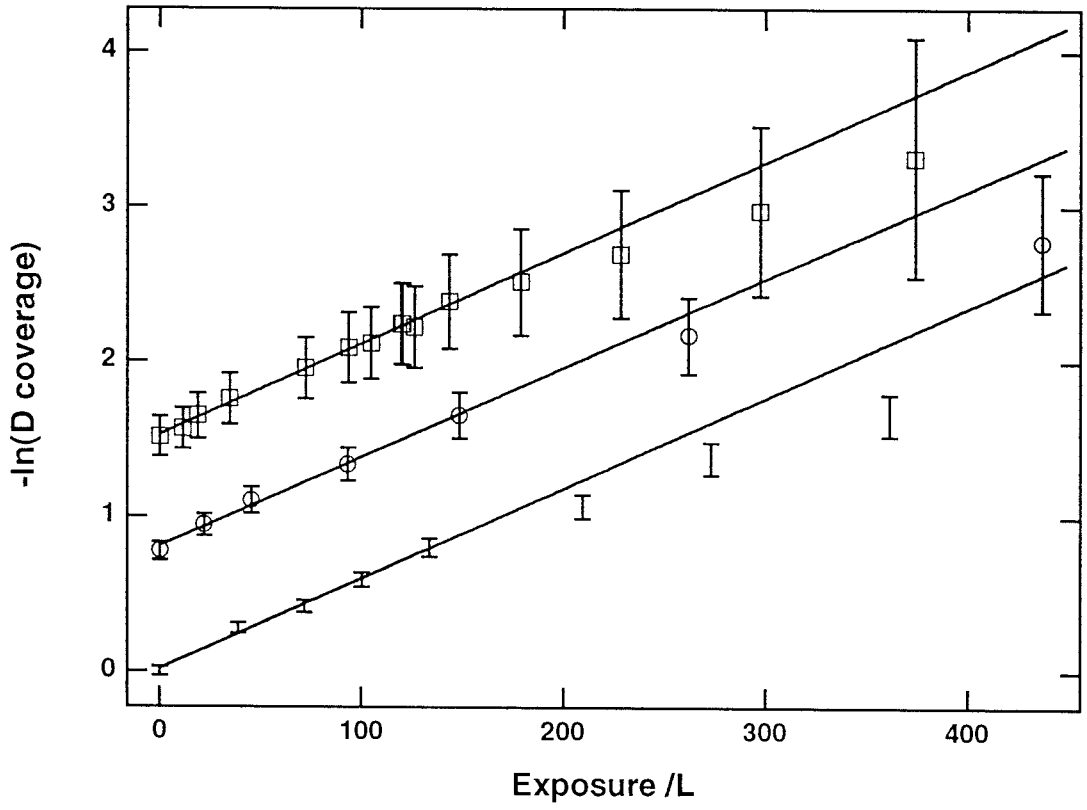

Figure (3). Plots of -ln(D coverage) against exposure to H· for initial D coverages of 1 ML (no symbols), 0.46 ML (○) and 0.22 ML (□) which give a rate constant of (0.31±0.01)k_s from the initial slopes only. The rate decreases more slowly than expected for first order kinetics after exposures of approximately 200 L.

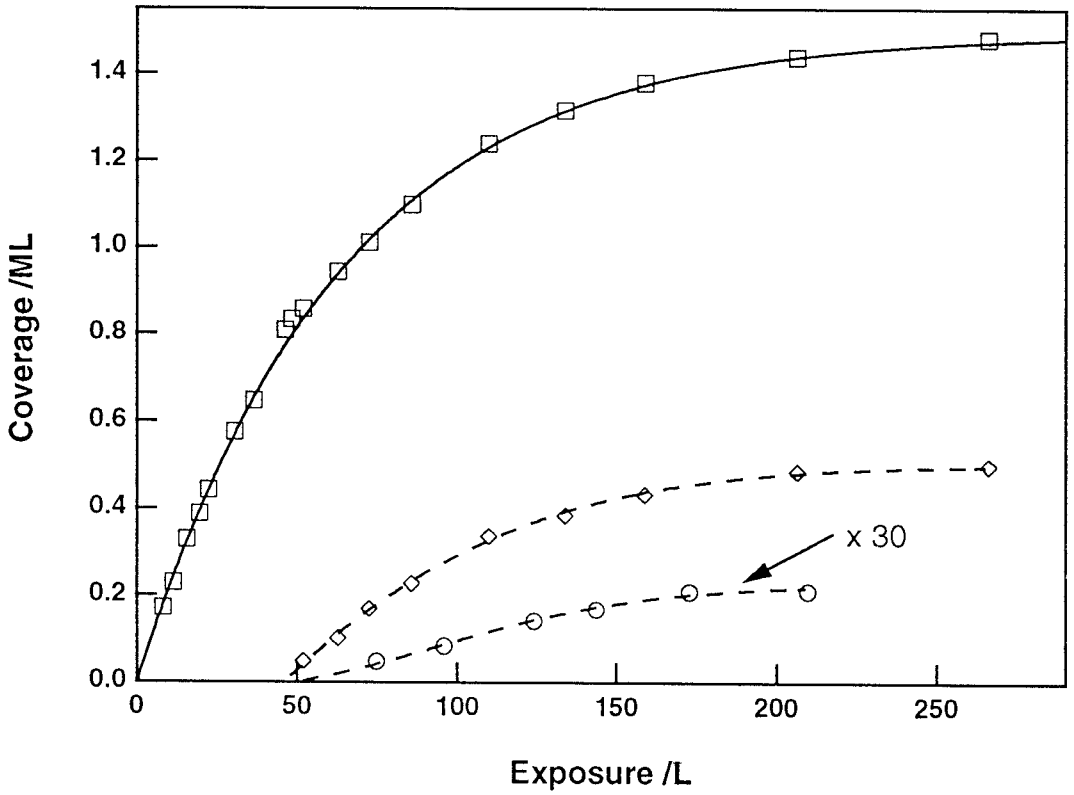

Figure (4). Uptake of D· at 373K; coverage corresponding to the integrated areas of both β_1 and β_2 TPD peaks (□), first order Langmuir kinetics (—), β_2 TPD peak area only (◇), TPD yield of SiD_4 (○) and spline through data (---).

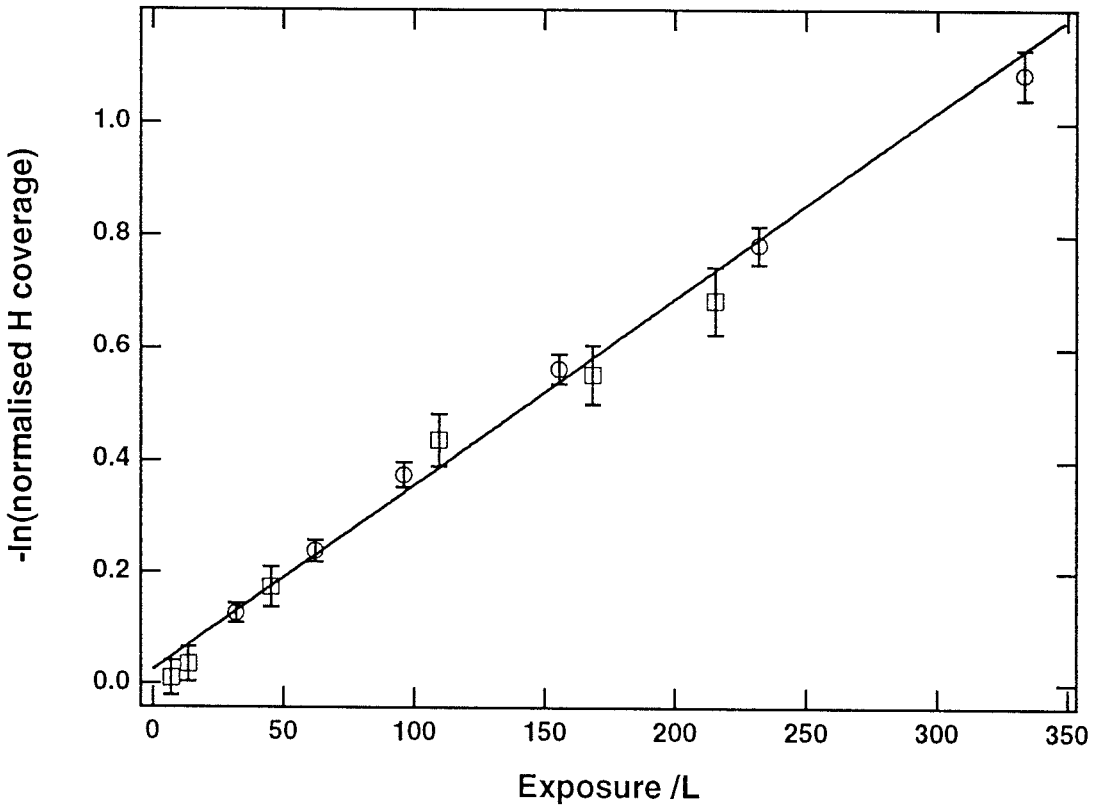

Figure (5). Plot of -ln(normalised H coverage) against exposure to D· at 373 K; abstraction from both dihydride and monohydride (O) and from initially monohydride only (□) with linear regression through the data (—).

abstraction and adsorption reactions. However, the initial increase of D coverage represents only the reaction

$$HSi\text{-}SiH + 2\ D\cdot \rightarrow 2\ HSiD \qquad (8)$$

and hence, by measuring the uptake of D· by a saturated monohydride phase, the rate constant for this reaction was determined as $(0.80\pm0.05)k_s$.

In agreement with these and other [3] results, Koleske *et al.* [2] find that abstraction from mixed monohydride and higher hydrides at 403 K is slower than from monohydride only at 673 K. They claim that dihydride and trihydride are less reactive than monohydride but do not seem to have considered the effect of surface temperature. Using their value for the activation energy, the rate constant for abstraction from monohydride at 403 K is calculated as 0.4 times that at 673 K in approximate agreement with their data at these temperatures. The data in figure (5) indicate that monohydride and dihydride are equally reactive. This is confirmed by infrared spectrocopy of hydrogenated porous silicon [24] which clearly shows that the intensities of the bands attributed to monohydride, dihydride and trihydride decrease uniformly with increasing D· exposure at 298 K.

4.3. DISCUSSION

A. The Hot Precursor Model

The relaxation of the surface Si-H stretching vibration has been reported in a series of studies [25-27] that represent a comprehensive investigation of energy transfer [28]. In these experiments, the relaxation of the v=1 Si-H stretching vibration on an unreconstructed Si(111) surface was measured by sum frequency generation (SFG) after excitation with a picosecond IR laser. At room temperature, the pure relaxation time, T_1, was found to be 800±100 ps whereas measured values for CO adsorbed on Cu(100) and Pt(111) are of the order of a few picoseconds [29, 30]. The vibrational relaxation of a CO to metal

surface bond is dominated by coupling to electron-hole pair excitation and intermolecular dipole-dipole interactions. Electron-hole pair excitation does not contribute to vibrational relaxation on silicon surfaces since the band gap (1.1 eV for intrinsic silicon at 300 K [31]) is much larger than a typical vibrational transition (0.26 eV for the v=1 ← v=0 transition of Si-H [32]) and dipole-dipole interactions are small due to the weak dynamic dipole of the Si-H bond (0.1 D [33] compared with 0.22 D for CO adsorbed on Cu(100) [34]). By examining line shapes as a function of surface temperature, inefficient coupling to multi-phonon excitations and to the much lower frequency Si-H bending vibration have been deduced as dominant processes in the relaxation of the Si-H stretching vibration. Remarkably, a relaxation lifetime of approximately 6 ns has recently been measured [35] for H adsorbed on Si(100)-2x1 at 100 K although defect sites significantly but unpredictably increase the rate of relaxation as the temperature is increased. Hence, vibrational energy accommodation during hydrogen adsorption on silicon is likely to be slow and hot precursor mechanisms can therefore be rationalised.

A hot precursor can lose energy by vibrational relaxation processes or by an inelastic collision with another adsorbed atom or molecule. Inelastic collisions are least important at low coverages and a random site occupation is expected but at higher coverages, loss of energy by inelastic scattering is likely to lead to some clustering [1, 8]. Hence, an essentially random distribution of hydrogen atoms is observed by STM [36] at coverages of approximately 0.07 ML whereas the data of Widdra *et al.* suggest complete pairing for coverages greater than 0.2 ML. However, some evidence for inelastic collisions is expected at intermediate coverages and this can be found in figure (4) of reference [36]. A "reaction map" was extracted from this image and is presented in figure (6). There are 99 occupied sites in a region of the image containing a total of 684 sites and hence the coverage is 0.145 ML. Theoretical calculations [37] predict

that hydrogen atoms diffuse mainly along the edges of dimer rows and that a much higher activation energy is associated with hopping to an adjacent row. The number of pairs of occupied sites along the edges of the dimer rows is then a crude analysis of the inelastic scattering process for hot precursors at low temperatures. If the occupation of sites is completely random then the number of pairs in figure (6) should be

$$\left(\frac{99}{684}\times\frac{1}{2}\times 7\right)+\left(\frac{99}{684}\times 2\times\frac{1}{2}\times 92\right)=14$$

since there are 7 occupied sites at the edges of the image with one adjacent site and 92 other occupied sites with two adjacent sites. A total of 25 pairs can be found in figure (6) and thus there is clear evidence for inelastic collisions along the edges of the dimer rows. There should be a similar correlation between occupied sites on Si(111)-7x7 after adsorption of hydrogen atoms at low temperature. Unfortunately, the STM image in figure (2) of reference [38] shows only adatom sites (the rest atom sites are not imaged) and the distribution of occupied sites plotted in figure (7) is indistinguishable from a random distribution. Subjective impression is very unsatisfactory but a statistical analysis such as that developed for a square lattice [39] is complicated for the Si(111)-7x7 reconstruction.

It is not surprising but nevertheless encouraging to find that the vibrational lifetime is of importance in both adsorption and desorption processes. Electronic excitation and consequently dissociation of the Si-H bond can be induced by field emitted electrons from an STM tip with a sample bias in excess of +6V [40]. However, at lower energies, a mechanism for multiple vibrational excitation of the Si-H bond by inelastic electron tunneling has been identified and shown to result in the desorption of atomic hydrogen. Hence, the efficiency of desorption by this excitation mechanism for H adsorbed on Si(100) is a consequence of the slow rate of vibrational relaxation.

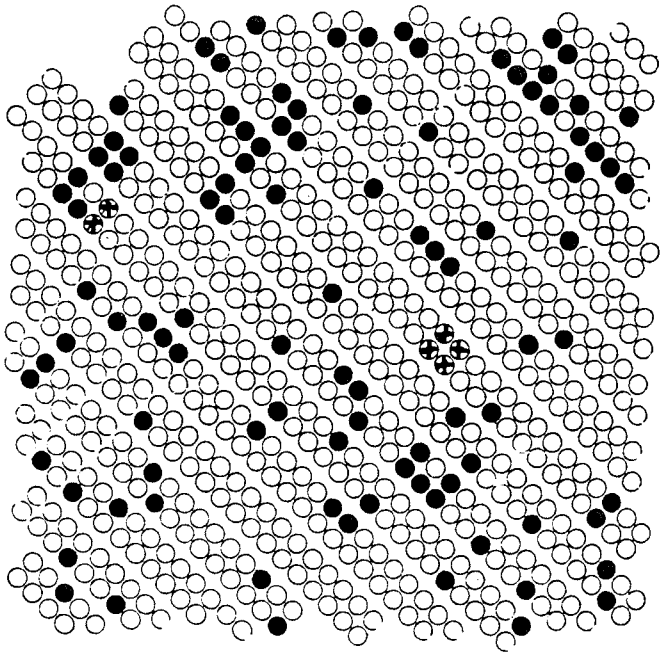

Figure (6). An STM "reaction map" extracted from figure (4) of reference [36] which shows the distribution of hydrogen atoms on Si(100) following adsorption of H· at room temperature. There are 99 occupied sites (●), 585 unoccupied sites (○) and 6 defect sites (x) in this region of the image.

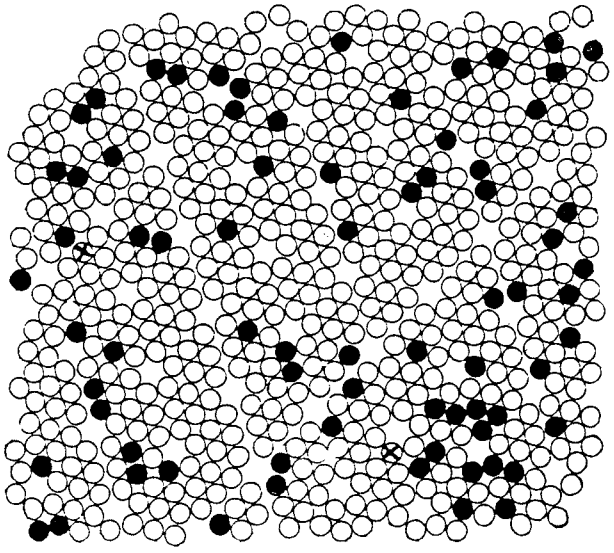

Figure (7). An STM "reaction map" extracted from figure (2) of reference [38] which shows the distribution of reacted adatoms (●) on Si(111)-7x7 following adsorption of H· at room temperature.

The activation barrier for diffusion of an adsorbed H atom along a dimer row has been calculated by *ab initio* methods as approximately 38 kcal mol^{-1} and 30 kcal mol^{-1} using cluster and slab models respectively [37, 41]. The degree of vibrational excitation required to surmount this barrier can be estimated by considering a molecular analogue. The harmonic frequency, ω_e, and the anharmonicity, x_e, of the Si-H bond in Me_3SiH have been calculated from measured fundamental and first overtone frequencies [42]. If the surface Si-H bond can be adequately described by a Morse potential using these parameters, then vibrational levels higher than v=5 or v=6 are above the diffusion barrier.

Slow vibrational relaxation of the Si-H bond provides a mechanism by which H can diffuse from one chemisorption well to another during adsorption at low surface temperatures. Widdra *et al.* [1] have calculated the sticking probability at 600 K as a function of coverage using equation (9) which was originally formulated to describe adsorption kinetics involving a mobile physisorbed precursor [5]. Using the notation of these authors, $P_{a,0}$ and P_a are the initial sticking probability and sticking probability respectively and κ is a constant such that $1/\kappa$ is a measure of the number of sites visited before localised chemisorption or desorption.

$$P_a(\theta) = P_{a,0}\left[1 + \kappa\theta/(1-\theta)\right]^{-1} \tag{9}$$

Hence, the rate of increase of coverage is given by equation (10)

$$\frac{d\theta}{dt} = -FP_r\theta + FP_{a,0}\left[1 + \kappa\theta/(1-\theta)\right]^{-1} \tag{10}$$

where F is the incident atomic flux and P_r is the reaction probability for abstraction. Integration yields an expression for ε, the exposure in terms of θ, the coverage

$$\varepsilon = \frac{1}{P_r(\kappa-1)(a-b)}\left\{(1+a(\kappa-1))\ln\left[\frac{(\theta-a)}{-a}\right]-(1+b(\kappa-1))\ln\left[\frac{(\theta-b)}{-b}\right]\right\} \tag{11}$$

where a and b are obtained from

$$a,b = \frac{P_r + P_{a,0} \pm \sqrt{(P_r+P_{a,0})^2 + 4P_r(\kappa-1)P_{a,0}}}{-2P_r(\kappa-1)} \tag{12}$$

and b is the saturation coverage. With $1/\kappa = 20$, Widdra *et al.* find that a high sticking probability is maintained until near saturation and hence a coverage of nearly 1 ML can be reconciled with a high probability for abstraction. Equation (9) might typically be applied, for example, to the adsorption of D_2O on Si(100) at 300 K [43]. In common with many other examples, the sticking probability is high and constant until 95% of the saturation coverage as a consequence of a long-lived extrinsic precursor. Thus a D_2O molecule incident at an occupied site becomes trapped in the physisorption potential well and can subsequently diffuse over many sites until it either dissociatively chemisorbs at two adjacent vacant sites or returns to the gas phase. This example is included here because it illustrates how a coverage independent sticking probability arises from physisorption at occupied chemisorption sites. However, a hot precursor is chemisorbed, in this case as a result of orbital overlap between hydrogen atom and silicon dangling bond. Within the extent of the description of H· adsorption given by Widdra *et al.*, there is no possibility for chemisorption at an already occupied dangling bond site. Hence, a fundamental objection to the use of equation (9) to describe the adsorption of H· is that trapping and diffusion over occupied sites is not explained by invoking a hot precursor. It is likely that at low temperatures, slow relaxation of the nascent Si-H bond allows diffusion from one dangling bond to the next and this feature is needed to explain the diffusion observed at 150 K. There does not seem any extension or relevance of

this phenomenon to adsorption at high temperatures when thermally activated diffusion is fast and some other mechanism is needed to introduce a coverage independent sticking probability.

B. A New Quasi-Equilibrium Model for Atomic Hydrogen Uptake at 635K

It is proposed here that the formation and reactions of dihydride species are important at 635 K and provide mechanisms for adsorption, migration and abstraction. The rate constant for adsorption at monohydride sites to give dihydride species is assumed to be high, since it is accepted that Widdra *et al.* are correct in recognising that a high sticking probability is required at monolayer or near monolayer coverages in order to compensate for abstraction. Hence, while the hot precursor model is likely to be important at 150 K and moreover is needed to explain the observed diffusion, it is of no consequence in this kinetic model for uptake at 635 K. It is unreasonable to dismiss the involvement of dihydride species, however transient, even at 635 K since some indication of a β_2 TPD peak is observed by reducing the surface temperature during adsorption by only 20 K. The apparent migration of the dihydride, which may be regarded as a chemisorbed precursor at 635 K since its eventual fate is either desorption or conversion to a monohydride, is possible by the isomerisation reaction given in equation (13).

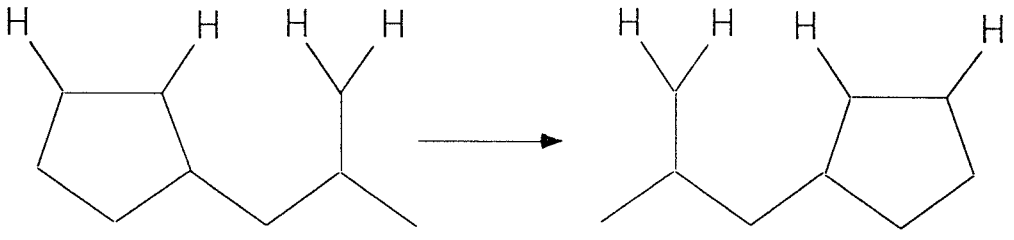

(13)

An activation energy for this process of about 38 kcal mol^{-1} is suggested by *ab initio* calculations [44] which is identical to that calculated for the diffusion of a hydrogen atom as a monohydride [37].

Two equilibria, which are represented by equations (14) and (15), have been proposed [21] to define the distribution of dihydride units, HSiH, doubly occupied dimers, HSi-SiH, singly occupied dimers, HSi-Si· and unoccupied dimers, Si=Si.

$$\text{HSi-SiH} + \text{Si=Si} \rightleftharpoons 2\ \text{HSi-Si}\cdot \tag{14}$$

$$\tfrac{3}{2}\text{HSi-SiH} \rightleftharpoons \text{HSi-Si}\cdot + \text{HSiH} \tag{15}$$

The TPD of molecular hydrogen via both β_1 and β_2 channels has been successfully modelled by using these equilibria to calculate the quasi-equilibrium coverages of each species [21]. Thus it is convenient to use the same model to describe adsorption and abstraction processes since diffusion of both monohydride and dihydride species is fast compared with the rate constants for abstraction and adsorption. If n_{00}, n_{10}, n_{11} and n_2 are the densities of unoccupied dimers, singly occupied dimers, doubly occupied dimers and dihydride species respectively and n is the density of chemisorbed hydrogen atoms, then

$$2n_{00}+2n_{10}+2n_{11}+n_2=N \text{ or } \theta_{00}+\theta_{10}+\theta_{11}+\theta_2=1 \tag{16}$$

and

$$n_{01}+2n_{11}+2n_2=n \text{ or } \tfrac{1}{2}\theta_{10}+\theta_{11}+2\theta_2=\Theta \tag{17}$$

where $n_{1i}/N=\theta_{1i}/2$ (i=0,1), $n_{00}/N=\theta_{00}/2$, $n_2/N=\theta_2$ and $n/N=\Theta$ by definition. Equations (18) and (19) describe the equilibria given in equations (14) and (15) and may be derived using standard statistical mechanical arguments and assuming that the only significant differences in the vibrational partition functions for the various species are due to differences in Si-H vibrations.

$$\frac{\theta_{10}^2}{\theta_{00}\theta_{11}} = \frac{4q_{10}^2}{q_{11}}\exp\left(-\frac{\epsilon_1}{kT}\right) \tag{18}$$

$$\frac{\theta_{10}\theta_2}{(\theta_{11}^3(1+\theta_2))^{1/2}} = \frac{q_{10}q_2}{q_{11}^{3/2}}\exp\left(-\frac{\epsilon_2}{2kT}\right) \tag{19}$$

The vibrational partition functions, q_{10}, q_{11} and q_2 for HSi-Si·, HSi-SiH and HSiH

respectively, can be calculated from published vibrational frequencies which are collated elsewhere [21]. Previously, the enthalpies, ϵ_1 and ϵ_2, have been determined from TPD data and include the π-bond energy and the σ-bond energy respectively [21]. Hence, the equilibrium coverage of each species can be calculated by numerically solving equations (16), (17), (18) and (19) for a given hydrogen coverage and surface temperature.

Using the definitions given above, the fractional coverage of unoccupied dangling bond sites available for adsorption is $\theta_{00}+\frac{1}{2}\theta_{10}$ and the fractional coverage of monohydride sites available for abstraction by an Eley-Rideal mechanism is $\theta_{11}+\frac{1}{2}\theta_{10}$. The adsorption, abstraction and desorption processes which result in dihydride formation and loss are represented by equations (20), (21) and (22) respectively where k_{di}, $2k_{HH}$ and k_d are the corresponding rate constants.

$$\text{HSi-SiH} + 2\text{H}\cdot \xrightarrow{k_{di}} 2\ \text{HSiH} \qquad (20)$$

$$\text{HSiH} + \text{H}\cdot \xrightarrow{2\,k_{HH}} \tfrac{1}{2}\text{HSi-SiH} + \text{H}_2 \qquad (21)$$

$$2\ \text{HSiH} \xrightarrow{k_d} \text{HSi-SiH} + \text{H}_2 \qquad (22)$$

It is important to note that equations (20) and (21) are not elementary reactions and do not purport to suggest the reaction mechanism. They do, however, represent the overall stoichiometry of these processes in terms of the surface species considered in this model. Desorption via the β_2 channel is believed to be a second order reaction involving two dihydride groups as indicated by equation (22). Hence, the overall rate of change of coverage due to desorption, adsorption and abstraction can be written as

$$\frac{d\Theta}{dt} = -k_d\theta_2^2 - k_{HH}(\theta_{11} + \tfrac{1}{2}\theta_{10}) - 2k_{HH}\theta_2 + k_{di}\theta_{11} + k_s(\theta_{00} + \tfrac{1}{2}\theta_{10}) \qquad (23)$$

where the rate constants k_s, k_{di} and k_{HH} are pseudo first order rate constants and incorporate the H· flux. As the flux is constant in these experiments, the order with respect to the H· flux is not significant and has not been ascertained. It is

convenient to obtain the surface coverage as a function of time or exposure by numerical integration of equation (23). The instantaneous rate, $-(d\Theta/dt)_i$ can be evaluated at time t_i using the values of θ_{00}, θ_{10}, θ_{11} and θ_2 calculated for an instantaneous coverage of Θ_i. After a finite time increment, Δt, the coverage increases to approximately $\Theta_{i+1}=\Theta_i+(d\Theta/dt)_i\times\Delta t$ and hence the calculation can be iterated until saturation.

C. Uptake at 635 K

For the purposes of this analysis, the total coverage minus the dihydride coverage, θ_2, is plotted against exposure at each iteration of the numerical integration since all the dihydride will have desorbed before the TPD is recorded, although the total coverage is used to continue with the calculation. However, if a technique could be used to measure the coverage during exposure, then the uptake plot obtained would be different and could exceed a coverage of 1 ML. The appropriate value of k_s is obtained from the initial gradient of the uptake plot in figure (1) and k_d at 635 K was calculated using the activation energy and pre-exponential factor reported previously [21]. Coverages of 1 ML or more require that k_{di} is greater than k_{HH} and it is unlikely that either k_{HH} or k_{di} is much larger than k_s. The values of k_{di} which give the best fit to the H· uptake data are plotted as a function of k_{HH} in figure (8) in addition to the mean deviation of the fit from the experimental data. Hence, it is determined that k_{HH} equal to $(0.85\pm0.05)k_s$ and k_{di} equal to $(1.06\pm0.06)k_s$ give the best fit, which is plotted in figure (9a), although it should be noted that all the points in figure (8) represent acceptable fits. The lowest reasonable value of k_{di} is considered to be $0.8k_s$, which is the measured rate constant for D· adsorption by a saturated monohydride phase at 373 K.

Clearly, an identical analysis can be applied to the D· uptake data with k_{HH} replaced by k_{DD}. It is found that the appropriate values of k_{di} are almost exactly

the same as those plotted for k_{HH} in figure (8). However, a unique best fit cannot easily be identified in this case since the data at coverages approaching 1 ML are fortuitously fitted well by first order Langmuir kinetics for which both k_{DD} and k_{di} are zero. Nevertheless, the fit plotted in figure 9(b), which was calculated k_{DD} and k_{di} set equal to $0.85k_s$ and $1.06k_s$ respectively, is more than satisfactory.

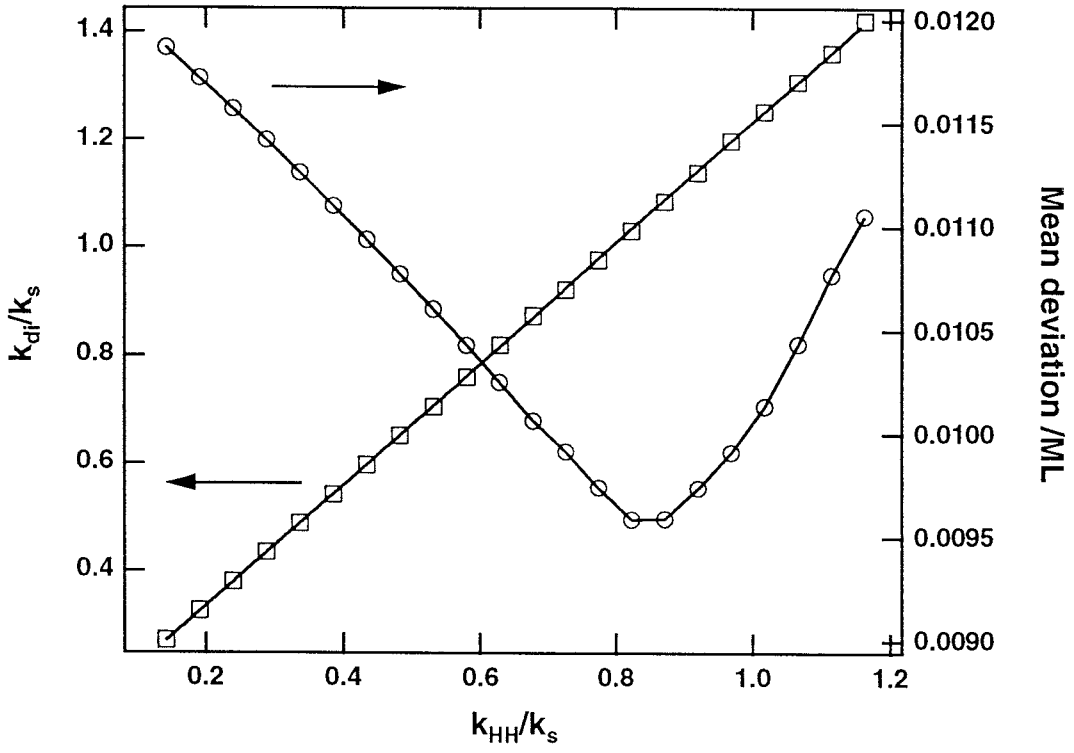

Figure(8). Plots of the value of k_{di} giving the best fit to the data (□) and the mean deviation of this fit from the data (○) as a function of k_{HH} .

D. Abstraction at 635 K

The model described above implies that hydrogen and deuterium can be lost from the surface by recombinative desorption via the β_2 channel as well as by abstraction. However, the rate of recombinative desorption is small compared with the rate of Eley-Rideal abstraction at equilibrium. It should be noted that the isomerisation reactions given in equations (13) and (24) do

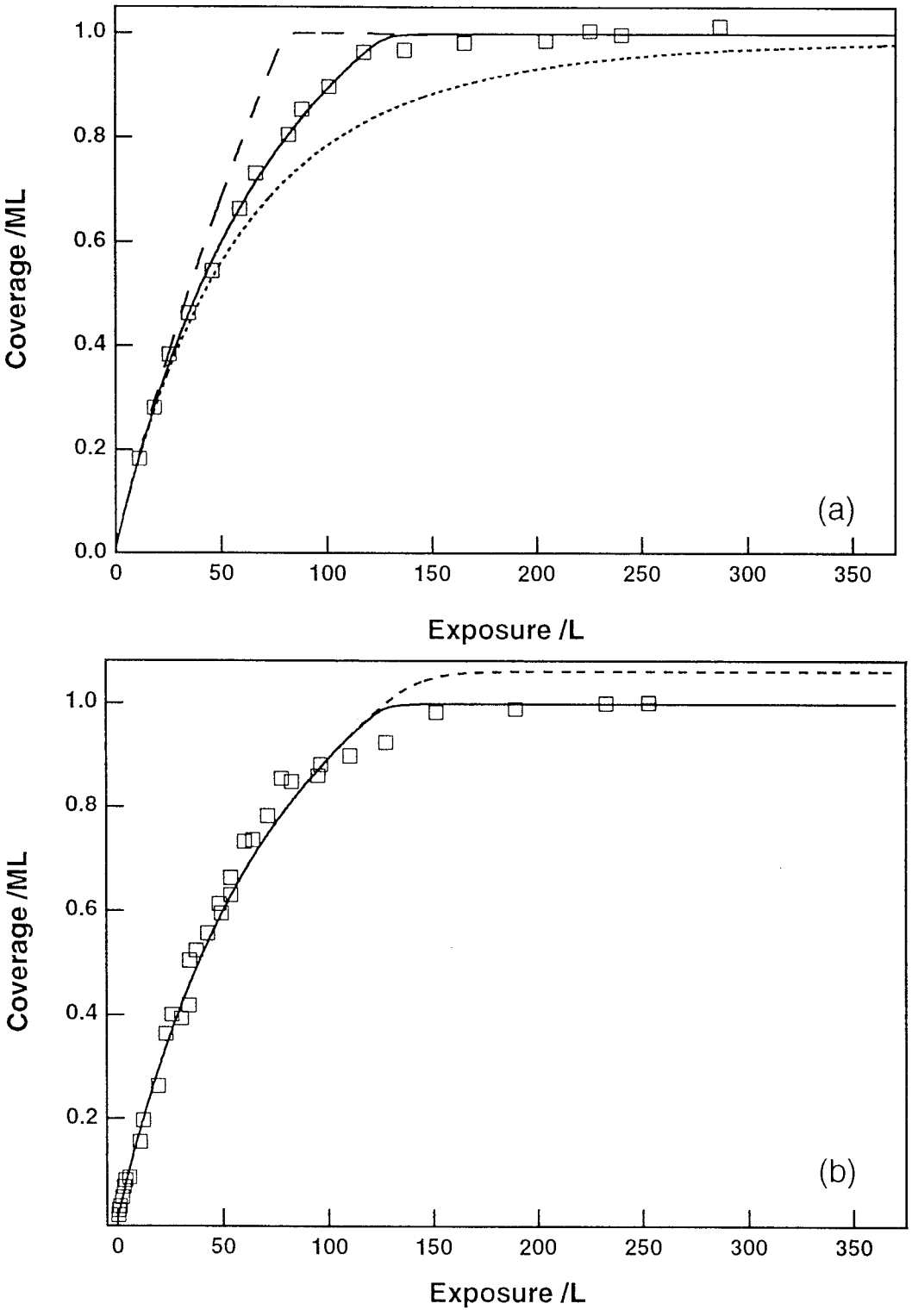

Figure (9). Best fit (—) to experimental data (□) for (a) H· and (b) D· uptake at 635 K equation (23). Also shown are simulated uptake plots using the minimum (···) and maximum (— —) values of k_{di} considered and the simulated coverage during exposure (---).

not preserve the initial identity of the surface species and establish a distribution of HSiH, HSiD and DSiD.

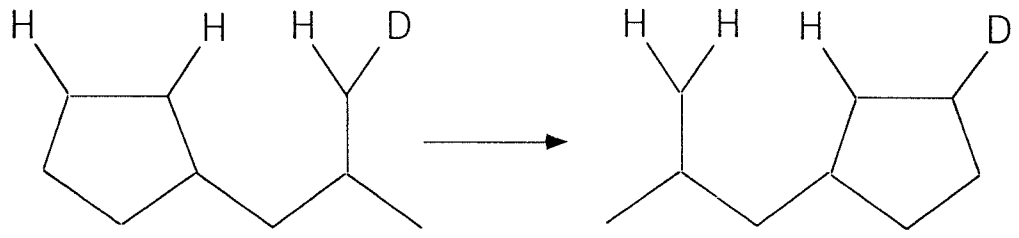

(24)

In agreement with the trend observed here, a recent study has found that the Eley-Rideal reaction probabilities for adsorbed D abstraction by H· and adsorbed H abstraction by D· on Ni(110) are 0.38 and 0.26 respectively [45]. Reaction probabilities and vibrational excitation have been addressed by detailed quantum mechanical calculations [2, 46-49] using various potential energy surfaces, but some aspects of the Eley-Rideal mechanism can be explained by a simple kinematic model [46] If D· collides with an adsorbed H atom, both atoms move towards the surface and subsequently make a second collision as the H atom rebounds from the surface. However, if H· collides with an adsorbed D atom it will be recoiled such that the H and D atoms move in opposite directions as the nascent H-D bond is formed. Hence, a reduced reaction probability is expected and rationalised for H· abstraction of adsorbed D compared with D· abstraction of adsorbed H. The highest reaction probability is expected when H· collides with adsorbed H or D· collides with adsorbed D because the second collision occurs when the atoms are some distance from the surface and the chemisorption potential is weak. The value of k_{HH} deduced from the H· uptake data in figure (9a) and the measured values of k_{HD} and k_{DH} are therefore consistent with this explanation.

The measured rate constant for loss of D during exposure to H· is $(0.31\pm0.01)k_s$ at initial D coverages of 1.0, 0.46 and 0.22 ML yet the rate decreases

more slowly than expected for first order kinetics as the reaction proceeds. According to the kinematic interpretation of abstraction, collisions that do not result in reaction may nevertheless leave the surface Si-H or Si-D bond vibrationally excited. Thus, at the threshold for thermal desorption via the β_1 channel, collision induced recombiative desorption must also be considered. Eilmsteiner *et al.* have recently reported [45] that both HD and D_2 are lost from a D covered Ni(110) surface during reaction with H· as a result of Eley-Rideal abstraction and collision induced desorption respectively. They find that 30 % of the D coverage is lost as D_2 and that the overall rate of reaction is close to second order with respect to D coverage. The contribution of collision induced desorption from doubly occupied dimers to the overall rate of loss of D during H· exposure will be very nearly independent of the initial coverage at 635 K (almost complete pairing except at very low coverages) but will become less significant as the D coverage is diluted by the increasing H coverage (two D atoms are lost from DSi-SiD whereas only one is lost from HSi-SiD). This behaviour is reflected by the data in figure (3) which show that the rate decreases more slowly than expected for first order kinetics, regardless of the initial coverage. It is clear from figure (2) that, within error limits, the abstraction of adsorbed H by D· is described well by first order kinetics. Collision induced desorption is less significant in this case because more of the collisions result in Eley-Rideal abstraction rather than vibrational excitation of the Si-H bond.

E. Uptake and Abstraction at 373 K

A 3x1 LEED pattern is observed after saturation at 380±20 K and has been attributed to an alternating lattice of doubly occupied dimers and dihydride units [53]. STM images of this phase show quite small but well-ordered domains and some incongruities where adjacent rows of dihydride units can be identified [14]. It would appear that local bond rearrangement is required even

at 380 K in order to attain and preserve an ordered 3x1 phase. It is unreasonable to suppose that all dangling bond sites are occupied before Si-Si bonds react to give dihydride species. It is more realistic to suggest that incident H· can react with doubly occupied dimers regardless of coverage. Hence, in figure (4), which shows the uptake of D· at 373 K, there is no distinct change in the sticking probability at the point at which the β_2 TPD peak is first observed or at 1 ML coverage. At low coverages only monohydride is observed by STM which is consistent with this mechanism if the dihydride is propagated across the surface until it encounters and reacts with a vacant dimer site. However, in view of its relatively high activation energy, it is likely that propagation by the isomerisation reaction is slow compared with the time-scale of the experiment and indeed some dihydride is identified by STM before all the dimer dangling bond sites are occupied [14]. The quasi-equilibrium approximation is invalid when the rate constant for diffusion or isomerisation is small compared the rate constants for adsorption and abstraction. However, given that evidence has been presented to suggest local bond rearrangement at 373 K and that the atomic hydrogen flux used in these experiments is small, application of the model as a first approximation to the uptake kinetics can be justified.

Further reaction of Si-Si bonds, probably at defect and step sites yields trihydride species which subsequently react to give silane during TPD and possibly also during H· exposure. Boland [14] has observed that etching (loss of silicon containing products) can be initiated at adjacent rows of dihydride units and it may be that this is responsible for the complex behaviour of the 3x1 phase after extended H· exposures [51]. Thus in addition to abstraction, loss of H or D by etching must also be considered at 373 K. The data in figure (4) show that the silane yield during TPD is a constant fraction of the β_2 TPD peak area which leads to the conclusion that approximately 1% of the dihydride species, probably at defects or step edges, can further react to give trihydride groups and

then silane. It seems likely that silane can be lost from the surface by reaction of trihydride groups with an incident hydrogen atom. The silane TPD yield is then representative of the steady state trihydride coverage that remains on the surface when the atomic hydrogen flux is turned off but which then reacts with an adjacent chemisorbed hydrogen atom during TPD. Silane has been detected [52] during exposure of Si(111) at 373 K to an H· flux in excess of 1 ML s^{-1}. The rate constant for loss of H as silane at 373 K is estimated as approximately 0.04 k_s from the reported data which is significantly less than the rate constant for abstraction measured in the present study. Moreover, trihydride formation is more facile on the Si(111)-7x7 reconstruction [53] and especially when the surface is aggressively etched. Since the rate of desorption via the β_1 and β_2 channels is insignificant at 373 K, it can be concluded that hydrogen adsorbed on Si(100) is removed predominantly by abstraction at 373 K and that silane loss can be ignored in this analysis.

The uptake plot predicted using the quasi-equilibrium model is compared with the experimental data in figure (10). The agreement is excellent when it is considered that the rate constants for abstraction and adsorption were obtained from independent experiments rather than by fitting the model to these data. A slightly slower rate of uptake is predicted by the model than suggested by the data which may be due to the inadequacy of the quasi-equilibrium approximation at this temperature. It is likely that the number of dangling bond sites is higher than the equilibrium prediction at less than about 1 ML due to slow dihydride propagation. The saturation coverages obtained by simulation and experiment are in particularly good agreement. Hence, it would appear that a coverage of 1.5 ML is obtained when abstraction and adsorption reactions are in equilibrium whereas previously 1.33 ML has been regarded as the ideal saturation coverage [14, 54]. Since a saturation coverage in excess of that corresponding to a perfect 3x1 phase is an equilibrium condition,

it can be concluded that the out of phase domain boundaries, and hence the domain sizes, are merely a microscopic reflection of a system at equilibrium.

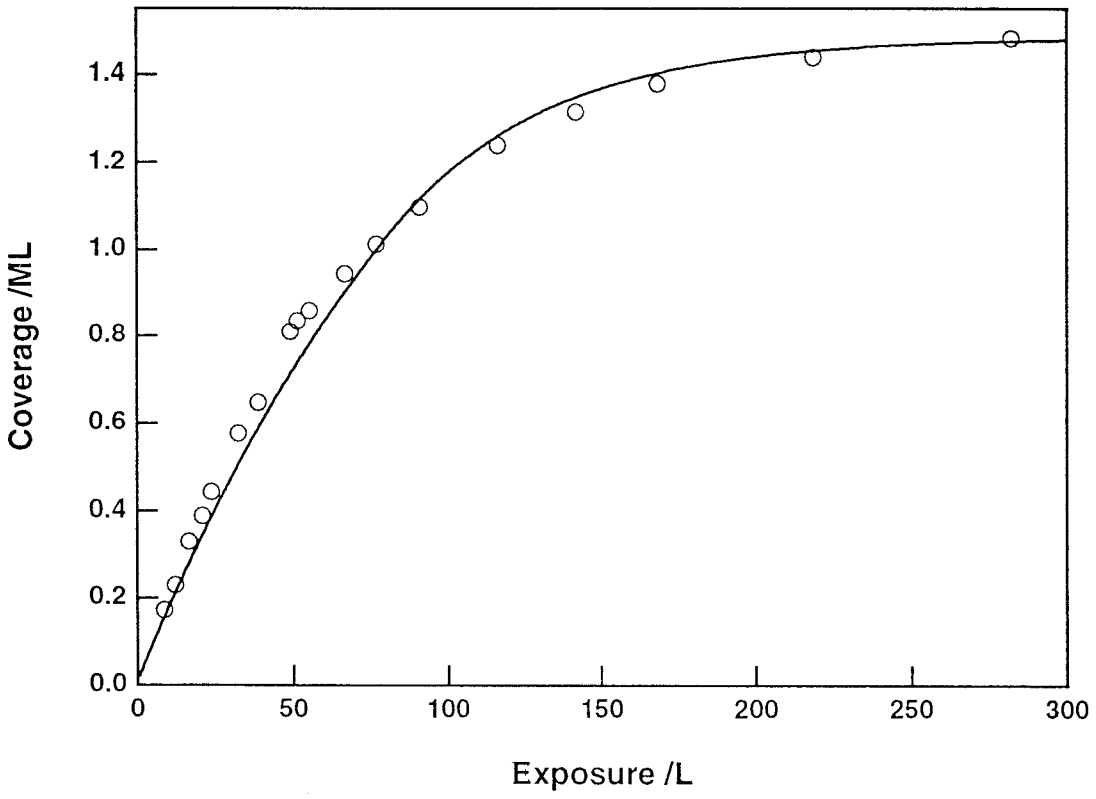

Figure (10). Simulation of D· uptake at 373 K using the quasi-equilibrium model with $k_{d1}=0.8k_s$ and $k_{DD}=0.28k_s$; simulation (—) and experimental data (○).

4.4. CONCLUSIONS

A quasi-equilibrium model has been developed to describe the uptake kinetics of atomic hydrogen on Si(100) at 373 K and 635 K. A simple consideration of only adsorption at dangling bond sites and Eley-Rideal abstraction cannot be reconciled with a saturation coverage of 1 ML at 635 K. It is argued that although hot precursor dynamics may be important at low temperatures, slow vibrational relaxation in the chemisorption potential well does not lead to an almost coverage independent sticking probability. Instead, it is proposed that a high sticking probability is maintained by reaction with doubly occupied dimers to give dihydride species which then propagate across

the surface by an isomerisation reaction. At 635 K, the rate constant for this reaction is high and at the H· flux used in the present experiments, the steady state coverage is slightly more than 1 ML. Subsequently, dihydride units either react with unoccupied dimer sites or molecular hydrogen is lost by desorption from two dihydride units (the β_2 desorption channel). The dihydride species may be regarded as a mobile chemisorbed precursor at high temperatures, although only the bonding arrangement is propagated by isomerisation. When the H· source is turned off, the steady state dihydride coverage is quickly lost to leave a monohydride coverage of 1 ML. Although the experimental data at both 373 K and 635 K can also be convincingly represented by first order Langmuir kinetics, this model for uptake does not take abstraction into account.

The abstraction reaction has been discussed in terms of an Eley-Rideal abstraction mechanism and a simple kinematic model. At 635 K, the initial rate constants for loss of D during exposure to H· are the same regardless of the initial coverage but the rate decreases less rapidly than expected for first order kinetics as the reaction proceeds. It is thought that this is a consequence of collision induced desorption. The uptake model also implies that a small amount of deuterium is lost as D_2 and HD via the β_2 thermal desorption channel at 635 K. The rate constant for abstraction from monohydride is the same as for abstraction from dihydride which implies that the geometric and electronic differences between these species are not important in this reaction.

Bond rearrangement at (380±20) K is required to attain and preserve a mostly ordered 3x1 phase during adsorption and abstraction. Hence, the model can be applied as a first approximation when the H· or D· flux is small. At 373 K, a coverage of 1.5 ML is maintained when adsorption and abstraction reactions are in dynamic equilibrium. This coverage is accommodated by small

3x1 domains with adjacent rows of dihydride at some boundaries. Loss of hydrogen as silane is shown to be of little importance in these experiments but further reactions of the saturated 3x1 phase during extended exposures were intentionally not pursued. It is likely that the adjacent rows of dihydride which are required at equilibrium also present sites for slow etching reactions.

4.5. REFERENCES

[1] W. Widdra, S.I. Yi, R. Maboudian, G.A.D. Briggs and W.H. Weinberg. Phys. Rev. Lett. 74 (1995) 2074.

[2] D.D. Koleske, S.M. Gates and B.Jackson, J. Chem. Phys. 101 (1994) 3301.

[3] M. Naitoh, H. Morioka, F. Shoji and K. Oura, Surf. Sci. 297 (1993) 135.

[4] C.C. Cheng, S.R. Lucas, H. Gutleben, W.J. Choyke and J.T. Yates Jr., J. Am. Chem. Soc. 114 (1992) 1249.

[5] P. Kisliuk, J. Phys. Chem. Solids. 3 (1957) 95.

[6] P.W. Tamm and L.D. Schmidt, J. Chem. Phys. 52 (1970) 1150.

[7] J. Harris and B. Kaesmo, Surf. Sci. 105 (1981) L281.

[8] H. Brune, J. Wintterlin, J. Trost, G. Ertl, J. Wiechers and R.J. Behm, J. Chem. Phys. 99 (1993) 2128.

[9] C.E. Wartnaby, A. Stuck, Y.Y. Yeo and D.A. King, J. Chem. Phys. 102 (1995) 1855.

[10] K-H. Allers, H. Pfnür, P. Feulner and D. Menzel, J. Chem. Phys. !00 (1994) 3985.

[11] C.T. Rettner, Phys. Rev. Lett. 69 (1992) 383.

[12] C.T. Rettner, J. Chem. Phys. 101 (1994) 1529.

[13] C.T. Rettner and D.J. Auerbach, Science 263 (1994) 365.

[14] J.J. Boland, Surf. Sci. 261 (1992) 17.

[15] J.F. O' Hanlon. A User's Guide to Vacuum Technology, 2nd ed., Wiley.

[16] T.A. Flaim and P.D. Ownby, J. Vac. Sci. Technol. 8 (1971) 661.

[17] R. Holanda, J. Vac. Sci. Technol. 10 (1973) 1133.

[18] D. Rapp and P. Englanda-Golden, J. Chem. Phys. 43 (1965) 1464.

[19] W.L. Walters and J.H. Craig, Jr., J. Vac. Sci. Technol. 5 (1968) 152.

[20] T. Sakurai, M.J. Cardillo and H.D. Hagstrum, J. Vac. Sci. Technol. 14 (1977) 397.

[21] M.C. Flowers, N.B.H. Jonathan, Y. Liu, A. Morris, J. Chem. Phys. 99 (1993) 7038.

[22] S.M. Gates, Roderick, R. Kunz and C.M. Greenlief, Surf. Sci. 207 (1989) 364.

[23] D. Mihelcic, R.N. Schindler and P. Potzinger, Ber. Bunsenges. Physik. Chem. 78 (1974) 82.

[24] J.A. Glass, Jr., E.A. Wovchko and J.T. Yates, Jr., Surf. Sci. 348 (1996) 325.

[25] P. Guyot-Sionnest, P. Dumas, Y.J. Chabal and G.S. Higashi, Phys. Rev. Lett. 64 (1990) 2156.

[26] P. Dumas, Y.J. Chabal, and G.S. Higashi, Phys. Rev. Lett. 65 (1990)1124.

[27] M. Morin, P. Jacob, N.J. Levinos, Y.J. Chabal and A.L. Harris, J. Chem. Phys. 96 (1992) 6203.

[28] R.R. Cavanagh, E.J. Heilweil and J.C. Stephenson, Surf. Sci. 299/300 (1994) 643.

[29] R.R. Cavanagh, J.D. Beckerle, E.J. Heilweil and J.C. Stephenson, Surf. Sci. 269/270 (1992) 113.

[30] M. Morin, N.J. Levinos and A.L. Harris, J. Chem. Phys. 96 (1992) 3950.

[31] CRC Handbook of Chemistry and Physics, 75th edition, Ed. D.R. Lide, CRC press (1994).

[32] Y.J. Chabal and K. Raghavachari, Phys. Rev. Lett. 53 (1984) 282.

[33] P. Jakob and Y.J. Chabal, J. Chem. Phys. 95 (1991) 2897.

[34] B.N.J. Persson and R. Ryberg. Solid State Commun. 36 (1980) 175.

[35] P. Guyot-Sionnest, P.H. Lin, E.M. Lin, E.M. Miller, J. Chem. Phys. 102 (1995) 4269.

[36] J.J. Boland, J. Vac. Sci. Technol. A10 (1992) 2458.

[37] C.J. Wu, I.V. Ionova and E.A. Carter, Phys. Rev. B49 (1994) 13488.

[38] J.J. Boland, Surf. Sci. 244 (1991) 1.

[39] A.J. Mayne, C.M. Goringe, C.W. Smith and G.A.D. Briggs, Surf. Sci. 348 (1996) 209.

[40] T.-C. Shen, C. Wang, G.C. Abeln, J.R. Tucker, J.W. Lyding, Ph. Avouris and R. E. Walkup, Science 268 (1995) 1590.

[41] A. Vittadini, A. Selloni and M. Casarin, Surf. Sci. Lett. 289 (1993) L625.

[42] J. McKean. J. Phys. Chem. 86 (1982) 307.

[43] M.C. Flowers, N.B.H. Jonathan, A. Morris and S. Wright, Surf. Sci. Surf. Sci. 351 (1996) 87.

[44] P. Nachtigall, K.D. Jordan, C. Sosa, J. Chem. Phys. 101 (1994) 8073.

[45] G. Eilmsteiner, W. Walkner and A. Winkler, Surf. Sci. 352-354 (1996) 263.

[46] B. Jackson and M. Persson, J. Chem. Phys. 96 (1992) 2378.

[47] B. Jackson and M. Persson, Surf. Sci. 269/270 (1992) 195.

[48] P. Kratzer and W. Brenig, Surf. Sci. 254 (1991) 275.

[49] M. Persson and B. Jackson, J. Chem. Phys. 102 (1985) 1078.

[50] Y.J. Chabal and K. Raghavachari, Phys. Rev. Lett. 54 (1985) 1055.

[51] D.T. Jiang, G.W. Anderson, K. Griffiths, T.K. Sham and P.R. Norton, Phys. Rev. B48 (1993) 4952.

[52] D.R. Olander, M. Balooch, J. Abrefah and W.J. Siekhaus, J. Vac. Sci. Technol. B5 (1987) 1404.

[53] J.J. Boland, Surf. Sci. 244 (1991) 1.

[54] C.C. Cheng and J.T. Yates, Jr., Phys. Rev. B43 (1991) 4041.

CHAPTER 5

THE DESORPTION OF MOLECULAR HYDROGEN FROM Si(100)-2x1 AND Si(111)-7x7 SURFACES

5.1. INTRODUCTION

Kinetic investigations of adsorption and desorption processes on metal surfaces have largely been superseded by methods providing dynamic information. In contrast to metals, however, the chemistry of silicon surfaces is dominated by surface reaction kinetics as a consequence of distinct covalent bonding, site specificity and the surface reconstruction. Although the dynamics of molecular hydrogen adsorption [1] and desorption [2-5] on and from silicon surfaces have been studied, microscopic models for the surface reaction remain controversial.

Unoccupied dimers, singly occupied dimers and doubly occupied dimers can be distinguished by STM [6-9] of sub-monolayer hydrogen coverages on Si(100)-2x1. Crucially, a thermodynamic propensity for doubly occupied dimers is observed as a consequence of the π-bond interaction such that paired dangling bonds are energetically more favourable than isolated dangling bonds for which there is no π-bonding [8, 9]. In addition to this pairing interaction, there is an effective clustering interaction between doubly occupied dimers in the same dimer row [8-10] which is evidenced by strings of doubly occupied dimers at low coverages. At higher coverages there is little impression of anisotropic clustering but there is a very clear separation into occupied and unoccupied areas [11].

The TPD of molecular hydrogen from Si(100) at low coverages is characterised by a single peak, labelled β_1, which represents desorption from monohydride species. At higher coverages, a second peak, labelled β_2, appears as the result of dimer bond breaking and desorption from dihydride species. Isothermal desorption measurements [12, 13] at high coverages have shown that desorption via the β_1 channel is first order in hydrogen coverage. It has been proposed that this is a consequence of desorption exclusively from doubly

occupied dimers [13]. D'Evelyn *et al.* have developed lattice gas models [10, 14] to describe the dynamic equilibrium between unoccupied dimers, singly occupied dimers and doubly occupied dimers. These models predict that the β_1 desorption channel will deviate from first order kinetics at low coverages. This has been confirmed experimentally by isothermal SHG measurements [15] for coverages less than 0.1 ML but clustering was not considered in the analysis. In a previous study [16], TPD data obtained for initial coverages between 0.05 and 1.5 ML were successfully simulated using a generalised lattice gas model but desorption at low coverages was not thoroughly investigated. In this chapter, carefully obtained TPD data resulting from low initial coverages are presented and analysed using a lattice gas model which involves both the π-bond energy and a clustering interaction between doubly occupied dimers.

Hydrogen coverages of less than 19/49 ML can be accommodated at the rest atom and adatom dangling bond sites of the Si(111)-7x7 reconstruction. STS [17] of adatom and rest atom positions on at low hydrogen coverages has confirmed that atomic hydrogen adsorbs at these sites and STM images [17] show that there is no disruption of the 7x7 unit cell. The role of corner hole dangling bonds is uncertain since they cannot be investigated by STM or STS. Ab initio density functional theory calculations [18] have predicted that the corner hole dangling bond sites are more reactive than both adatom and rest atom sites. Moreover, vibrational spectroscopy [19] of low hydrogen coverages has inferred that hydrogen adsorbs preferentially at corner hole sites.

The TPD of molecular hydrogen from Si(111) at low coverages is also characterised by a single peak, labelled β_1, which represents desorption from monohydride species. A second peak, labelled β_2, appears at higher coverages as the result of adatom back-bond breaking and desorption from dihydride and trihydride species. At high coverages, hydrogenated adatom clusters are

initially prominent and a complex chemistry involving the decomposition of these islands and the subsequent formation of a ($\sqrt{3}$x$\sqrt{3}$) R30° phase is revealed as desorption proceeds [17, 20]. All evidence suggests that the 7x7 reconstruction remains intact during desorption of low initial hydrogen coverages but desorption of high coverages involves substantial surface reconstruction even when only low hydrogen coverages remain. Hence, the desorption kinetics will depend on the chemical history in addition to the coverage and surface temperature. Isothermal measurements [21] of desorption via the β_1 channel for coverages between 0.2 and 0.8 of saturation hydrogen coverage have been interpreted in terms of second order kinetics. Recently, a two site model involving two competing second order desorption channels has been developed and used to simulate β_1 TPD peaks for a wide range of coverages [22]. Although both channels are required in order to fit the TPD data at moderate and high coverages, only one channel is important at low coverages according to this model. However, Heinz *et al.* [23] have found that an empirical order number of 1.5±0.2 is appropriate for coverages less than 0.2 ML using SHG and have proposed a different two site model to explain the observed kinetics. It is the purpose of the present study to determine the kinetics for hydrogen desorption from Si(111) at low coverages using TPD and thereby suggest a suitable mechanism.

5.2. THE PROBLEM OF AMBIENT WATER ADSORPTION

Early STM images of nominally clean Si(100)-2x1 surfaces appeared to show missing dimer defect densities from 10 to 20% but the crystals were left to cool for up to three hours after annealing in these experiments [24]. However, ambient H_2O is a significant contribution to the residual gas pressure in most vacuum systems and adsorbs on Si(100)-2x1 with unity sticking probability at room temperature. More recent STM studies have shown that most missing dimer defects arise from dissociative water adsorption [25, 26] and that defect

densities of only 1% can be observed if the surface is imaged quickly after annealing [11].

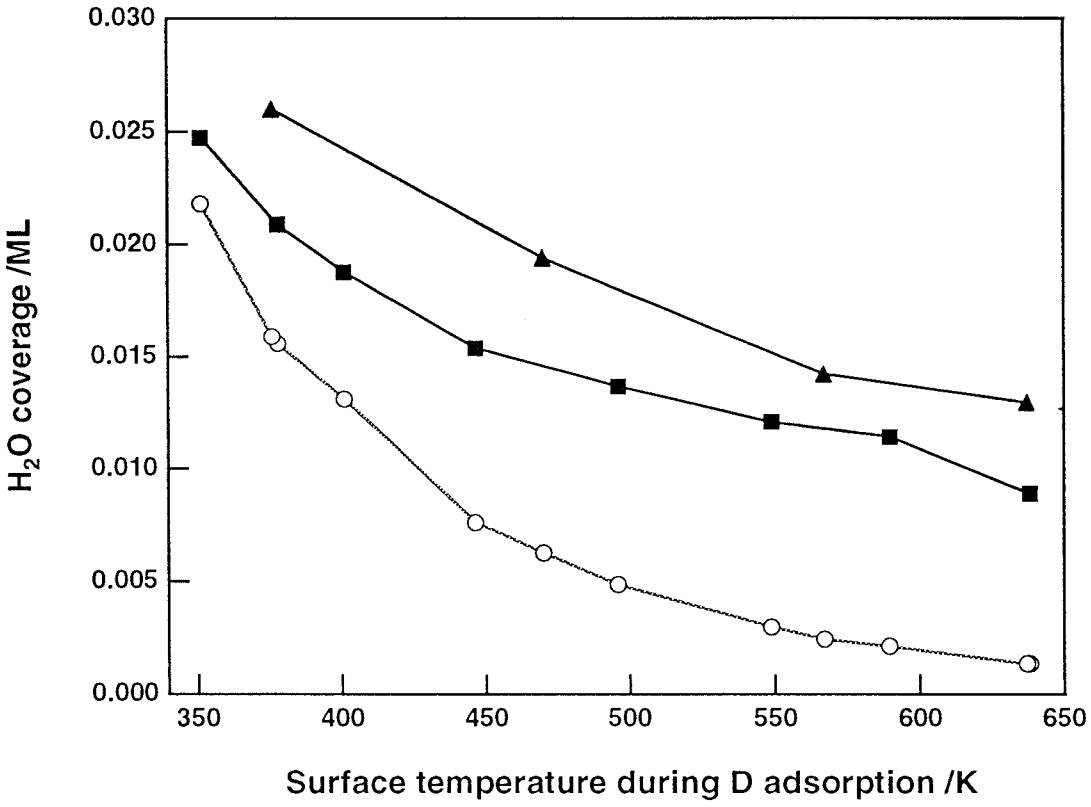

Figure (1). Measured H_2O coverage after D atom exposure using D_2 pressures of $1x10^{-7}$ mbar (■) and $2x10^{-7}$ mbar (▲) and the H_2O coverage calculated using an ambient H_2O pressure of $4x10^{-11}$ mbar and the measured temperature during each experiment (○).

In the present study of desorption at very low deuterium coverages, the problem of ambient water adsorption has been thoroughly addressed. It is particularly important that the total coverage of hydrogen and deuterium is used in the analysis. In order to measure the amount of water adsorption it is convenient to titrate the hydrogen coverage arising from dissociative H_2O adsorption with an excess of deuterium. All hydrogen is then lost as HD during TPD which is much easier to measure than a smaller H_2 signal superimposed on a large and noisy background. The H_2O coverages measured by TPD after cooling from 1150 K and exposure to atomic deuterium are plotted

in figure (1). The sticking probability for water as a function of surface temperature has been measured elsewhere in this work and can be used to calculate the amount of H_2O adsorption if the partial pressure of H_2O and the surface temperature as a function of time during the experiments are known. It is immediately obvious from figure (1) that more H_2O adsorbs when the D_2 pressure is doubled which suggests that either H_2O is displaced from the chamber walls or that the D_2 gas was contaminated with a very small amount of H_2O. Nevertheless, it is clear that if the D_2 pressure were reduced to zero, the calculated and measured water adsorption would be in excellent agreement considering the very low coverages involved. The surface temperature during exposure to deuterium atoms was 640 K and the D_2 pressure was $1x10^{-8}$ mbar in the experiments which follow and hence the estimated H_2O coverage is 0.004 ML.

5.3. DESORPTION KINETICS OF HYDROGEN FROM Si(100)

A. The partition function for chemisorbed hydrogen atoms

The partition function, Q, for any system is defined by equation (1) in which g_i and ε_i are the degeneracy and the energy of the ith level respectively.

$$Q = \sum_i g_i e^{-\varepsilon_i / k_B T} \tag{1}$$

An atom localised on a lattice site has vibrational energy but the total energy of the system may also include an attractive or repulsive interaction with other adsorbed atoms. Thus the total partition function can be factorised into two components which represent the single particle partition function and the lattice partition function as given in equation (2).

$$Q_{surface} = \sum_{vibrations} g_{vibrations} \exp\left(-\varepsilon_{vibrations}/k_B T\right) \times \sum_{lattice} g_{lattice} \exp\left(-\varepsilon_{lattice}/k_B T\right) \times \exp\left(-D_0^{Si-H}/k_B T\right) \tag{2}$$

A hydrogen atom adsorbed at a dangling bond site has three degrees of freedom which can be identified with one stretching vibration and two bending vibrations (perpendicular and parallel to the dimer bond). Similarly, two hydrogen atoms adsorbed on both dangling bonds of a single dimer have six degrees of freedom which can be identified with symmetric and asymmetric stretching vibrations and four bending vibrations. The contribution of all the vibrations to the partition function is calculated using equation (3) in which υ_i are the measured vibrational frequencies collated in table (1).

$$q_{vibrations} = \sum_i \frac{\exp(h\nu_i / 2k_B T)}{\exp(h\nu_i / k_B T) - 1} \tag{3}$$

The location of the zero energy level is arbitrarily chosen as the dissociation limit of the Si-H bond and it is important that the same zero energy level is used throughout this analysis. The zero point energy for each vibrational mode has been included in equation (3) and hence the Si-H bond dissociation energy, $D_0^{Si\text{-}H}$, is the minimum of the Si-H potential well.

B. A Chemical Approach to Surface Equilibria

A detailed model of the desorption kinetics at low coverages must include the clustering interaction but it is a reasonable approximation to consider only the pairing interaction, especially at higher coverages. A model has been developed [16] which is particularly useful when dihydride species contribute to the surface equilibria. Although the elementary surface reactions are unknown and may be complex, the distribution of singly occupied dimers, HSi-Si·, doubly occupied dimers, HSi-SiH, unoccupied dimers, Si=Si and dihydride units, HSiH, can be defined by the two equilibria represented by equations (4) and (5).

$$\text{HSi-SiH} + \text{Si=Si} \rightleftharpoons 2\ \text{HSi-Si}\cdot \tag{4}$$

Table (1). Frequencies of Si-H and Si-D vibrations used to calculate the vibrational partition function.

vibration	Si-H frequency /cm^{-1}	Si-D frequency /cm^{-1}
H-SiSi stretch*	2093 [27]	1523 [27]
H-SiSi bend*	621 [28]	419 [28]
H-SiSi-H sym. stretch	2088 [27]	1519 [27]
H-SiSi-H asym. stretch	2099 [27]	1528 [27]

* It has been assumed that the Si-H and Si-D stretching frequencies for HSi-Si· and DSi-Si· are equal to the mean of the symmetric and asymmetric stretching frequencies for HSi-SiH and DSi-SiD respectively. However, singly occupied dimers are both electronically (charge transfer and correlation effects) and geometrically (buckled rather than symmetric) different to doubly occupied dimers. Additionally, there is a chemical interaction (coverage dependence of the vibrational frequencies) of 9 cm^{-1} for hydrogen and 7.5 cm^{-1} for deuterium [27]. These subtle effects are of little consequence when calculating the partition function.

$$\tfrac{3}{2}\text{HSi-SiH} \rightleftharpoons \text{HSi-Si}\cdot + \text{HSiH} \qquad (5)$$

The equilibrium constants describing these equilibria are given by equations (6) and (7) in which q_{10}, q_{11} and q_2 are the vibrational partition functions for HSi-Si·, HSi-SiH and HSiH respectively and ϵ_1 and ϵ_2 are the enthalpy changes for the forward reactions.

$$\frac{\theta_{10}^2}{\theta_{00}\theta_{11}} = \frac{4q_{10}^2}{q_{11}}\exp\left(-\frac{\epsilon_1}{kT}\right) \qquad (6)$$

$$\frac{\theta_{10}\theta_2}{(\theta_{11}^3(1+\theta_2))^{1/2}} = \frac{q_{10}q_2}{q_{11}^{3/2}}\exp\left(-\frac{\epsilon_2}{kT}\right) \qquad (7)$$

If n_{00}, n_{10}, n_{11} and n_2 are the densities of unoccupied dimers, singly occupied dimers, doubly occupied dimers and dihydride species respectively, n is the density of chemisorbed hydrogen atoms and N is the density of surface silicon atoms, then

$$2n_{00}+2n_{10}+2n_{11}+n_2=N \text{ or } \theta_{00}+\theta_{10}+\theta_{11}+\theta_2=1 \quad (8)$$

and

$$n_{10}+2n_{11}+2n_2=n \text{ or } \tfrac{1}{2}\theta_{10}+\theta_{11}+2\theta_2=\Theta \quad (9)$$

where $n_{1i}/N=\theta_{1i}/2$ (i=0,1), $n_{00}/N=\theta_{00}/2$, $n_2/N=\theta_2$ and $n/N=\Theta$ by definition. The values of ϵ_1 and ϵ_2 can be regarded as being approximately equal to the π-bond energy and the σ-bond energy respectively although any differences in the Si-H bond energies must also be taken into account [29, 30]. Equations (6), (7), (8) and (9) can be solved numerically to yield the equilibrium coverages of Si=Si, HSi-Si·, HSi-SiH and HSiH at a given temperature and total coverage.

Desorption via the β_2 channel results in a decrease in the dihydride coverage and is thought to be second order with respect to hydrogen coverage [16, 31]. It is generally assumed that molecular hydrogen is lost by reaction between two adjacent dihydride units as shown in figure (2a). This is vindicated by the STM image [32] represented by figure (2b) which shows the formation of epitaxial dimers from disilane fragments. Clearly some adjacent SiH_2 units have been imaged before reaction. Hence, the overall rate equation for desorption including both β_1 and β_2 channels is

$$-\frac{d\Theta}{dt}=\nu_a\times\theta_{11}\times\exp(-E_a/kT)+\nu_b\times\theta_2^2\times\exp(-E_b/kT) \quad (10)$$

which can be evaluated using the calculated values of θ_{11} and θ_2.

C. The one dimensional lattice gas problem

The one dimensional lattice gas problem can be solved exactly by considering a canonical ensemble of N distinguishable lattice sites of which n are occupied. A combinatorial analysis is given here so that it can then be adapted to a lattice of dimers and is essentially that described by Hill [33].

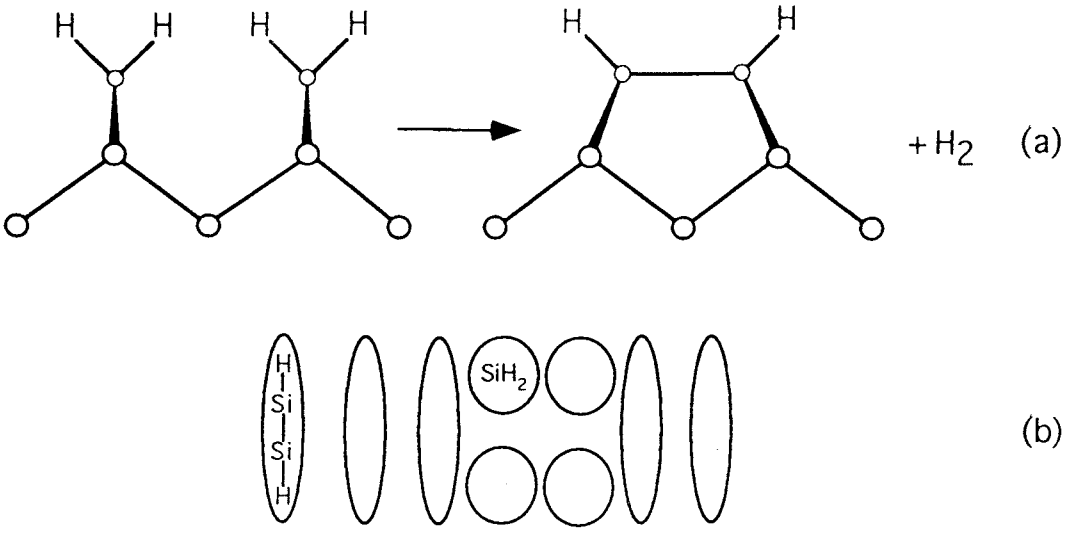

Figure (2). The reaction between two adjacent dihydride units shown in (a) is confirmed by the STM image represented by (b).

If there is an interaction potential, ω, between nearest neighbour pairs of sites then the total energy of a particular configuration is $P_{11}\omega$, where P_{11} is the number of nearest neighbour pairs of occupied sites. If a line is drawn from each occupied site to its two neighbours as in figure (3), then 2n lines will be drawn.

Figure (3). A total of 2n lines are drawn if a line is drawn between each occupied site and its neighbours.

Hence,

$$2n = 2P_{11} + P_{10} \tag{11}$$

and

$$P_{11}\omega = (n - {}^{P_{10}}/_{2})\omega \tag{12}$$

where P_{10} is the number of pairs of nearest neighbour sites with one site empty and the other occupied. It follows from equation (2) that the lattice partition

function can be written as

$$q_{lattice} = \sum_{P_{10}} g(n, N, P_{10}) \exp\left[-(n - P_{10}/2)\omega / k_B T\right] \tag{13}$$

where the summation is over all values of P_{10} consistent with a given coverage. The configuration degeneracy, g(n, N, P_{10}), is the number of different ways in which n atoms can be distributed on N sites with P_{10} pairs of adjacent occupied and unoccupied sites.

Consider a small lattice comprising of seven occupied sites and six unoccupied sites which are represented by 1's and 0's respectively in figure (4).

1 1 1|0 0|1|0|1|0 0|1 1|0

Figure (4). A lattice of thirteen sites occupied by seven atoms. Each boundary between an occupied site and an unoccupied site is indicated by a vertical line and represents a 10 pair.

A 10 pair occurs at each boundary between a group of 1's and a group of 0's and therefore it follows that there are (P_{10}+1)/2 groups of 1's and (P_{10}+1)/2 groups of 0's. Let

$$Y = \frac{P_{10} + 1}{2} \tag{14}$$

be the number of groups of either 1's or 0's. For a given value of P_{10}, the number of groups remains fixed and hence the configuration degeneracy is the number of different ways that the 1's and 0's can be assigned to these groups. Each group of 1's must have at least one member so the number of arrangements is the number of ways the remaining

$$X = n - \frac{P_{10} + 1}{2} \tag{15}$$

1's can be assigned. The solution to this problem given by Ising [34] for a ferromagnetic system is described in detail below since it is then readily adapted to hydrogen atoms adsorbed on a one dimensional lattice of silicon dimers. There are X+Y 1's in total which can be written as 1+1+1+1+1+1+1 with plus signs between each. Groups can be selected and written as (1+1+1)+(1+1)+(1)+(1) or (1+1)+(1)+(1+1)+(1+1) for example with the number of excluded plus signs equal to Y-1. If seven 1's are to be arranged into four groups then there are six ways of choosing the first plus sign, five ways of choosing the second and four ways of choosing the third, making a total of 6!/3! or 120 ways of selecting the groups. However, the order in which the plus signs are selected makes no difference and thus it is necessary to divide by 3!, the number of ways that the same three plus signs can be selected. In the general case,

$$number\ of\ arrangements = \frac{(X+Y-1)!}{X!(Y-1)!} \tag{16}$$

which becomes

$$number\ of\ arrangements = \frac{n!}{(P_{10}/2)!\,[n-(P_{10}/2)]!} \tag{17}$$

by substitution. The corresponding number of ways of arranging the groups of 0's can be obtained by replacing n by N-n in equation (17) and thus finally, the configuration degeneracy of n atoms on a lattice of N sites with P_{10} boundaries is given by equation (18).

$$g(n,N,P_{10}) = \frac{n!(N-n)!}{[n-(P_{10}/2)]!\,[N-n-(P_{10}/2)]!\,[(P_{10}/2)!]^2} \tag{18}$$

The lattice partition function can be evaluated by the maximum term method when this expression for g(n, N, P_{10}) is substituted into equation (13). Although the summation is strictly over all possible values of P_{10}, there will be one term

that makes an overwhelming contribution to the summation if n is large. This term can be identified using

$$\frac{\partial \ln q_{lattice}}{\partial P_{10}} = 0 \tag{19}$$

which yields

$$\frac{(\frac{n}{N} - \alpha)(1 - \frac{n}{N} - \alpha)}{\alpha^2} = e^{-\omega/kT} \tag{20}$$

where

$$\alpha = \frac{P_{10}}{2N} \tag{21}$$

when the value of P_{10} corresponds to the maximum term in the sum.

D. Hydrogen atoms adsorbed on a one dimensional lattice of silicon dimers

The clustering interaction is likely to be a consequence of bond strain as suggested by Boland [11]. Unoccupied dimers are buckled such that the two second layer atoms bound to the up end are pulled together whereas those bound to the down end are pushed apart and hence the bond strain is minimised when adjacent dimers buckle in opposite directions. Doubly occupied dimers are invariably reported to be symmetric (not buckled) and have a longer dimer bond length which must result in strain in the bonds to second layer atoms at the boundary between an unoccupied dimer and a doubly occupied dimer. The lattice energy is then determined by the number of these boundaries and is therefore reduced by clustering. Although there is some lattice strain coupling between adjacent dimer rows such that the out-of-phase c(4x2) reconstruction is preferred over the in-phase p(2x2) reconstruction, there seems to be little correlation between adjacent HSi-SiH strings at low coverage. The distribution of singly occupied dimers appears to be random and only in a few cases are they adjacent to doubly occupied dimers. This is entirely

consistent with the explanation given above since it has been shown that singly occupied dimers are buckled [34] and therefore do not introduce lattice strain. It is not clear why singly occupied dimers are buckled. The buckling orientation of many dimers in the same dimer row is pinned by the influence of one singly occupied dimer and this can be imaged by STM (but only filled state images clearly show the buckling). The dimer flipping process requires charge transfer from the up atom to the down atom as shown in figure (5) but this will be much more difficult when an electronegative hydrogen atom is adsorbed on the up atom. Hence, a singly occupied dimer becomes locked in one orientation and many other unoccupied dimers in the same row are prevented from flipping by coupling of the strain through second layer atoms. It is possible that the buckling orientation is flipped by diffusion of the hydrogen atom to an adjacent site but this will occur rarely on the time-scale of a room temperature STM experiment.

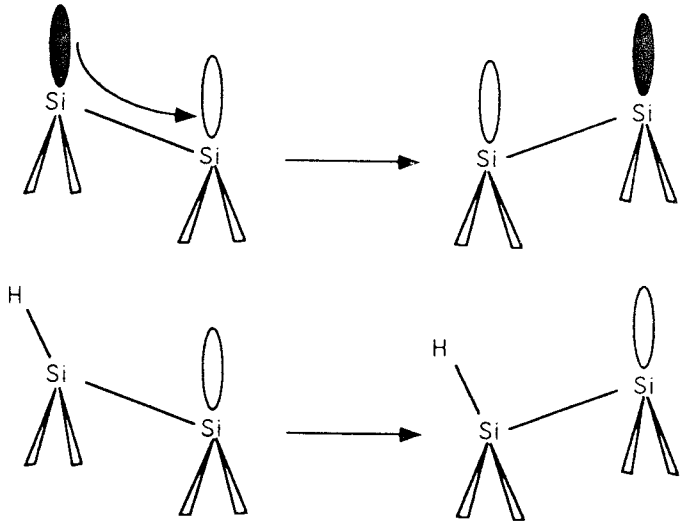

Figure (5). Charge transfer occurs during the flipping vibration of unoccupied dimers. This vibration is made much more difficult when a hydrogen atom is adsorbed on the up atom.

If it can be assumed that there is an effective clustering interaction between pairs of doubly occupied dimers, then the analysis of a one

dimensional lattice gas described above can be applied. A typical section of the lattice might look like figure (6) in which doubly occupied dimers are represented by 1's, singly occupied dimers by A's and unoccupied dimers by 0's.

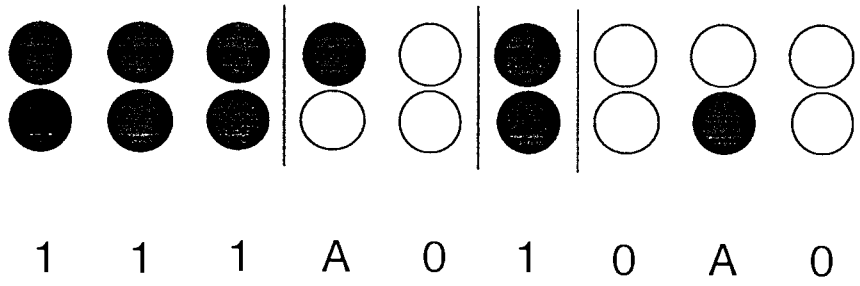

Figure (6). A row of occupied (●) and unoccupied (○) dimer sites with each P_{1x} boundary indicated by a vertical line.

The total energy of a particular arrangement of doubly occupied dimers, singly occupied dimers and unoccupied dimers is the sum of both clustering and pairing interactions and is defined as

$$Total\ energy = -P_{11}\omega + \frac{\epsilon_1 n_{10}}{2} \tag{22}$$

where ω is the attractive interaction between two adjacent doubly occupied dimers and ϵ_1 is the energy required to unpair a doubly occupied dimer. It is necessary to express P_{11}, the number of adjacent pairs of doubly occupied dimers, in terms of P_{1x}, the total number of 10 and 1A boundaries using

$$P_{11} = \left(n_{11} - \frac{P_{1x}}{2} \right) \tag{23}$$

which follows from equation (11). Hence, the lattice partition function can be written as

$$q_{lattice} = \sum_{n_{10}}^{\min(n,N-n)} \sum_{P_{1x}}^{\min(n-n_{10}-1,N-n+n_{10}+1)} g(n,N,P_{1x},n_{10}) \exp\left[\left\{ -\omega\left(n_{11} - \frac{P_{1x}}{2} \right) + \frac{\epsilon_1 n_{10}}{2} \right\} \Big/ k_B T \right] \tag{24}$$

in which the limits of the summation reflect the mass and site balance

requirements dictated by equations (8) and (9). Clearly, the evaluation of the configuration degeneracy, $g(n, N, P_{1x}, n_{10})$, will be similar to the evaluation of $g(n, N, P_{10})$ for a simple one dimensional lattice gas but is made more complicated by the permutations of A's and 0's. Some of the many possible configurations that have the same energy as the example shown in figure (6) are given in figure (7) with each configuration split into groups of 1's and groups of 0's and A's. Groups can be chosen from the A's and 0's by excluding plus signs as before but it is then necessary to count other permutations of A's and 0's. For example, (A+0+0)+(A+0) can be chosen from A+0+0+A+0 but (0+A+0)+(A+0) can be chosen from 0+A+0+A+0 by excluding the same plus sign. In general,

$$\begin{matrix}\textit{number of permutations} \\ \textit{of A's and 0's}\end{matrix} = \frac{(n_{00}+n_{10})!}{n_{00}!\,n_{10}!} \tag{25}$$

which is the number of different ways that the A's and 0's can be placed in order. There are four ways of choosing two groups from A+0+0+A+0 but there are ten permutations of the A's and 0's and hence, there are a total of forty different ways of arranging just the A's and 0's. In addition, it is obvious from figure (6) that each singly occupied dimer can be arranged in two different ways so that for each configuration identified above there are in fact $2^{n_{10}}$ configurations which must be counted.

$$\begin{aligned}
&111A010A0 \quad or \quad (1+1+1)+(1)\ and\ (A+0)+(0+A+0)\\
&11A0110A0 \quad or \quad (1+1)+(1+1)\ and\ (A+0)+(0+A+0)\\
&1A01110A0 \quad or \quad (1)+(1+1+1)\ and\ (A+0)+(0+A+0)\\
&1A00111A0 \quad or \quad (1)+(1+1+1)\ and\ (A+0+0)+(A+0)\\
&10A0111A0 \quad or \quad (1)+(1+1+1)\ and\ (0+A+0)+(A+0)
\end{aligned}$$

.....and many other configurations

Figure (7). Some of the many possible degenerate configurations corresponding to n_{10}=2 and P_{1x}=3.

It follows from these arguments that the surface partition function can be written as

$$Q_{surface} = \sum_{n_{10}} \sum_{P_{1x}} \frac{n_{11}!\left[(n_{00}+n_{10})!\right]^2 2^{n_{10}}}{\left[\left(N_{10}/2\right)!\right]^2\left[n_{11}-\left(N_{10}/2\right)\right]!\left[\left(n_{00}+n_{10}\right)-\left(N_{01}/2\right)\right]!n_{00}!n_{10}!} \times q_{10}^{n_{10}} q_{11}^{n_{11}} \times \exp\left[\left\{-\omega\left(n_{11}-\frac{P_{1x}}{2}\right)+\frac{\epsilon_1 n_{10}}{2}\right\}\Big/ k_B T\right] \tag{26}$$

by explicitly including the configuration degeneracy in equation (24). The summation is again complicated and therefore the partition function is evaluated by using the maximum term method. The most important configuration is identified by simultaneously solving the conditions defined by

$$\frac{\partial \ln Q_{surface}}{\partial P_{1x}} = 0 \tag{27}$$

and

$$\frac{\partial \ln Q_{surface}}{\partial n_{10}} = 0 \tag{28}$$

since the configuration degeneracy is a function of both n_{10} and P_{10}. These derivatives are easily evaluated by applying Stirling's approximation and substituting n_{00} and n_{11} in equation (26) for terms in N, n and n_{10}. Solving equation (27) yields

$$\frac{\left(n_{11}-\frac{P_{1x}}{2}\right)\left(\frac{N}{2}-n_{11}-\frac{P_{1x}}{2}\right)}{\left(\frac{P_{1x}}{2}\right)^2} = \exp(\omega/k_B T) \tag{29}$$

which is the simple one dimensional lattice gas result derived earlier and solving equation (28) yields equation (30).

$$\frac{\left(\frac{N}{2}-n_{11}\right)^2\left(n_{11}-\frac{P_{1x}}{2}\right)\left(\frac{N}{2}-n+n_{11}\right)}{n_{11}\left(\frac{N}{2}-n_{11}-\frac{P_{1x}}{2}\right)n_{10}^2} = \frac{q_{11}}{4q_{10}^2}\exp\left[\left(\epsilon_1+\omega\right)/k_B T\right] \tag{30}$$

Equations (29) and (30) are equivalent to those given by D'Evelyn *et al.* [10] without derivation and can be solved numerically to give the coverage of doubly occupied dimers.

E. Analysis of the experimental results

The TPD data were simulated by numerical integration of the rate equation for desorption. The quasi-equilibrium coverage of doubly occupied dimers was calculated by numerically solving equations (29) and (30) for the instantaneous total coverage, Θ, and the measured surface temperature, T. After each time increment, Δt, the change in coverage is approximately $(d\Theta/dt)\Delta t$ where $d\Theta/dt$ is the instantaneous desorption rate calculated from

$$-\frac{d\Theta}{dt} = \nu_a \times \theta_{11} \times \exp(-E_a / k_B T) \qquad (31)$$

assuming that ν_A and E_a do not change with coverage.

The variation of TPD peak temperatures with coverage is plotted in figure (8). The departure from first order kinetics at low coverages is clearly demonstrated by a sharp increase in peak temperature for initial coverages less than about 0.15 ML. Previous studies [12, 13] have indicated that desorption at higher coverages can be described by first order kinetics but the present data show a small but discernable increase in the TPD peak temperature for initial coverages greater than 0.15 ML. Initial simulations indicated that without the inclusion of the clustering interaction, the precipitous rise in peak temperature at low coverages and the TPD peak shapes could not be reconciled with a single value of the pairing energy. However, if attention is confined to the low coverage regime, the peak temperatures, peak shapes and the onset of first order kinetics at higher coverages suggest a pairing interaction of (3.2±0.2) kcal mol^{-1} and a clustering interaction of (5±0.5) kcal mol^{-1}. Some examples of TPD peaks simulated using these values for ϵ_1 and ω with ν_A and E_A equal to $1x10^{15}$ s^{-1}

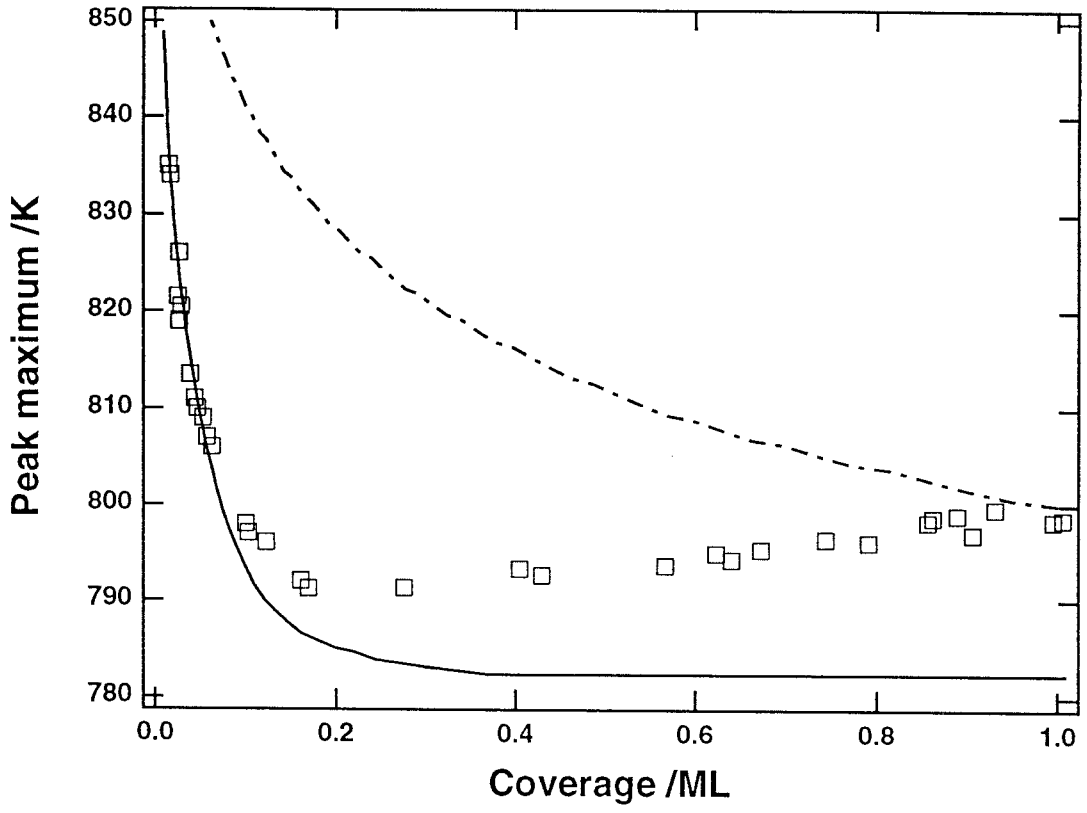

Figure (8). TPD peak temperatures predicted using the pairing and clustering model (—) and an empirical rate equation [37] for an atomically rough surface (— · —)are compared with the experimental data (□).

and 56.0 kcal mol^{-1} respectively are compared with the experimental data in figure (9). The validity of the model and the values assigned to ϵ_1, ω, ν_A and E_A are confirmed by an excellent fit to the data at low coverages, but it is conceded that the increase in peak temperature between 0.15 and 1.0 ML cannot be interpreted using the simple rate equation given above. A complete description of the desorption kinetics at all coverages must recognise that the pre-exponential factor and the activation energy are coverage dependent. Indeed, the microscopic model implies that the activation energy for desorption depends on the occupation of neighbouring sites; two 10 or 1A boundaries are lost by desorption from an isolated doubly occupied dimer but two are created by desorption from the middle of a string of doubly occupied

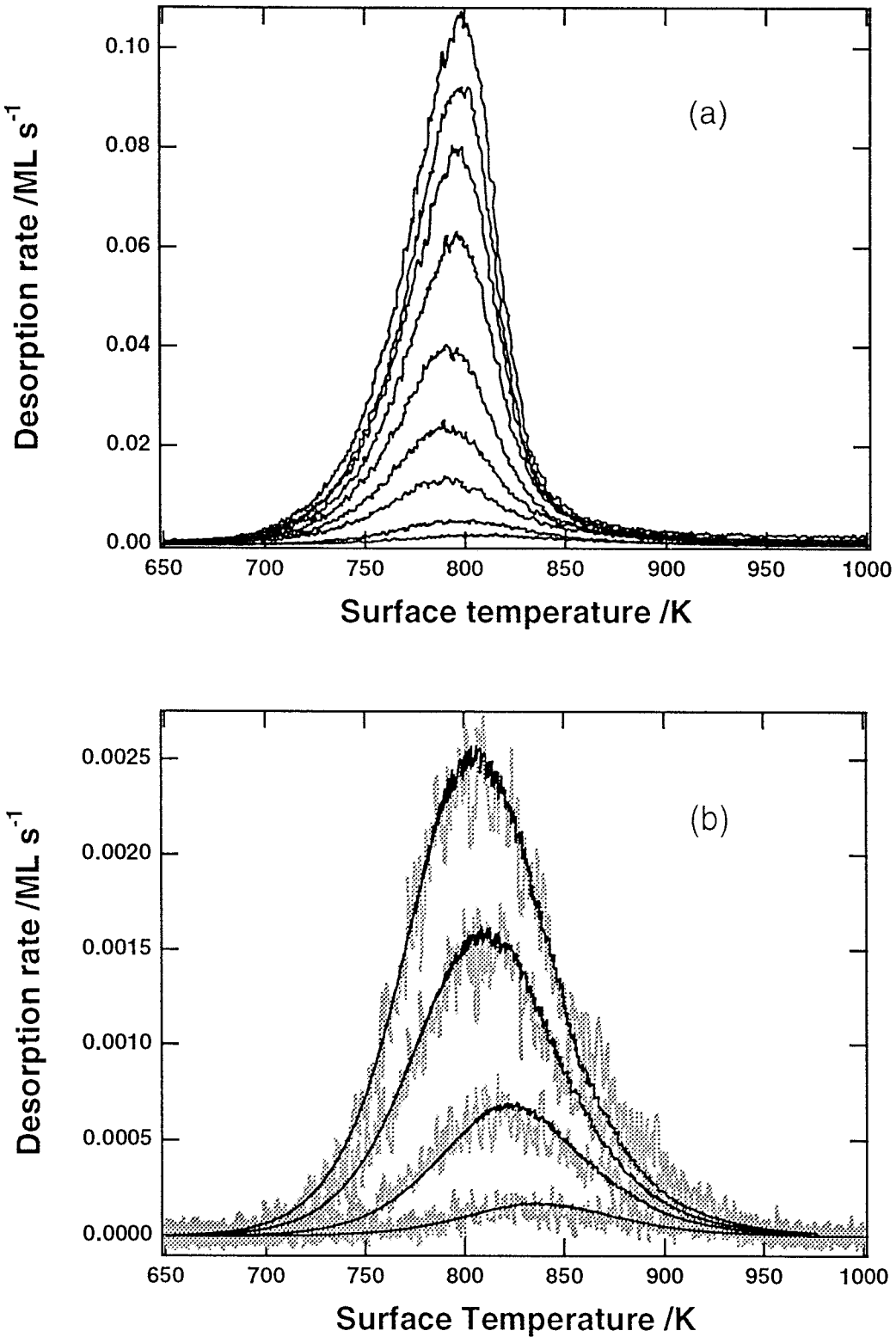

Figure (9). The experimental TPD data in (a) are characteristic of first order kinetics at high coverages but careful analysis reveals complex kinetic behaviour. Experimental TPD data (grey) and TPD simulated using the pairing and clustering model (black) are compared in (b). The data in (b) result from total coverages (deuterium and hydrogen from 0.004 ML of H_2O) of 0.015, 0.026, 0.046 and 0.062 ML.

dimers. In general, the effective pre-exponential factor and activation energy are extracted from desorption rates using, for example, the variation of heating rate method [36], but an empirical rate equation is of little value here.

The desorption of hydrogen from an atomically rough Si(100) surface has been reported [37]. Hydrogen coverages between 0.06 and 0.97 ML were prepared by quenching epitaxial growth from silane. An empirical rate equation fits the data well and can be used to simulate TPD for comparison with the present data. Rather than compare peak shapes, the peak temperatures plotted in figure (8) more clearly demonstrate the very different kinetics. It is likely that the subtle interactions that lead to pairing and particularly clustering on a nominally perfect Si(100) surface are overwhelmed by the distorted geometries of an atomically rough surface.

F. The rate of desorption from equilibrium thermodynamics

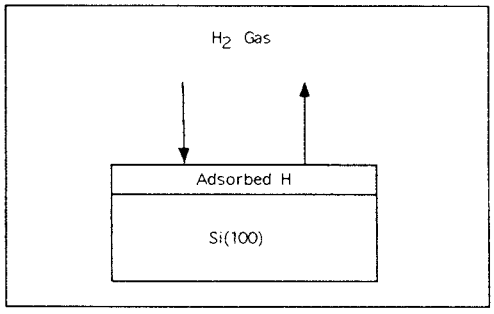

Figure (10). Molecular hydrogen gas is in equilibrium with hydrogen adsorbed on Si(100) when the rates of adsorption and desorption are equal.

The rate equation for desorption can be obtained directly from equilibrium considerations without explicitly including a pre-exponential factor and activation energy [38]. The system described by figure (10) is at equilibrium when the surface coverage of hydrogen is such that the total free energy of the system is minimised at constant number of molecules, volume

and temperature. This requirement can be expressed more conveniently in terms of chemical potentials as

$$\mu_{gas} = \mu_{surface} \tag{32}$$

where the surface is a two component condensed phase consisting of both the adsorbed hydrogen and the silicon surface. The total partition function for H_2 in the ideal gas approximation can be written as

$$Q_{gas} = \left(\frac{2\pi m k_B T}{h^2}\right)^{3/2} V \times Q_{internal} \times \exp(-D_0^{H-H}/k_B T) \tag{33}$$

where $Q_{internal}$ is the partition function for vibrations and rotations and D_0^{H-H} is the dissociation energy of an H_2 molecule. Differentiating ln Q_{gas} with respect to the number of H_2 molecules in the gas phase yields the chemical potential

$$\mu_{gas} = D_0^{H-H} - k_B T \ln\left[\left(\frac{2\pi m k_B T}{h^2}\right)^{3/2} \frac{k_B T}{P} \times Q_{internal}\right] \tag{34}$$

and hence,

$$P = \left(\frac{2\pi m k_B T}{h^2}\right)^{3/2} k_B T \times Q_{internal} \times \exp\left[\left(\mu_{gas} - D_0^{H-H}\right)/k_B T\right] \tag{35}$$

is the corresponding H_2 pressure. At equilibrium, the chemical potentials of the gas phase and hydrogen adsorbed on the surface are equal so μ_{gas} can be replaced by $\mu_{surface}$. The rate of adsorption is given by the Hertz-Knudsen equation

$$rate\ of\ adsorption = \frac{s(\Theta,T)P}{(2\pi m k_B T)^{1/2}} \tag{36}$$

where

$$s(\Theta,T) = s_0(T) \times \theta_{00} \tag{37}$$

is the coverage and temperature dependent sticking probability. The surface

and gas temperature dependence of the initial sticking coefficient, $s_0(T)$, has been measured using SHG and molecular beam techniques [1, 39]. Detailed balance demands that H_2 adsorbs only at unoccupied dimers if desorption occurs only from doubly occupied dimers and that the rate of adsorption equals the rate of desorption at equilibrium. Hence, substituting equations (35) and (37) into equation (36) and equating the rate of desorption to the rate of adsorption yields

$$\begin{aligned} rate\ of\ desorption = s_0(T)\theta_{00}\left(\frac{2\pi m k_B T}{h^3}\right)k_B T \times Q_{internal} \\ \times \exp\left[\left(2\mu_{surface} - D_0^{H-H}\right)/k_B T\right] \end{aligned} \tag{38}$$

in which all the dynamical information about adsorption and desorption is contained in the sticking probability, $s_0(T)$. The chemical potential of hydrogen adsorbed on the surface can be evaluated using

$$\mu_{surface} = -k_B T \frac{\partial \ln Q_{surface}}{\partial n} \tag{39}$$

where $Q_{surface}$ is defined by equation (2).

It was naïvely implied earlier that the only significant differences in vibrational partition functions for singly occupied dimers, doubly occupied dimers and unoccupied dimers are due to the Si-H vibrations, but it is likely that the lower frequency Si-Si vibrations are much more important. The π-bonding interaction or Peierls distortion must surely have some effect on the vibrations of the surface silicon atoms. Numerous calculations using a variety of methods find that the dimer bond length in doubly occupied dimers is longer than in unoccupied dimers, although there is no convincing experimental evidence at present [40]. The pairing and clustering model developed above is a detailed description of the surface perturbation and models for other systems look crude by comparison [41, 42]. The lattice strain

associated with doubly occupied dimers has been identified with the clustering interaction, ω, whereas the π-bond interaction and other correlation effects involving dangling bonds are included in the pairing interaction, ϵ_1. However, Si-Si vibrations are undoubtedly crucial to the evaluation of the surface partition function and to the successful application of equation (38). Surface phonon frequencies from theoretical calculations or experimental measurements are presently sparse and it is unreasonable to speculate what they might be or which should be included in the vibrational partition function.

5.4. DESORPTION KINETICS OF HYDROGEN FROM Si(111)

A. Microscopic kinetic model

Previously it has been found that the β_1 desorption channel cannot be adequately described by a single second order desorption process for all coverages less than 19/49 ML [22]. Two second order desorption channels, designated AA and AB have been proposed and represent recombinative desorption from adjacent rest atom sites and adjacent rest atom and adatom sites respectively. The kinetic model requires that the Si-H bond is stronger for hydrogen adsorbed at rest atoms than for hydrogen adsorbed at adatoms by an amount denoted as ΔE.

There is no clear experimental evidence for preferential adsorption on Si(111)-7x7 at rest atom sites rather than adatom sites. It should be noted that any analysis of site preference must take into account the relative number of adatom and rest atom sites and that hydrogen atom adsorption at low temperatures does not result in an equilibrium distribution. However, there is a very distinct propensity for adsorption at the rest atom sites of the Ge(111)-c(2x8) reconstruction such that no reacted adatoms can be observed at very low hydrogen coverages [43]. There are equal numbers of rest atoms and adatoms

in this reconstruction and it is thought that charge transfer from adatoms to rest atoms leaves the adatom dangling bond state almost empty. STS of the Si(111)-7x7 reconstruction [44] has indicated that the rest atom dangling bond state is fully occupied and that the center adatom dangling bond state is almost empty. In this case, less electron density is withdrawn from the corner adatoms compared with the center adatoms because each center adatom has two rest atom neighbours whereas each corner adatom has only one. Occupied state STM images [43] of Ge(111)-c(2x8) show that the adatoms surrounding a reacted rest atom become bright and this is attributed to reverse charge transfer from the rest atom to the nearest adatoms. Theoretical calculations [43, 44] confirm that the higher electron density available at rest atom sites and relaxation of the reconstruction results in stronger bonding at these sites compared with adatom sites. In particular, ΔE is calculated to be 5 kcal mol^{-1} using the density functional approximation [45] but it is suggested that this value will decrease as more electron density is transferred to the adatoms. Previously, TPD data have been successfully analysed [30] using ΔE equal to 2.5 kcal mol^{-1} and no attempt was made to introduce a coverage dependence.

The equilibrium coverages of hydrogen adsorbed at rest atoms, θ_A, and at adatoms, θ_B, can be calculated for a given value of ΔE. The rate of desorption is then given by

$$-N\frac{d\Theta}{dt} = \nu_{AA}\theta_A^2 \exp(-E_{AA}/RT) + \nu_{AB}\theta_A\theta_B \exp(-E_{AB}/RT) \qquad (39)$$

where N is the number of silicon atoms in one monolayer, Θ is the total hydrogen atom coverage, ν_{AA} and ν_{AB} are pre-exponential factors and E_{AA} and E_{AB} are activation energies for desorption.

B. Simulation of experimental results

The TPD data were simulated by numerical integration of the rate

equation for desorption using the calculated quasi-equilibrium values of θ_A and θ_B. Experimental data were obtained for initial coverages less than 0.14 ML. At these coverages desorption occurs almost entirely via the AA channel resulting in desorption kinetics that are characteristic of a single second order process. Experimental and calculated peak temperatures are plotted as a function of coverage in figure (11) and examples of experimental and simulated TPD data are plotted in figure (12). An excellent fit to the experimental data is obtained for E_{AA} and ν_{AA} equal to 57 kcal mol^{-1} and $2x10^{15}$ s^{-1} respectively. The values of ΔE, E_{AB} and ν_{AB} are set equal to 2.5 kcal mol^{-1}, 57 kcal mol^{-1} and $1x10^{15}$ s^{-1} respectively in accord with a previous analysis of higher coverage TPD data [30].

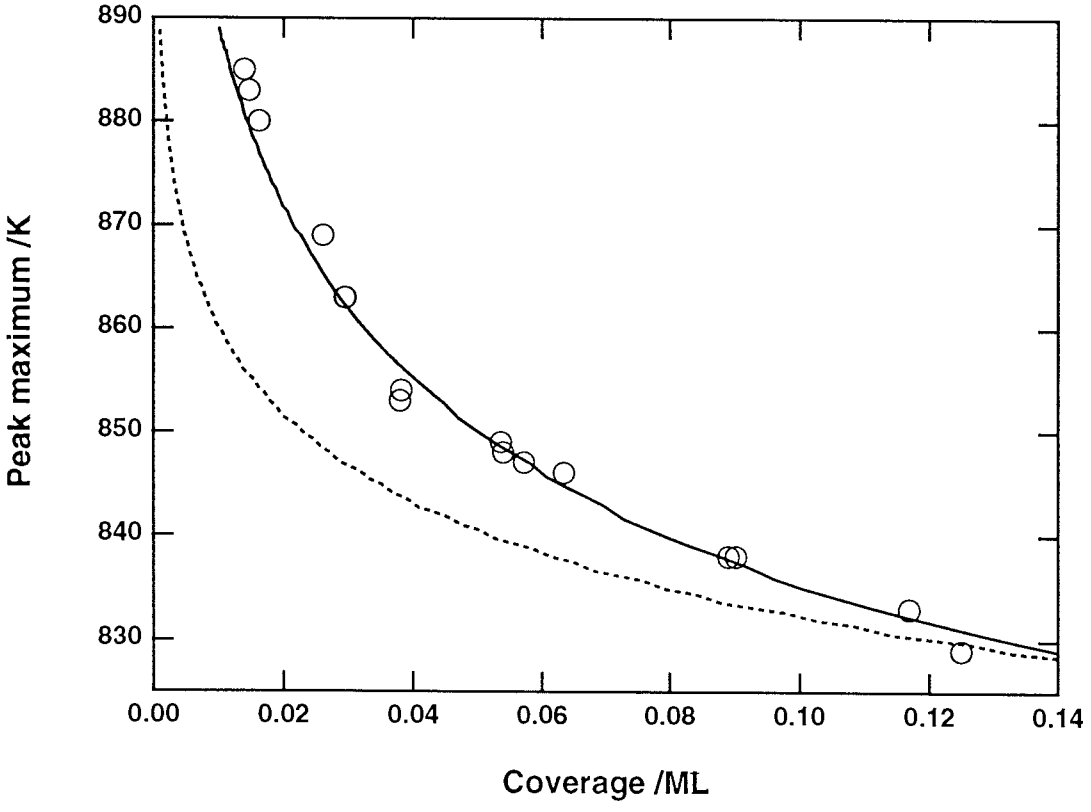

Figure (11). Measured TPD peak maxima (O) and maxima of TPD peaks simulated using the two site model with E_{AA} and ν_{AA} equal to 57 kcal mol^{-1} and $2x10^{15}$ s^{-1} respectively (—). Also shown are the maxima of TPD peaks (····) simulated using the empirical rate equation determined by SHG [23].

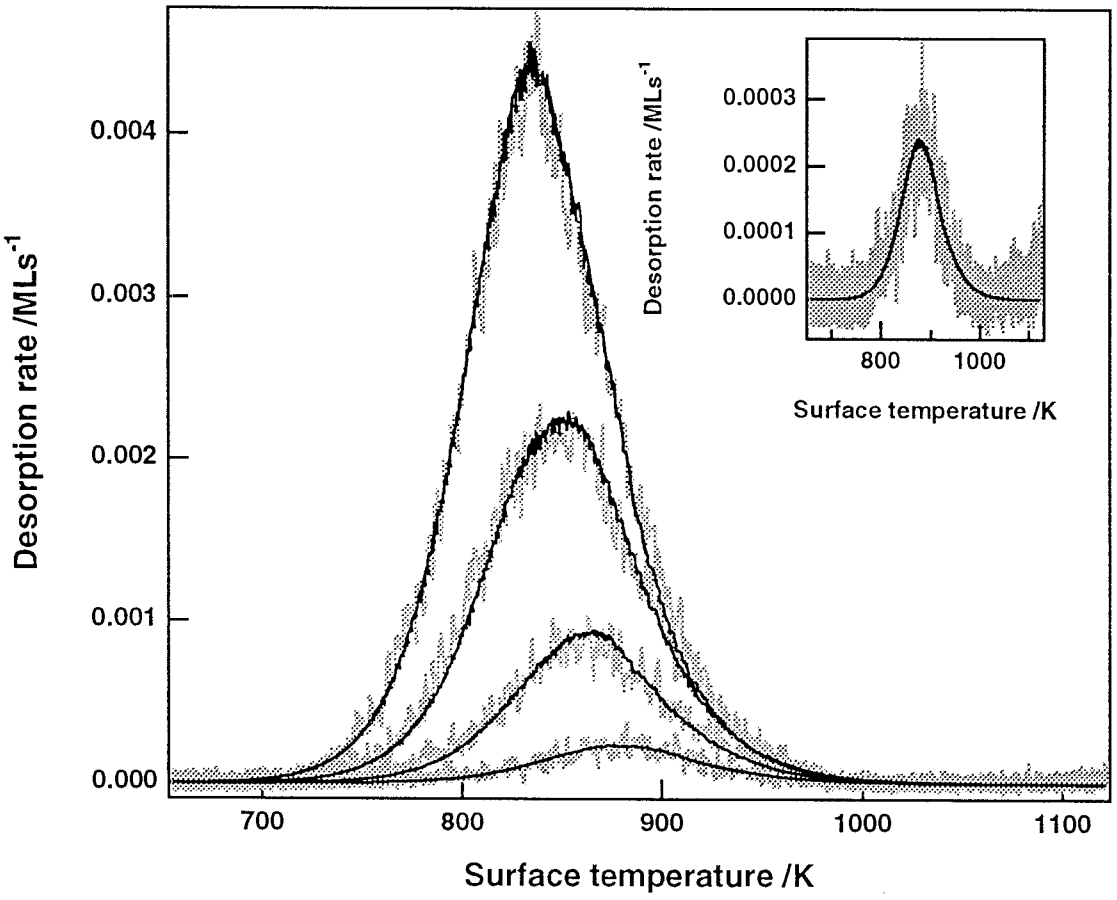

Figure (12). Experimental TPD data (·····) and simulations (—) using a two site model (essentially second order kinetics at these coverages) with E_{AA} and ν_{AA} equal to 57 kcal mol^{-1} and $2x10^{15}$ s^{-1} respectively. These data result from initial coverages (deuterium and hydrogen from 0.004 ML of ambient water adsorption) of 0.015, 0.029, 0.053 and 0.089 ML. The inset shows the smallest TPD peak more clearly.

5.5. A MINOR DESORPTION CHANNEL

Atomic hydrogen adsorption on Si(100) at room temperature results in some patches of an ordered dihydride phase but also yields surface trihydride species [8]. The adatom back-bonds of the Si(111)-7x7 reconstruction are strained and readily react to give adatom trihydride. Trihydride groups on both Si(100) and Si(111) can migrate during exposure to hydrogen atoms and at high coverages by diffusing to adjacent sites made vacant by abstraction. STM [8] and TPD [46, 47] have identified two reaction channels, which depend on the surface temperature, the rate of heating, the hydrogen atom flux and the local

chemical environment. The appearance of adatom islands and dimer strings on Si(111) and Si(100) respectively [8] is evidence for silicon-silicon bond formation between trihydride groups and loss of hydrogen from the surface. A broad H_2 TPD feature (usually labelled β_3) extending from about 200 K to the onset of the β_2 TPD peak is thought to arise from this reaction [47]. Silane desorbs during TPD with a peak maximum at approximately 600 K and is attributed to reaction between trihydride groups and monohydride, dihydride or other trihydride groups. The product yields for these two reaction channels are correlated and increase with decreasing surface temperature during adsorption [46, 47].

A mostly ordered 3x1 phase consisting of alternating rows of dihydride and monohydride can be prepared by atomic hydrogen adsorption at 380±20 K. However, adjacent rows of dihydride are found at some domain boundaries and it is here that some local etching is observed [8]. The yield of silane during TPD is almost at its minimum value [46] but the surface reactions are likely to be somewhat simpler for the generally well-defined 3x1 phase. Some SiD_4 and D_2 TPD data are compared in figure (13). The asymmetry and coverage independent maxima of the SiD_4 TPD peaks are characteristic of first order kinetics. Pseudo first order kinetics are expected since the reaction must involve a very small concentration of trihydride and a very large excess of dihydride and monohydride. However, these TPD peaks are too broad to reconcile with a single one-step reaction and are undoubtedly the consequence of complex reactions.

5.6. DISCUSSION

The kinetic models for hydrogen desorption from Si(100)-2x1 and Si(111)-7x7 both require that the rate of hydrogen atom diffusion is such that quasi-equilibrium distributions of the surface species are maintained. Optical

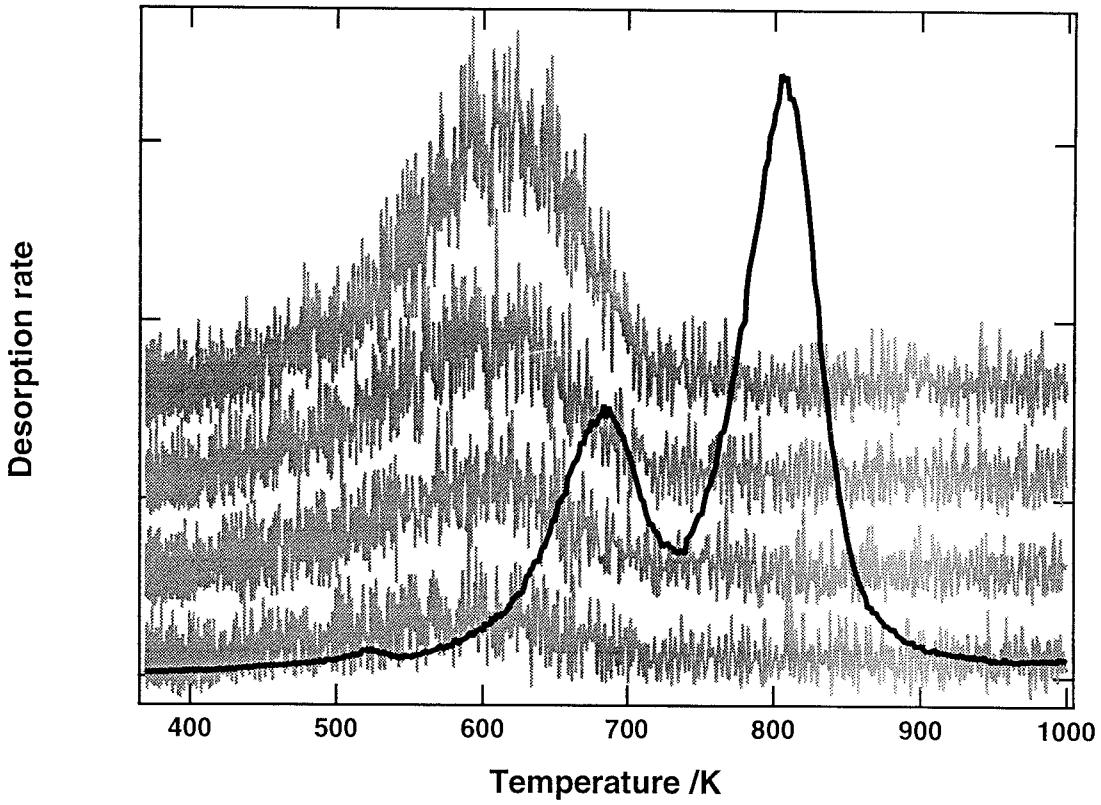

Figure (13). A very small amount of deuterium is lost as SiD_4 (·····) during TPD with a peak maximum at approximately 600K but only when the initial D coverage is greater than 0.85 ML. The D_2 TPD data (—) shown for comparison have been scaled and represent a coverage of 1.5 ML whereas the largest SiD_4 peak corresponds to only 0.01 ML.

second harmonic diffraction measurements from a submonolayer grating of hydrogen adsorbed on Si(111)-7x7 [48] have determined that the diffusion activation energy and pre-exponential factor are 34.5±4.6 kcal mol^{-1} and 10^{-3} cm^2 s^{-1} respectively. First principles calculations have predicted that hydrogen atom diffusion on Si(100)-2x1 is anisotropic. Wu *et al.* [49] find that the activation energy and pre-exponential factor for diffusion parallel to the dimer rows are 38.1±1.7 kcal mol^{-1} and $4.0x10^{\pm0.5}$ cm^2s^{-1} respectively whereas the activation energy and pre-exponential factor for diffusion perpendicular to the dimer rows are 62.8±6.4 kcal mol^{-1} and $4.8x10^{-1\pm1.8}$ cm^2s^{-1} respectively. Vittadini *et al.* [50] calculate an activation energy for diffusion parallel to the dimer rows of approximately 30 kcal mol^{-1} but find that the activation energy for diffusion

perpendicular to the dimer rows is only approximately 41.5 kcal mol^{-1}. It can be concluded that the diffusion of hydrogen atoms on Si(111)-7x7 and parallel to the dimer rows on Si(100)-2x1 is not rate limiting and sufficient to maintain quasi-equilibrium distributions at 800 K.

There has been much discussion in the literature concerning the possible involvement of defect sites in surface processes, especially at low coverages. Step edges are generally accepted to be the most common defect on metal surfaces [51] and have been invoked in adsorption [52], surface reaction [51] and desorption mechanisms [53]. Large area STM topographs of Si(100)-2x1 surfaces have established terrace defect densities ranging from 10% to less than 1% [11, 24]. However, high defect densities may be largely due to adsorption of ambient H_2O [25, 26] rather than method of preparation. Very low defect densities on Si(100)-2x1 surfaces have been observed following saturation with hydrogen and chlorine at high temperatures [8, 54]. STM images [11] infer that molecular hydrogen desorption events, evidenced by the appearance of unoccupied dimers, are not associated with either steps or defect sites. It has been demonstrated in this chapter that the observed kinetics are consistent with microscopic models which neither imply nor invoke the involvement of defect sites.

The internal state distributions of hydrogen desorbed from silicon surfaces have been measured by REMPI [2-4]. Despite the differences in surface structure and kinetics, the rovibrational distributions are found to be approximately the same for desorption from both Si(111) and Si(100) surfaces and via both β_1 and β_2 channels. On the basis of these results and theoretical calculations [55-57], it has been suggested that molecular hydrogen desorbs from an intermediate dihydride species involving only one silicon atom. The mechanism by which the dihydride intermediate is created on the Si(100)-2x1

surface has been the subject of much debate. Ab initio calculations [56] and density functional theory [57] have been used to investigate the desorption of hydrogen from silicon clusters and have indicated that desorption from a doubly occupied dimer via a dihydride intermediate is characterised by an activation energy that is considerably higher than that measured experimentally. However, a recent density functional study [58] using a repeated slab geometry has shown that desorption from a doubly occupied dimer is associated with an activation energy of 55-58 kcal mol^{-1} and a transition state localised over a single silicon atom.

The discrepancies between results obtained from cluster and repeated slab geometries may be due to the inadequacies of the silicon cluster model which comprises a single dimer in the surface layer, four silicon atoms in the second layer, two silicon atoms in the third layer and one silicon atom in the fourth layer. Typically, the atoms in the bottom two layers are held in their rigid lattice positions whereas the top two layers are allowed to relax. Repeated slab geometries generally involve six or more layers with the top four allowed to relax. Experimentally, ion scattering measurements [59] have demonstrated that there is significant reconstruction in at least the first four layers of the Si(100)-2x1 surface, suggesting that small silicon clusters are poor representations of the real surface.

5.7 CONCLUSIONS

The two site model for desorption of hydrogen from Si(111)-7x7 described earlier is found to be entirely consistent with the experimental TPD data and cannot be distinguished from second order kinetics at low coverages. Isothermal SHG measurements have suggested a significant departure from second order kinetics at low coverages and are characterised by an empirical order number of 1.5±0.2. The expected coverage dependence of the TPD peak

temperatures for a kinetic order number of 1.5 is shown to be inconsistent with the experimental data.

A simple lattice gas model involving only the pairing interaction does not adequately describe the desorption of hydrogen from Si(100), except as an approximation at high coverages. A more detailed model including both the pairing and clustering interactions successfully reconciles the TPD peak shapes and peak temperatures at low coverages but it is conceded that a complete description of the desorption kinetics at all coverages must include a coverage dependent activation energy and pre-exponential factor.

5.8. REFERENCES

[1] K.W. Kolasinski, W. Nessler, K-H Bornscheuer and E. Hasselbrink, J. Chem. Phys. 101 (1994) 7082.

[2] S.F. Shane, K.W. Kolasinski and R.N. Zare, J. Chem. Phys. 97 (1992) 1520 .

[3] K.W. Kolasinski, S.F. Shane and R.N. Zare, J. Chem. Phys. 96 (1992) 3995.

[4] S.F. Shane, K.W. Kolasinski and R.N. Zare, J. Chem. Phys. 97 (1990) 3704.

[5] Y-S. Park, J-Y. Kim and J. Lee, J. Chem. Phys. 98 (1992) 757.

[6] Y.W. Mo and M.G. Lagally, Surf. Sci. 248 (1991) 313.

[7] R.M. Tromp, R.J. Hamers and J.E. Demuth, Phys. Rev. Lett. 55 (1985) 1303.

[8] J.J. Boland, Surf. Sci. 261 (1992) 17.

[9] J.J. Boland, Phys. Rev. Lett. 67 (1991) 1539.

[10] Y.L. Yang and M.P. D'Evelyn, J. Vac. Sci. Technol. A11 (1993) 2200.

[11] J.J. Boland, J. Vac. Sci. Technol. A10 (1992) 2458.

[12] K. Sinniah, M.G. Sherman, L.B.Lewis, W.H. Weinberg, J.T. Yates, Jr. and K.C. Janda, J. Chem. Phys. 92 (1990) 5700.

[13] M.L. Wise, B.G. Koehler, P. Gupta, P.A. Coon and S.M. George, Surf. Sci. 258 (1991) 166.

[14] M.P. D'Evelyn, Y.L. Yang and L.F. Sutcu, J. Chem. Phys. 96 (1992) 852.

[15] U. Höfer, L. Li and T.F. Heinz, Phys Rev B45 (1992) 9485.

[16] M.C. Flowers, N.B.H. Jonathan, Y. Liu and A. Morris, J. Chem. Phys. 99 (1993) 7038 .

[17] J.J. Boland, Surf. Sci. 244 (1991) 1.

[18] K.D. Brommer, M. Galván, A. Dal Pino Jr., J.D. Joannopoulos, Surf. Sci. 314 (1994) 57.

[19] Y.J. Chabal, Phys. Rev. Lett. 50 (1983) 1850.

[20] Y. Morita, K. Mika and H. Tokumoto, Surf. Sci. 325 (1995) 21.

[21] B.G. Koehler, C.H. Mak, D.A. Arthur, P.A. Coon and S.M. George, J. Chem. Phys. 89 (1988) 1709.

[22] M.C. Flowers, N.B.H. Jonathan, Y. Liu and A. Morris, J. Chem. Phys. 102 (1995) 1034.

[23] G.A. Reider, U. Höfer and T.F. Heinz, J. Chem. Phys. 94 (1991) 4080.

[24] R.J. Hamers, R.M. Tromp and J.E. Demuth, Phys. Rev. B34 (1986) 5343.

[25] L. Andersohn and U. Köhler, Surf. Sci. 284 (1993) 77.

[26] M. Chander, Y.Z. Li, J.C. Patrin and J.H. Weaver, Phys. Rev. B48 (1993) 2493.

[27] Y. J. Chabal and K. Raghavachari, Phys. Rev. Lett. 53 (1984) 282.

[28] H. Froitzheim, U. Köhler and H. Lammering, Surf. Sci. 149 (1985) 537.

[29] P. Nachtigall and K.D. Jordan, J. Chem. Phys. 101 (1994) 2648.

[30] M.C. Flowers, N.B.H. Jonathan, Y. Liu and A. Morris, J. Chem. Phys. 101 (1994) 2650.

[31] P. Gupta, V.L. Colvin and S.M. George, Phys. Rev. B37 (1988) 8234.

[32] J.J. Boland, Phys. Rev. B44 (1991) 1383.

[33] T.L. Hill, Statistical Thermodynamics, Addison-Wesley, Reading, MA, 1960.

[34] Ising, Z. Physik, 31 (1925) 253.

[35] M.J. Bronikowski, Y. Wang, M.T. McEllistrem, D. Chen and R.J. Hamers, Surf. Sci. 298 (1993) 50.

[36] J.L. Taylor and W.H. Weinberg. Surf. Sci. 78 (1978) 259.

[37] M. Suemitsu, K.-J. Kim and N. Miyamoto, Phys. Rev. B49 (1994) 11480.

[38] H.J. Kreuzer and S.H. Payne in Dynamics of Gas-Surface Interactions, Eds. C.T. Rettner and M.N.R. Ashfold, The Royal Society of Chemistry.

[39] P. Bratu, K.L. Kompa and U. Höfer, Chem. Phys. Lett. 251 (1996) 1.

[40] K.W. Kolasinski, Int. J. Mod. Phys. B9 (1995) 2753.

[41] V.P. Zhdanov, Surf. Sci. 209 (1989) 523.

[42] A.V. Myshlyavtsev and V.P. Zhdanov, J. Chem. Phys. 92 (1990) 3909.

[43] T. Klitsner and J.S. Nelson, Phys. Rev. Lett. 67 (1991) 3800.

[44] R. Wolkow and Ph. Avouris, Phys. Rev. Lett. 60 (1988) 1049.

[45] A. Vittadini and A. Selloni, Phys. Rev. Lett. 75 (1995) 4756.

[46] S.M. Gates, R.R. Kunz and C.M. Greenlief, Surf. Sci. 207 (1989) 364.

[47] C.C. Cheng and J.T. Yates, Jr., Phys. Rev. B43 (1991) 4041.

[48] G.A. Reider, U. Höfer and T.F. Heinz, Phys. Rev. Let. 66 (1991) 1994.

[49] C.J. Wu, I.V. Ionova and E.A. Carter, Phys. Rev. B 49 (1994) 13488.

[50] A. Vittadini, A. Selloni and M. Casarin, Surf. Sci. Let. 289 (1993) L625.

[51] D.F. Johnson and W.H. Weinberg, J. Chem. Phys. 101 (1994) 6289.

[52] H. Karner, M. Luger, H.P. Steinrack, A. Winkler and K.D. Rendulic, Surf. Sci. 163 (1985) L641.

[53] J.A. Serri, J.C. Tully, M.J. Cardillo, J. Chem. Phys, 19 (1983) 1530.

[54] J.J. Boland Adv. Phys. 42 (1993) 129.

[55] P. Nachtigall, K. D. Jordan and K.C. Janda, J. Chem. Phys. 95 (1991) 8652.

[56] C.J. Wu, I.V. Ionova and E.A. Carter, Surf. Sci. 295 (1993) 64.

[57] P. Nachtigall, K.D. Jordan and C. Sosa, J. Chem. Phys. 101 (1994) 8073.

[58] A. Vittadini and A. Selloni, Chem. Phys. Lett. 235 (1995) 334.

[59] R.M. Tromp, R.G. Smeenk, F.W. Saris and D.J. Chadi, Surf. Sci. 133 (1983) 137.